Technische Universität München
Fakultät für Chemie

Quantum-Chemical Investigations into the Photophysics and Photochemistry of Bioorganic Molecules

Dissertation

zur Erlangung des akademischen Grades

Doktor der Naturwissenschaften

vorgelegt von

Deniz Tuna

geboren in Duisburg

Garching b. München, 2014

TECHNISCHE UNIVERSITÄT MÜNCHEN

Theoretische Chemie

Quantum-Chemical Investigations into the Photophysics and Photochemistry of Bioorganic Molecules

Deniz Tuna

Vollständiger Abdruck der von der Fakultät für Chemie der Technischen Universität München zur Erlangung des akademischen Grades eines

Doktors der Naturwissenschaften

genehmigten Dissertation.

Vorsitzender: Univ.-Prof. Dr. Aymelt Itzen

Prüfer der Dissertation:

1. Univ.-Prof. Dr. Wolfgang Domcke
2. Univ.-Prof. Dr. Ville R. I. Kaila
3. Hon.-Prof. Dr. Walter Thiel, Universität Düsseldorf (schriftliche Begutachtung)

   Univ.-Prof. Dr. Steffen J. Glaser (mündliche Prüfung)

Die Dissertation wurde am 27. Februar 2014 bei der Technischen Universität München eingereicht und durch die Fakultät für Chemie am 10. April 2014 angenommen.

Abstract

This thesis is concerned with computational investigations into the photophysics and the photochemistry of bioorganic molecules using *ab initio* methods. Five bioorganic molecules of physiological or biological significance have been investigated *in vacuo*. The photophysical properties, such as the vertical singlet excitation energies, were computed and the photochemical reactivity was elucidated by exploring the potential-energy profiles of the relevant photochemical reaction paths. The conical intersections relevant for the studied processes were optimized and analyzed. The employed *ab initio* methods comprise second-order perturbation theory with a complete-active-space-self-consistent-field reference (CASPT2//CASSCF), the approximate coupled-cluster method of second order (CC2), and the algebraic-diagrammatic-construction method of second order (ADC(2)). The studied molecules include adenosine, a building block of nucleic acids, urocanic acid, a UV filter found in the epidermis of human skin, kynurenine, a UV filter found in the human ocular lens, oligomers of 5,6-dihydroxyindole, the building blocks of the human skin pigment eumelanin, and glucose, an archetypical carbohydrate. Our investigations aimed at identifying the photochemical mechanisms responsible for radiationless excited-state deactivation of electronically excited states and for the exceptionally high photostability of the studied molecules. Our results provide a detailed level of insight into the photophysical and photochemical properties of these isolated biomolecules without the perturbative effect of the environment. On the one hand, some of our studies were motivated by previously obtained spectroscopic findings, on the other hand, our studies may motivate future spectroscopic investigations.

Zusammenfassung

Diese Arbeit befasst sich mit der rechnergestützten Untersuchung der Photophysik und Photochemie von bioorganischen Molekülen mit *ab-initio*-Methoden. Fünf bioorganische Moleküle von physiologischer oder biologischer Bedeutung wurden *in vacuo* untersucht. Die photophysikalischen Eigenschaften, wie etwa die vertikalen Singulett-Anregungsenergien, wurden berechnet und die photochemische Reaktivität wurde über die Berechnung der Potentialenergieprofile der relevanten photochemischen Reaktionspfade aufgeklärt. Die für die untersuchten Prozesse relevanten konischen Durchschneidungen wurden optimiert und analysiert. Die verwendeten *ab-initio*-Methoden umfassen Störungstheorie zweiter Ordnung für eine *complete-active-space-self-consistent-field*-Referenzfunktion (CASPT2//CASSCF), die genäherte *coupled-cluster*-Methode zweiter Ordnung (CC2), sowie die *algebraic-diagrammatic-construction*-Methode zweiter Ordnung (ADC(2)). Die untersuchten Moleküle umfassen Adenosin, ein Baustein der Nukleinsäuren, Urocansäure, ein UV-Filter in der Epidermis der menschlichen Haut, Kynurenin, ein UV-Filter in der menschlichen Augenlinse, Oligomere von 5,6-Dihydroxyindol, welche als Bausteine des menschlichen Hautpigments Eumelanin auftreten, und Glucose, ein archetypisches Kohlenhydrat. Unsere Untersuchungen zielten auf die Identifikation der photochemischen Mechanismen, die für die strahlungslose Deaktivierung von elektronisch angeregten Zuständen und für die außergewöhnlich hohe Photostabilität der untersuchten Moleküle verantwortlich sind, ab. Unsere Studien eröffnen ein detailliertes Verständnis der photophysikalischen und photochemischen Eigenschaften dieser isolierten Biomoleküle ohne den störenden Einfluss der Umgebung. Auf der einen Seite wurden einige unserer Studien durch vorherige spektroskopische Beobachtungen motiviert, auf der anderen Seite könnten unsere Studien weitere spektroskopische Untersuchungen motivieren.

This doctoral thesis is a publication-based thesis. The work presented in this thesis has been published in international scientific journals, has been submitted for publication in an international scientific journal, or is in preparation for submission to an international scientific journal by the time of submission of this thesis. This thesis provides an introduction to the field of computational investigations into the photophysics and photochemistry of bioorganic molecules. A broad overview on the employed theoretical concepts and ab initio methodologies is given. A short summary of three published papers, one submitted manuscript, and one manuscript in preparation as well as a description of my contribution to each piece of work is given. A Discussion and Conclusions section integrates our work into the existing literature on each studied system and provides an outlook for future studies. Three published papers are found as attachments to this thesis. The submitted manuscript and the manuscript in preparation are not attachments to this thesis to avoid prior-to-publication issues, nevertheless, these two manuscripts will be made available to the reviewers of this thesis.

D.T., Garching b. München, February 2014

The presented work was performed from January 2010 to February 2014 in the Department of Chemistry of Technische Universität München under the supervision of Prof. Dr. Wolfgang Domcke.

Contents

Chapter 1

Introduction

Molecules with a closed valence shell possess a singlet electronic ground state. A number of photophysical processes can be induced when a molecule absorbs a photon. The valence electrons of small organic molecules typically absorb wavelengths in the ultraviolet part of the electromagnetic spectrum. When a photon interacts with the transition dipole moment of a molecule, the molecule can be excited to an electronically excited state. Following absorption of a photon, the molecule can deactivate back to the electronic ground state via radiative deactivation, that is, by emission of a photon, or by a radiationless transition, which is called internal conversion. Radiative deactivation processes between electronic states of like multiplicity are known as fluorescence. Alternatively, the molecule may populate a triplet state via a so-called intersystem-crossing process. In this case, it may again relax to the ground state via radiative deactivation. Radiative deactivation processes between states of unlike multiplicity are known as phosphorescence. Due to the weak spin-orbit interaction in molecules containing only first-row atoms, phosphorescence typically proceeds on a much longer timescale than fluorescence. All processes mentioned thus far—absorption, rearrangement of the electronic structure of the molecule, radiationless transitions between electronically excited states of like or unlike spin multiplicity, fluorescence, and phosphorescence—are known as photophysical processes. Jablonski diagrams have been of wide use in recent decades to describe such processes.[1,2]

Photochemical processes, on the other hand, are characterized by the formation of a different chemical species following light absorption. More precisely, the reactant, which is photoexcited, and the photoproduct, which is generated after the system has deactivated back to the electronic ground state, are not chemically identical in the case of a photochemical reaction. In many cases, photochemical reaction products are formed via nonadiabatic processes between adiabatic potential-energy surfaces in regions where the latter are very

close in energy.[1]

For many applications in chemistry, the Born–Oppenheimer adiabatic approximation, which separates the movement of the nuclei and the electrons, is a reasonable approximation to facilitate the description of the energetic landscape of a chemical reaction. The very notion of a potential-energy surface stems from this approximation.[3] When two Born–Oppenheimer potential-energy surfaces come close in energy, the assumption that forms the basis of the Born–Oppenheimer approximation—well-separated energy levels of the electronic states—becomes invalid. Therefore, in regions of energetically closely-spaced adiabatic potential-energy surfaces the nuclei can no longer be regarded as moving in the potential of a single electronic state. The coupling of adiabatic potential-energy surfaces is determined by the nonadiabatic coupling matrix.[1,4–11]

Radiationless deactivation processes, that is, processes that convert electronic energy into vibrational energy, such as internal conversion and intersystem crossing, have been rationalized by Jablonski diagrams in the past. However, Jablonski diagrams are not able to capture the dynamic nature of an internal-conversion process. Today, it is an established notion that ultrafast photochemical processes, including internal conversion, which proceed on a subpicosecond timescale, are mediated by crucial points on the excited-state potential-energy surfaces, so-called conical intersections.[1,5–11] Molecules undergoing excited-state deactivation can, in fact, undergo substantial geometrical change along the reaction path leading to the relevant conical intersection. In case the photochemical reaction regenerates the reactant, which is known as an aborted photochemical reaction, the net result is a radiationless excited-state deactivation process.[1,2,10–12]

Critical points for excited-state chemistry and photochemistry are conical intersections, that is, points of degeneracy of at least two potential-energy surfaces. These points are characterized by a complete breakdown of the Born–Oppenheimer approximation. The nonadiabatic coupling of the involved electronic states diverges at the point of conical intersection. Conical intersections between the first singlet excited-state potential-energy surface (S_1) and the electronic ground-state potential-energy surface (S_0) can be of comparable significance for excited-state reactions of closed-shell molecules as are transition states for ground-state reactions. Conical intersections mediate the internal conversion between states of like multiplicity. The determination of the energetic location and the optimization of the geometry of S_1/S_0 conical intersections is a crucial step in the analysis of a photochemical reaction.[1,5–12]

Another important step in the elucidation of photochemical reactions is the exploration of the energy profiles of the relevant excited-state potential-

energy surfaces from the Franck–Condon region of the initially populated excited state—vertically above the potential well of the ground-state potential-energy surface—to the relevant conical intersections. This is the photochemical reaction path. If this photochemical reaction path is barrierless, one can assume that the associated photochemical reaction process is efficient, that is, it is kinetically dominant. If, on the other hand, the reaction path involves sizable barriers and/or local minima, the associated conical intersection may not be of relevance. It is known that a large number of conical intersections can be located for each molecular system, but many of these are either too high in energy or are separated by too high barriers from the Franck–Condon region as to be of relevance.[10–12]

The description of the photophysics and photochemistry of molecules by computational means requires the use of methodologies that are able to describe electronically excited states. The results presented in this thesis have been obtained by using state-of-the-art *ab initio* quantum-chemical methods. These include wavefunction-based post-Hartree–Fock methods, namely, CASPT2//CASSCF, CC2, and ADC(2).[13–17] The use of such high-level computational methods imposes severe limitations on the applicable system size. The current practical limit for a feasible treatment of systems with the above-mentioned methods employing a basis set of double-zeta quality is about 400 electrons if geometry optimizations are required and about 1000 electrons if single-point energy evaluations suffice. Therefore, it is generally impossible to treat a biologically relevant molecular system in a realistic environment, for example, in a solvation shell or in a protein environment, with these quantum-chemical methodologies.

Photostable molecules are able to efficiently convert electronic energy into vibrational energy. By converting electronic energy into harmless vibrational energy of the electronic ground state on a femtosecond timescale—the typical timescale of a molecular vibrational period and thus of many elementary steps of chemical reactions—a photostable molecule is able to effectively quench the population of highly reactive electronically excited states before potentially destructive chemical reactions can proceed. This rapid dissipation of electronic energy after the population of an excited state prevents the molecule from undergoing chemical transformation in response to light absorption. Many molecules found in nature have been shown to possess an exceptionally high degree of photostability towards UV irradiation from the sun.[18]

The exploration of the relevant photochemical reaction mechanisms which provide biological molecules with a high degree of UV photostability has been a topic of active research in recent decades. The fruitful interplay between spectroscopy and computational chemistry has provided comprehensive insight

into the efficient excited-state deactivation mechanisms in organic molecules that are responsible for the photostability of UV filters and various classes of biomolecules.[18,19] The investigation of isolated nucleobases as well as nucleobase pairs has been a hot topic since the beginning of the millennium. It was found that isolated nucleobases can deactivate to the electronic ground state in an ultrafast manner via ring-puckering processes, which break the planar structure of aromatic rings. Nucleobase Watson–Crick pairs, which exhibit two or three interbase hydrogen bonds, possess an additional mechanism for excited-state deactivation,[20–24] which is driven by electronically excited states of charge-transfer character and proceeds via the forward-backward transfer of a proton.[25–29]

The radiationless deactivation mechanism via electron-driven proton transfer mediated by an excited singlet state of charge-transfer character was previously identified in a number of biomolecular systems. It has been shown to be one of the relevant deactivation mechanisms in nucleobase pairs found in the double helix of DNA,[27–29] and in peptides.[30–32] All in all, these findings as well as the results obtained within the present work suggest that excited-state deactivation via electron-driven proton transfer is a ubiquitous photoprotective mechanism in the building blocks of life as well as in various other biomolecular systems exhibiting intramolecular hydrogen bonds.[18,19]

Herein, explorations of the UV-absorption behavior and of photochemical reaction paths are presented. The photoabsorption step can be characterized by the calculation of the vertical excitation energies and the associated oscillator strengths of singlet excited states. The reactivity of the molecule in the electronically excited state can be elucidated by the computation of the energy profiles of the potential-energy surfaces of the relevant singlet excited states along selected reaction paths. These excited-state potential-energy surfaces govern the motion of the nuclei after photoexcitation. Insight into the topography of these singlet excited-state potential-energy surfaces, that is, into the location of local minima and saddle points as well as the slope of these surfaces, helps in understanding the photochemical reactivity and in identifying the possible photoproducts.[12]

Bioorganic molecules constitute the foundation of life throughout all kingdoms of nature. They fulfill a multitude of biological functions and come in different sizes: from very small organic molecules like amino acids, carbohydrates, and oligopeptides to larger molecules such as vitamins, hormones, pheromones, neurotransmitters, and lipids. They can be distinguished from biopolymers such as proteins and polysaccharides by their molecular weight: typically, the weight of these small bioorganic molecules does not exceed 900 au.[33] The biomolecules considered in this thesis are found in nature and are exposed to

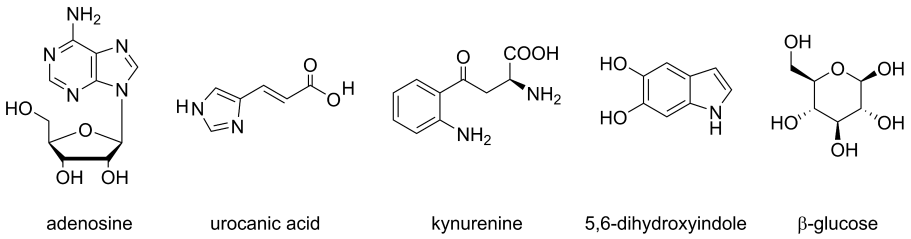

Figure 1: Structural formulas of the molecules considered in this thesis: adenosine, urocanic acid, kynurenine, 5,6-dihydroxyindole, and β-glucose.

the UV light emitted from the sun. Over the course of evolution, some of these biomolecules may have been incorporated into their biological environment because of their photoprotective capacity towards UV irradiation (for example, melanin, urocanic acid, and kynurenine), while others may have to persist in an environment where UV irradiation is present, although it is not the primary function of these molecules to act as UV filters *per se* (for example, nucleosides and glucose).

In the present context, organic molecules can be classified into three categories. Molecules whose function it is to absorb the UV light of the sun and thus prevent UV photodamage to surrounding molecular structures (which do not necessarily possess such photoprotective properties themselves), are known as UV filters. Examples of such molecules are melanin and kynurenine. Molecules which have a different primary function and have to persist in an environment where the occasional absorption of a UV photon cannot be prevented constitute the second category. Examples for these are nucleobases, nucleosides, nucleotides, peptides, proteins, and carbohydrates. The third category comprises molecules which actively use UV photons to undergo a designated photochemical change. Examples for this type are the retinal chromophore in rhodopsin—the photoisomerization of retinal initiates a reaction cascade that results in the visual process—and photolyases, which repair DNA photodamage by using the energy of absorbed UV photons. The molecules considered in this thesis cover the first two categories.

The five molecules that have been investigated as part of the doctoral work presented in this thesis are shown in Figure 1. These are adenosine, a building block of nucleic acids, urocanic acid, a UV filter found in the epidermis of human skin, kynurenine, a UV filter found in the human ocular lens, oligomers of 5,6-dihydroxyindole, the building blocks of eumelanin and thus the natural sunscreen and color pigment of human skin, and β-glucose, an archetypical carbohydrate.

Adenosine is a building block of nucleic acids and of the nucleotides adenosine monophosphate, adenosine diphosphosphate, and adenosine triphosphate,

which act as the molecular energy carriers in cells. While the past decade has seen an enormous amount of research directed at the understanding of the photophysical and photochemical properties of nucleobases and nucleobase pairs,[20–24] the investigation of nucleosides has not been pursued in the same vigorous manner. The first resonant two-photon ionization mass spectrum of a jet-cooled nucleoside was recorded in 2000.[34] Computational studies on nucleosides concerned with the possible conformations[35,36] and with vertical excitation energies were performed previously.[37,38] Only last year, a spectroscopic study revealed that isolated adenosine exhibits a significantly shorter excited-state lifetime than adenine.[39] This experimental finding indicates the existence of an efficient mechanism for excited-state deactivation in adenosine, that is not existent in adenine. This discovery motivated us to initiate a computational investigation into the photochemical deactivation mechanisms in adenosine which are introduced by the interplay of the nucleobase and the ribose moieties.

Urocanic acid is a chromophore found in the epidermis of human skin, where its E isomer is produced from the amino acid histidine. It acts as a UV filter and thus as a natural sunscreen in human skin. Upon UV absorption, it can undergo $E \rightarrow Z$ photoisomerization or radiationless deactivation without undergoing stereochemical transformation. The photoinduced formation of the Z isomer may have detrimental health effects, since (Z)-urocanic acid has been linked to photoimmunosuppression.[40–42] Urocanic acid has been the focus of research for about three decades and researchers of a number of disciplines such as photobiology, photochemistry, spectroscopy, immunology, and dermatology have been involved in these investigations. Many spectroscopic studies have been performed on urocanic acid in aqueous solution.[40–44] Computational studies have been performed on various aspects of the ground-state[45,46] and excited-state chemistry[47–51] of urocanic acid. While there have been many computational studies on this molecule, no study had so far been concerned with the photochemical reaction mechanisms responsible for the high photostability of this molecule. A peculiar experimental finding, the wavelength-dependent quantum yield for E/Z photoisomerization, has not been conclusively resolved. This motivated us to conduct a comprehensive study concerned with the photochemical mechanisms responsible for the UV-filtering capacity of this molecule.

Kynurenines are UV filters found in the human ocular lens, where they are produced from the amino acid tryptophan.[52] Their function is the absorption of UV radiation in the lens, such that only visible light is transmitted to the retina. The age-related decline in the concentration of kynurenines in the lens has been linked to age-related cataract formation.[53] These molecules have attracted the attention of researchers in the fields of photochemistry, pho-

tobiology, spectroscopy, ophthalmology, biochemistry, and organic chemistry. Numerous spectroscopic studies have been performed on kynurenines in aqueous solution.[54–58] Kynurenine has been found to be exceptionally photostable, which is apparent from its high quantum yield for internal conversion and its negligible quantum yields for intersystem crossing and for fluorescence.[57] Also, a few computational studies have been concerned with the vertical excitation energies and the simulation of the UV-absorption spectra in the gas phase and in solution.[56,58,59] However, a computational study aimed at the exploration of the photochemical mechanisms responsible for the exceptionally efficient UV-filtering capacity of these molecules had not been performed. This motivated us to initiate a comprehensive study employing both static explorations of the photochemical reaction paths for excited-state deactivation and nonadiabatic trajectory-surface-hopping molecular-dynamics simulations.

5,6-Dihydroxyindole is the simplest building block of eumelanin. Other building blocks are indole-2-carboxylic acid and 5,6-dihydroxyindole-2-carboxylic acid. Eumelanin is a biopolymer derived from the amino acid tyrosine which acts as a natural skin pigment and as a UV filter to protect the skin from excessive UV photodamage. It is also responsible for developing a sun tan. Though the elucidation of the structure of eumelanin is a complicated endeavor due to its complex composition and amorphous state, considerable progress has been made in recent years.[60–62] The main components of eumelanin are oligomers formed from the three aforementioned building blocks. It has been proposed that polymeric eumelanin consists of a complex structure, which exhibits three levels of aggregation: the first level is constructed by π-stacking of the oligomers, which forms protomolecular "discs"; the second level is constructed by edge-to-edge aggregation and renewed π-stacking of the discs formed in the first level; at the third level, the second-level structures again accumulate to construct large conglomerates of structures of sizes of up to 200 nm.[60] A number of spectroscopic studies has been performed on the monomeric building blocks in solution.[63–67] Also, computational studies have been concerned with the photophysics and the photochemistry of the monomeric building blocks.[63,66,68–70] A rather comprehensive computational study investigated the monomers, oligomers, and stacked species using semiempirical methods.[71–73] However, a systematic and comprehensive investigation into the effects of progressing oligomerization and of π-stacking using accurate *ab initio* methods has not been performed so far.

Glucose is an archetypical representative of the molecular class of carbohydrates. It is the monomeric building block of cellulose, which is the most abundant organic material found on earth.[74] Many computational and experimental studies of carbohydrates performed in the past have been concerned

with various properties as well as with the chemical reactivity in the electronic ground state.[75–77] Previously reported work on the identification of the most stable conformers of β-glucose was especially helpful as a starting point for our study.[78–85] However, no computational study concerning the UV-absorption behavior or the excited-state chemistry had been performed on any carbohydrate thus far. The occurrence of carbohydrates in many biomolecular systems, such as nucleic acids and glycoproteins, motivated us to investigate the photophysical and photochemical properties of this representative hexose carbohydrate.

We have performed investigations of these bioorganic molecules in their isolated and neutral form, that is, *in vacuo*, irrespective of the environment of these molecules in their natural function. This approach allows the use of accurate *ab initio* methods and provides insight into the intrinsic photophysical and photochemical properties of the molecule without the interference of perturbative effects originating from the environment, that is, solvation effects or the effects of a protein environment.[86] These environmental effects, in general, modify the intrinsic properties of the isolated molecule. An understanding of these intrinsic properties is a prerequesite for the investigation of the same molecular system in a more realistic environment, for example, embedded in a solvation shell or in a protein cavity (that is, *in aquo* or *in situ*). The computational treatment of these more extended systems, on the other hand, requires the use of different methodological approaches from the ones we have been using. Our results are also the basis for performing photoinduced nonadiabatic molecular-dynamics simulations aimed at unraveling the timescales and the statistical distributions of the photochemical processes in the studied systems.

The goal of the present work was the elucidation of photophysical properties and photochemical reaction mechanisms responsible for the absorption behavior, the high photostability, and the photochemical reactivity of the studied systems. The tackling of these flexible molecular systems is often complicated by the existence of a large number of tautomers, isomers, and conformers. Therefore, a careful selection of the relevant structures is a crucial step at the beginning of each study. Moreover, each system calls for a careful evaluation of the available computational methods in order to ascertain which method and level of theory offers a satisfying accuracy at a reasonable level of computational cost. Adenosine, urocanic acid, kynurenine, and 5,6-dihydroxyindole possess a chromophore moiety, which simplifies the computational treatment due to the existence of π orbitals. We were the first to perform *ab initio* calculations of the photophysics and photochemistry of a carbohydrate, glucose, and had no previous studies to guide us in this case. A considerable amount of time was spent on testing several levels of *ab initio* theory to ascertain which one is suitable for the description of this class of compounds. Another

difficulty that complicated the computational treatment of the five systems presented in this work was the absence of symmetry: adenosine, kynurenine, and glucose do not possess any molecular symmetry; urocanic acid and 5,6-dihydroxyindole possess C_s symmetry in their planar forms, which we had to abandon for the exploration of the largest number of the considered photochemical reaction pathways (in the case of urocanic acid) and for obtaining more realistic structures (in the case of oligomers of 5,6-dihydroxyindole).

The next chapter presents the theoretical concepts for the description of conical intersections as well as the available techniques for the optimization of conical intersections and for the exploration of photochemical reaction paths. Following this, a brief description of the employed *ab initio* methodologies, which have been used to obtain the results of this thesis, is given. In the third chapter, the three published papers, the submitted manuscript, and the manuscript in preparation, which constitute this thesis, are summarized and the individual contributions of the candidate are described. The last chapter summarizes the results for each of the studied molecules in the context of the existing literature and provides an outlook on future work.

Chapter 2

Theoretical Concepts and Computational Methods

The theoretical concepts of conical intersections and techniques for the optimization of conical intersections as well as for the exploration of photochemical reaction paths are described in this chapter. The computational methods that have been used for the investigation of the molecular systems comprising this thesis are nowadays well established and in wide use for various applications in computational chemistry. The following presentations of the computational methods focus on the general idea of each method, its strengths and weaknesses, and the benefits of using a particular method in the treatment of the excited-state chemistry of bioorganic molecules. Since the underlying theory is too lengthy and technical to be presented in a concise manner, the interested reader is referred to the original literature or available compendia on electronic-structure methods.[13,14,16]

2.1 Conical Intersections and Photochemical Reaction Paths

A conical intersection can be characterized by the geometry of the molecule and the topography of the two (or more) intersecting potential-energy surfaces. At a point of conical intersection, only two nuclear-displacement vectors of the molecular system can lift the degeneracy in first order, which are the branching-space vectors. The gradient-difference vector, $\mathbf{g}$, points in the direction of maximal splitting between the two potential-energy surfaces. The nonadiabatic-coupling vector, $\mathbf{h}$, points in the direction of maximal coupling of the two adiabatic electronic states. The analysis of these branching-space vectors helps in determining the chemical process that is mediated by a particular

conical intersection. The topography of the involved potential-energy surfaces in the branching space in close proximity to a conical intersection resembles the shape of a double cone. This double cone is obtained when the energies of the involved potential-energy surfaces are plotted against the nuclear displacements of the two branching-space vectors. The topography of the lower adiabatic potential-energy surface in close proximity to the conical intersection can provide insight into the relative yields of the photoproducts, which can be formed after passage through the conical intersection. The remaining $3N - 8$ molecular degrees of freedom form the so-called intersection seam, on which the degeneracy is retained along a hyperline.[1,7–11]

Several methods for the geometry optimization of conical intersections are available. Common to most of these methods is the doubly-constrained approach that minimizes the energy of the upper potential-energy surface while also minimizing the energy gap between the two intersecting potential-energy surfaces. The calculation of the gradients of the energy as well as the nonadiabatic couplings of the two intersecting potential-energy surfaces allows the computation of the branching-space vectors.[87–91] Furthermore, the calculation of a linear approximation of the energy of the intersecting potential-energy surfaces allows the determination of the topographical properties of a particular conical intersection.[92] A few years ago, a novel method for the optimization of minimum-energy conical intersections was put forward, which we have made extensive use of. This method allows the optimization of conical intersections without the need to evaluate nonadiabatic couplings and therefore allows the use of any electronic-structure method capable of describing electronically excited states, but for which analytical nonadiabatic couplings are not yet available.[93]

For the optimization of the geometry of conical intersections and for the calculation of the nuclear-displacement vectors of the branching-space vectors as well as the linear approximation of the energy of the intersecting potential-energy surfaces at the CASSCF level (*vide infra*) we have used the Columbus 7.0 program package.[94] In other cases, we have used the program CIOpt[93] coupled to the Turbomole 6.3.1 program package[95] to optimize the geometry of conical intersections at the mixed ADC(2)/MP2 level (*vide infra*).

The exploration of the reaction path from the Franck–Condon region to the relevant conical intersections is accomplished mainly via four techniques. The first technique is the rigid scan, where the internal coordinate identified as a suitable approximation for the exploration of the photochemical reaction is changed in increments, and single-point energy evaluations are performed along the obtained reaction path. The starting geometry used for this approach is usually chosen to be the ground-state equilibrium geometry or the optimized

geometry of a conical intersection. The second technique is the relaxed scan, where the molecular geometry is optimized for the relevant electronic state while keeping one internal coordinate fixed. This internal coordinate is usually chosen to approximate the desired reaction coordinate. The third technique is the linear interpolation in internal coordinates. Here, the internal coordinates of two molecular structures are used to interpolate molecular structures in between these two original structures. Usually, the two starting structures of choice are the ground-state equilibrium geometry and the optimized geometry of the conical intersection. The approximate reaction path is then obtained via single-point energy calculations along the interpolated path. The fourth method is the construction of the minimum-energy path. This technique uses the constrained optimization of the molecular geometry on a hypersphere, that is, the search for the optimal geometry is performed in the subspace of all molecular geometries found on the surface of a hypersphere of chosen radius. By proceeding along multiple steps of fixed radius, this procedure can find the minimum-energy path available on the potential-energy surface.[12,96]

2.2 *Ab Initio* Electronic-Structure Methods

2.2.1 CASSCF

The complete-active-space self-consistent-field (CASSCF) method is a multiconfigurational self-consistent-field (SCF) method. The wavefunction is expanded as a linear combination of configurations (that is, of the Hartree–Fock determinant and excited determinants). The configurations are usually chosen as configuration state functions, which are pure spin states. The orbital space of the system is partitioned into three subsets: the inactive occupied orbitals, the active orbitals (which contain occupied and unoccupied orbitals of the Hartree–Fock reference wavefunction), and the inactive unoccupied orbitals. Within the active space of molecular orbitals, a full-CI (full configuration interaction) calculation is performed. In contrast to the CI method, not only are the CI coefficients being optimized in the CASSCF procedure, but also the molecular orbitals. The choice of the active space depends on the chemical problem that one wants to study.[13,14,16] For the work of this thesis, the state-averaged CASSCF method was used, in which the average of the energy of several selected electronic states is minimized.[13–17,97–99]

The use of a multiconfigurational method like the CASSCF method is imperative for systems with a quasi-degenerate ground state and advantageous for treating electronically excited states, where a multitude of excited states can be close in energy. The drawback of the CASSCF method is the lack of

dynamic correlation: only a small portion of the correlation energy of the electrons is captured by the CASSCF method. The dynamic electron-correlation energy needs to be recovered by improving the CASSCF reference wavefunction using variational or perturbational methods. Among such methods are the multi-reference configuration-interaction (MRCI) treatment or second-order perturbation theory. One of the methods based on perturbation theory, the CASPT2 method, will be discussed in the subsequent section.[13–17,99]

Analytical energy gradients for the state-averaged CASSCF method have been available for a few decades. The geometries obtained by geometry optimization at the CASSCF level are usually of sufficient accuracy, while the accuracy of the energy is poor. The low computational cost and the reasonable accuracy of the optimized geometries is the reason for the widespread application of this method for the optimization of transition states, equilibrium geometries of electronically excited states, and conical intersections.[13,14,16,99]

For the calculations at the SA-CASSCF level we have used the program packages Columbus 7.0,[94] Molcas 7.6,[100] and Molpro 2006.1.[101]

2.2.2 CASPT2

In the ansatz of complete-active-space perturbation theory (CASPT) the zeroth-order wavefunction is a CASSCF wavefunction. Second-order perturbation theory based on a CASSCF reference wavefunction is known as CASPT2.[13,14,16,102] For the treatment of the systems presented in this thesis we have used both the single-state CASPT2[102,103] and the multi-state CASPT2[104] methods. In the latter method, the single-state CASPT2 energies are allowed to interact via an effective Hamiltonian. This procedure can remedy problems arising when the single-state CASPT2 approach is used in regions of energetically closely-spaced potential-energy surfaces.

A problem that often arises in the use of the CASPT2 method are so-called intruder states. These can occur when the perturbational energy correction leads to a substantial lowering of the energy of an electronic state that has not been captured by the CASSCF reference wavefunction. An *ad hoc* solution for this problem is the use of a level-shift, which adds a constant to the zeroth-order Hamiltonian. This can remove the intruder states in the energy range of interest, but also deteriorates the accuracy of the computed energies.[105,106]

CASPT2 has been of wide use for performing single-point energy evaluations for geometries optimized at the CASSCF level or for the computation of vertical excitation energies. The combination of CASSCF-optimized geometries with CASPT2-corrected energies is one of the most commonly used combinations of methods in the field of computational photochemistry. This combination is known as the CASPT2//CASSCF methodology.[13–17,99]

Geometry optimizations employing numerical CASPT2 gradients[107] for the systems considered in this thesis are possible, but too costly for routine application.

For the calculations at the CASPT2//CASSCF level we have used the program packages Molcas 7.6[100] for MS-CASPT2 calculations and Molpro 2006.1[101] for SS-CASPT2 calculations.

2.2.3 CC2

The CC2 (approximate second-order coupled cluster with singles and doubles) method is based on an approximation in the CCSD (coupled cluster with singles and doubles) model, which involves the simplification of the doubles equations by retaining only the terms correct through first order. The singles equations, which have a negligible effect on the energy, but are crucial for obtaining accurate molecular properties, are retained in their original form. This approximation reduces the scaling from N^6 for the CCSD method to N^5 for the CC2 method (N being the number of basis functions). The CC2 method yields an energy which is correct through second order (instead of an energy which is correct through third order as is the case for CCSD) and, therefore, an energy of similar accuracy as the MP2 method.[108–110]

The formalism employing a linear-response function, which does not require the explicit calculation of an excited-state wavefunction, makes CC2 an efficient method for the calculation of excitation energies, oscillator strengths, and various molecular properties. The linear-response function for CC2 is defined via a Jacobi matrix, whose eigenvalues provide the CC2 excitation energies.[108,109] The accuracy of excitation energies is comparable to the accuracy of the MP2 energy for the electronic ground state of closed-shell systems.[13,108–110]

Like all single-reference coupled-cluster methods, the CC2 method may break down in regions close to conical intersections. As a single-reference method, CC2 is also inappropriate for systems with an electronic ground state of multiconfigurational character. Moreover, since the double excitations are approximated in zeroth-order perturbation theory, CC2 is also inappropriate for excited states which are dominated by doubly excited configurations (this would require to use the much costlier CC3 method).[108–110]

The CC2 method provides reasonable results for the excited states of organic molecules.[110–112] Analytical gradients available at the CC2 level offer an efficient way to optimize the geometries of excited states.[109,110,113]

For the calculations at the CC2 level we have been using the program package Turbomole 6.3.1.[95]

2.2.4 ADC(2)

The algebraic-diagrammatic construction of second order, ADC(2), is a polarization-propagator scheme, and, as such, explicitly devised for the computation of excitation energies, oscillator strengths, and molecular properties. A second-order perturbation expansion is applied to a Hermitian secular matrix, which contains singly and doubly excited determinants of the Hartree–Fock reference wavefunction.[109,114,115] The ADC(2) method scales as N^5, as does CC2. The advantage of the ADC(2) method compared to the CC2 method is the fact that the excitation energies are obtained as the eigenvalues of a Hermitian secular matrix, whereas in the CC2 method the excitation energies are obtained as the eigenvalues of a non-Hermitian Jacobi matrix. This is the reason why CC2 often fails in the vicinity of conical intersections, while ADC(2) may perform well in such cases.[15,17,109]

The ADC(2) method provides a very efficient way to obtain excitation energies, oscillator strengths, and molecular properties of organic molecules of reasonable accuracy. While the standard deviation from experimentally determined values is a little larger than at the CC2 level, the ADC(2) method is more stable in near-degeneracy regions.[112] Analytical gradients available at the ADC(2) level offer an efficient way to optimize the geometries of excited states for larger molecules.[109]

For the calculations at the ADC(2) level we have been using the program package Turbomole 6.3.1.[95]

Chapter 3

Summaries of Publications and Manuscripts

In this chapter, the three published papers, the submitted manuscript, and the manuscript in preparation, which comprise the work of this thesis, are summarized. These five projects are presented in the order in which they were submitted for publication. The individual contributions of the candidate to each piece of work are described. The three published papers are attachments to this thesis. To avoid prior-to-publication issues, the submitted manuscript and the manuscript in preparation are not attachments to this thesis, but will be made available to the reviewers of this thesis.

3.1 Electronically Excited States and Photochemical Reaction Mechanisms of β-Glucose

Summary of "Electronically excited states and photochemical reaction mechanisms of β-glucose" by *Deniz Tuna, Andrzej L. Sobolewski, and Wolfgang Domcke*: *Phys. Chem. Chem. Phys.* **2014**, *16*, 38−47. (*Featured on the cover of issue 1.*)

The vertical excitation energies of one conformer of β-glucose (that is, β-D-glucopyranose) were computed with three *ab initio* methods. The UV-absorption spectrum was simulated and several types of photochemical reaction mechanisms were explored with *ab initio* methods. We found that low-lying singlet excited states are of $n\sigma^*$ nature and of partial Rydberg character. They originate from the excitation of an electron from lone-pair orbitals of the oxygen

atoms of OH groups to σ^* orbitals of O–H bonds. The simulated absorption spectrum shows a broad absorption in the UV-C region. We explored two types of photochemical reaction processes: hydrogen-detachment processes that are driven by O–H antibonding $n\sigma^*$ states and ring-opening processes driven by C–O or C–C antibonding $n\sigma^*$ states. We were able to fully characterize each of the five possible O–H hydrogen-detachment reaction paths including the optimization of the relevant S_1/S_0 conical intersections. We also explored a C–O ring-opening process and proved the existence of C–C ring-opening processes. Analyses of the topography of the potential-energy surfaces at the relevant conical intersections suggest that the probability of aborted photochemical reactions is higher than the probability of generation of photoproducts. Our results indicate that the O–H hydrogen-detachment processes rather than the C–O ring-opening processes dominate the photochemistry of glucose due to the involvement of the light hydrogen atom, although these processes are mediated by conical intersections of higher energy. We compared the O–H hydrogen-detachment processes driven by $n\sigma^*$ states in glucose to the well-known O–H and N–H hydrogen-detachment processes driven by $\pi\sigma^*$ states in several aromatic molecules. We also compared the photochemistry of glucose to the well-studied photochemistry of methanol—which can be regarded as a "methylene-hydrate" and, as such, as a building block of carbohydrates—and pointed out similarities. This is the first *ab initio* calculation dealing with the excited-state chemistry of a carbohydrate. Our predictions have yet to be confirmed by spectroscopic experiments.

Individual contributions of the candidate:

I explored the available options for the computation of vertical excitation energies and photochemical reaction processes of carbohydrates using several quantum-chemistry program packages. The methodologies and levels of theory were benchmarked to ascertain which kind of methodology is suitable for the description of the excited-state chemistry of carbohydrates and which level of theory is appropriate for balancing accuracy and efficiency. I thoroughly explored the current state of knowledge in the field of carbohydrate chemistry to select a suitable conformer and to integrate our publication into the various scientific communities of computational chemistry, spectroscopy, and carbohydrate chemistry. I co-designed and progressively extended the research of this project, performed all the calculations, analyzed and interpreted the data, and created the tables, graphs, and figures. I wrote and submitted the manuscript, replied to the reviewers' comments, and handled all correspondence with editors (as corresponding author).

3.2 Mechanisms of Ultrafast Excited-State Deactivation in Adenosine

Summary of "Mechanisms of Ultrafast Excited-State Deactivation in Adenosine" by *Deniz Tuna, Andrzej L. Sobolewski, and Wolfgang Domcke*: *J. Phys. Chem. A* **2014**, *118*, 122−127.

This investigation was motivated by the experimental finding that laser-desorbed samples of jet-cooled adenosine do not give a signal in the resonant two-photon ionization mass spectrum, in contrast to adenine. This hints at the existence of an ultrafast radiationless excited-state deactivation mechanism in adenosine that is not existent in adenine. We explored the electron-driven proton-transfer process for a *syn* conformer exhibiting a 5′-O–H···N3 intramolecular hydrogen bond and an *anti* conformer exhibiting a 2′-O–H···N3 intramolecular hydrogen bond. These processes are mediated by an excited singlet state of charge-transfer character, which involves a translocation of electron density from the ribose moiety to the adenine moiety. We found that this process should be able to compete with the well-known ring-puckering deactivation processes inherent to the adenine moiety on energetic grounds, since the relevant conical intersections are lower in energy than the ring-puckered conical intersections. We postulate that the lack of a barrier along the relevant photochemical reaction path as well as the involvement of the light hydrogen atom in the proton-transfer deactivation process (in contrast to the involvement of the heavier carbon atoms, nitrogen atoms, and amino groups in the ring-puckering deactivation processes of the adenine moiety) leads to a shorter timescale for this process, which can explain the non-existence of a resonant two-photon ionization signal in the mass spectrum. We propose an experimental test to confirm our predictions. Also, we suggest that this mechanism may have been of relevance in the chemical evolution of life when the first nucleosides emerged from simpler precursors.

Individual contributions of the candidate:

I tested several *ab initio* methods to ascertain which one was most suited for tackling this relatively large system, and decided on the ADC(2) method. I used a new approach and a new program to optimize the conical intersections of this system. I extended the original design of the research, performed all the calculations, analyzed and interpreted the data, proposed an experimental test to confirm our predictions by spectroscopic means, and created the graphs and figures. Finally, I wrote and submitted the manuscript, replied

to the reviewers' comments, and handled all correspondence with editors (as corresponding author).

3.3 Photochemical Mechanisms of Radiationless Deactivation Processes in Urocanic Acid

Summary of "Photochemical Mechanisms of Radiationless Deactivation Processes in Urocanic Acid" by *Deniz Tuna, Andrzej L. Sobolewski, and Wolfgang Domcke*: *J. Phys. Chem. B* **2014**, *118*, 976−985.

We considered two rotamers of each of the N3H and N1H tautomers of urocanic acid, as well as the isomers resulting from $E \rightarrow Z$ photoisomerization of these four initial isomers. We computed the vertical singlet excitation energies and the oscillator strengths of eight isomers at two levels of theory and performed a detailed analysis of the energy profiles of the relevant singlet excited-state potential-energy functions along the photoisomerization reaction path as well as along several reaction paths for excited-state deactivation. We identified a deactivation mechanism via electron-driven proton transfer, which is mediated by an excited singlet state of charge-transfer character in an intramolecularly hydrogen-bonded Z isomer, as well as two mechanisms inherent to the imidazole moiety: the N–H hydrogen-detachment process and the ring-puckering process. We optimized and analyzed the relevant S_1/S_0 and S_2/S_1 conical intersections for each of the considered photochemical processes. We characterized the branching-space vectors of all the optimized conical intersections and analyzed the topography of the potential-energy surfaces in close proximity to the S_1/S_0 conical intersection for the photoisomerization process of one isomer. This topography suggests that the progression of an aborted photochemical process and a successful photoisomerization process should be of equal probability. For the E/Z photoisomerization process we compare the energy profiles of the $\pi\pi^*$ state with the corresponding profile of the V state of ethylene. We offer a novel interpretation of previously obtained spectroscopic findings by pointing out the reversed order of the $n\pi^*$ and $\pi\pi^*$ excited singlet states in the N3H and N1H tautomers. This reversed order suggests that the N3H tautomers are responsible for the wavelength-dependent photoisomerization quantum yield, since the S_1 state of these tautomers is the $n\pi^*$ state, whose excitation allows the system to proceed only along the photoisomerization process. All other radiationless deactivation processes outlined in

this work become accessible with the excitation to the bright $\pi\pi^*$ state, which is the S_2 state in these tautomers. In the N1H tautomers, where the S_1 state is the $\pi\pi^*$ state, all processes compete from the onset of the absorption. This investigation provides novel insight into the photochemical mechanisms for radiationless excited-state deactivation in urocanic acid. Our results demonstrate the efficient UV-filtering capacity of urocanic acid.

Individual contributions of the candidate:

I carefully tested a number of parameters for the CASSCF method: the active space and the state-averaging had to be specifically designed for the computation of the vertical excitation energies, for the computation of the energy profiles of each of the studied photochemical processes, as well as for the optimization of the various conical intersections of each of the studied processes. Moreover, the performance of the SS- and the MS-CASPT2 methods had to be compared and, finally, the level-shift for the CASPT2 method had to be optimized. I designed most of the research, performed all the calculations, analyzed and interpreted the data, and created the tables, graphs, and figures. Finally, I wrote and submitted the manuscript, replied to the reviewers' comments and handled all correspondence with editors (as corresponding author).

3.4 How Kynurenines Protect the Retina from Sunburn: A Joint Electronic-Structure and Dynamics Study

Summary of "How Kynurenines Protect the Retina from Sunburn: A Joint Electronic-Structure and Dynamics Study" by *Deniz Tuna, Nađa Došlić, Momir Mališ, Andrzej L. Sobolewski, and Wolfgang Domcke*: *submitted*.

We considered two conformers of kynurenine and one conformer of 3-hydroxykynurenine O-β-D-glucoside. For kynurenine, we performed a joint study employing static explorations of photochemical reaction paths and nonadiabatic trajectory-surface-hopping molecular-dynamics simulations. We explored the photochemical reaction paths for radiationless excited-state deactivation via electron-driven proton-transfer processes, which are mediated by excited singlet states of charge-transfer character, and optimized the conical intersections for these processes at the ADC(2) level. The explorations of the excited-state reaction paths suggest that *cis* kynurenine, which exhibits an in-

tramolecular hydrogen bond between the ring-amino group and the keto group, can deactivate via ring-N–H···O=C proton transfer, while *trans* kynurenine, which exhibits an intramolecular hydrogen bond between the tail-amino group and the keto group, can deactivate via tail-N–H···O=C proton transfer. Additionally, we identified a number of ring-puckering deactivation mechanisms which are inherent to the phenyl moiety. For the nonadiabatic dynamics simulations, we propagated trajectories for the *cis* and *trans* conformers of kynurenine at the TDDFT level. These simulations suggest that kynurenine deactivates on a femtosecond-to-picosecond timescale via electron-driven proton transfer. While *cis* kynurenine indeed deactivates via ring-N–H···O=C proton transfer (as suggested by the explorations of the reaction paths), *trans* kynurenine tends to undergo *trans*→*cis* isomerization before also deactivating via ring-N–H···O=C proton transfer. Only a few trajectories for *trans* kynurenine deactivated via tail-N–H···O=C proton transfer or other proton-transfer processes. The dynamics simulations therefore suggest that the ring-N–H···O=C proton-transfer deactivation process is the dominant deactivation process in kynurenines, irrespective of the conformer. Additionally, we also explored a deactivation process for an intramolecularly hydrogen-bonded conformer of 3-hydroxykynurenine O-β-D-glucoside. Here, a proton transfer from an OH group of the glucose moiety to the ring-amino group of the aniline moiety can occur, namely, a 6′-O–H···N2 proton transfer. We compared our findings on kynurenine with the excited-state deactivation processes in peptides, and our findings on 3-hydroxykynurenine O-β-D-glucoside with the results from our previous studies of adenosine and glucose. We propose novel interpretations of previously obtained spectroscopic findings in light of the obtained results. This study provides a new level of mechanistic insight into the exceptionally efficient UV-filtering capacity of kynurenines.

Individual contributions of the candidate:

I tested the performance of the multiconfigurational CASPT2//CASSCF methodology against the CC2 and ADC(2) linear-response methods for the description of this rather large system and decided on the ADC(2) method for production runs. I carefully explored the available conformers of kynurenine and 3-hydroxykynurenine O-β-D-glucoside, and ascertained which conformers could be of relevance for excited-state deactivation processes. I designed the entire study and performed all static *ab initio* calculations for the computation of vertical excitation energies, the exploration of photochemical reaction paths, the optimization of conical intersections, and analyzed and interpreted these data. I co-designed the scope of the dynamics simulations together with our collaborator Nađa Došlić and coordinated regularly with her and Momir

Mališ, who performed the dynamics simulations, to ensure a seamless complementarity between the static explorations of reaction paths and the dynamics simulations. I created all graphs and figures for the electronic-structure part of the manuscript. Finally, I wrote the manuscript and submitted it (as corresponding author).

3.5 *Ab Initio* Study of the Photophysics of Eumelanin: Onset of the Electronic Absorption Spectra of Isolated and π-Stacked Oligomers of 5,6-Dihydroxyindole

Summary of "*Ab Initio* Study of the Photophysics of Eumelanin: Onset of the Electronic Absorption Spectra of Isolated and π-Stacked Oligomers of 5,6-Dihydroxyindole" by *Deniz Tuna, Anikó Udvarhelyi, Andrzej L. Sobolewski, Wolfgang Domcke, and Tatiana Domratcheva*: *in preparation.*

In this study, we investigated the effect of oligomerization of 5,6-dihydroxyindole and π-stacking of oligomers of 5,6-dihydroxyindole on the onset of the electronic absorption spectra. We selected a reasonable number of isomers for each degree of oligomerization, namely, of monomers, dimers, trimers, tetramers, and pentamers. Apart from these isolated oligomers, we also considered stacked monomers, stacked dimers, and stacked trimers, as well as triply-stacked monomers and triply-stacked dimers. We optimized the ground-state equilibrium geometries of these species at the MP2/cc-pVDZ level and calculated the vertical excitation energies and oscillator strengths of the two lowest excited singlet states at the CC2/cc-pVTZ level of theory (due to the significant computational cost of the calculations for the larger systems, we had to compromise on computing only the two lowest excited singlet states to be able to simulate the onset of the electronic absorption spectra). Our study provides novel insight into the photophysical properties of oligomers as well as π-stacked structures of 5,6-dihydroxyindole and reveals to which extent oligomerization and π-stacking result in a red-shift of the electronic absorption spectrum.

Individual contributions of the candidate:

I designed the research together with our collaborator Tatiana Domratcheva. I tested the basis-set dependence of the excitation energies at the CC2 level to

ascertain which basis-set size is necessary to balance accuracy and computational cost. I selected which oligomers to calculate and selected a reasonable number of isomers of each oligomer size. I performed the geometry optimizations and the computations of the CC2 vertical excitation energies, analyzed and interpreted the data, and created the graphs and figures. I wrote the manuscript as it is at the time of submission of this thesis.

Chapter 4

Discussion and Conclusions

The goal of this work is the exploration of the photophysical properties and the photochemical mechanisms of bioorganic molecules of physiological or biological significance using *ab initio* methods. For this, we have selected the following molecules: adenosine, a building block of nucleic acids, urocanic acid, a UV filter found in the epidermis of human skin, kynurenine, a UV filter found in the human ocular lens, oligomers of 5,6-dihydroxyindole, the building blocks of eumelanin and a color pigment of human skin, and β-glucose, an archetypical carbohydrate. These studies have been conducted together with a longtime collaborator of the research group of Wolfgang Domcke, Andrzej L. Sobolewski (Institute of Physics, Polish Academy of Sciences, Warsaw, Poland).

Our investigations of adenosine have provided an explanation of a recently published spectroscopic observation that suggests a significantly shorter excited-state lifetime for adenosine than for adenine.[39] We identified a mechanism in a 5′-O–H···N3 intramolecularly hydrogen-bonded *syn* and a 2′-O–H···N3 intramolecularly hydrogen-bonded *anti* conformer of adenosine for excited-state deactivation via electron-driven proton transfer which is mediated by an excited singlet state of charge-transfer character. The relevant conical intersection for this mechanism is lower in energy than the well-known C2- and C6-ring-puckered conical intersections inherent to the adenine moiety.[116–118] We optimized these conical intersections at the ADC(2) level. The photochemical reaction path connecting the Franck–Condon region with the relevant proton-transfer conical intersection was found to be barrierless. We suggest that the favorable energetics, the barrierless reaction path, and the involvement of the light hydrogen atom (in contrast to the displacements of the heavier carbon atoms, nitrogen atoms, and amino groups involved in the ring-puckering deactivation processes inherent to the adenine moiety) are responsible for the shorter excited-state lifetime of adenosine observed in the spectroscopic experiments. We have proposed an experimental test to confirm

our predictions, which involves the blocking of all OH groups in adenosine by alcohol-protecting groups and repeating the spectroscopic experiments. We suggest that the presented mechanism may have been of relevance in the chemical evolution of life when the first nucleosides emerged from simpler precursors.[119]

In the case of urocanic acid, we have provided a systematic analysis of the vertical excitation energies of eight rotamers and tautomers. We optimized the relevant S_1/S_0 and S_2/S_1 conical intersections involved in the various photochemical processes and identified a number of photochemical mechanisms for radiationless deactivation of photoexcited urocanic acid. Among these processes are the photoisomerization process, an electron-driven proton transfer for an intramolecularly hydrogen-bonded Z isomer, an N–H hydrogen-detachment process, as well as a ring-puckering process inherent to the imidazole moiety.[120] These findings suggest that urocanic acid possesses the intrinsic ability to act as a natural sunscreen, that is, a UV filter. We compared the topography of the potential-energy surface of the $\pi\pi^*$ state along the photoisomerization reaction coordinate with the topography of the potential-energy surface of the V state of ethylene.[121] We have also provided novel insight into the photoisomerization process of urocanic acid, which has been the subject of controversial debate,[40,43,44,47,51] and provided a new interpretation of previously obtained spectroscopic findings.[43,44,122] The photoinduced population of the $\pi\pi^*$ state of urocanic acid allows the system to access the entirety of the identified mechanisms for excited-state deactivation, all of which compete with the photoisomerization process. In the N3H tautomers, the $n\pi^*$ state is the S_1 state and the excitation to the $n\pi^*$ state via intensity-borrowing from the nearby $\pi\pi^*$ state allows the system to access only the photoisomerization process, since the other radiationless deactivation processes are not accessible. Only by exciting the $\pi\pi^*$ state, which is the S_2 state, do these processes become available in the N3H tautomers. In the N1H tautomers, on the other hand, the S_1 state is the $\pi\pi^*$ state and all radiationless deactivation processes, including the photoisomerization process, compete from the onset of the absorption. This suggests that the wavelength-dependent quantum yield for photoisomerization[40,43,44,122] is a property of the N3H tautomers in the gas phase. Due to the shift of the absorption energies in solution, this effect might not be the underlying cause for the wavelength-dependent photoisomerization quantum yield measured in solution.[40,43,44,122] We have significantly advanced the understanding of the photochemical properties and the available mechanisms for radiationless deactivation of this molecule, although there is more work to be done before a complete and conclusive understanding will have been gained. Nonadiabatic molecular-dynamics simulations and the computa-

tion of the vertical excitation energies including solvent effects are necessary steps to gain further insight into the wavelength-dependent photoisomerization quantum yield.[123]

For kynurenine, we explored the photochemical reaction paths for radiationless excited-state deactivation by *ab initio* electronic-structure calculations and by nonadiabatic trajectory-surface-hopping molecular-dynamics simulations. We have thus identified a number of photochemical mechanisms responsible for the highly efficient UV-filtering capacity of these molecules.[54–58] We explored two electron-driven proton-transfer processes from the two amino groups to the keto group which are mediated by excited states of charge-transfer character. The relevant excited-state potential-energy profiles are well below the vertical excitation energies of the lowest absorbing $\pi\pi^*$ state and exhibit negligible barriers. The ring-puckering process inherent to the phenyl moiety was shown to exhibit an apparent barrier similar to the analogous process in benzene and aniline.[124–127] We optimized the conical intersections for each of these deactivation processes. The mechanistic picture suggested by the static exploration of the energy profiles of the photochemical reaction paths was reinforced by nonadiabatic dynamics simulations of the *cis* and *trans* conformer, which were carried out by our collaborators Nađa Došlić and Momir Mališ (Division of Physical Chemistry, Ruđer Bošković Institute, Zagreb, Croatia). We found that kynurenine deactivates on a femtosecond-to-picosecond timescale mainly via proton-transfer processes from amino groups to the keto group. As suggested by the exploration of the excited-state reaction paths, radiationless deactivation in the *cis* conformer of kynurenine proceeds mainly via the ring-N–H$\cdots$O=C proton-transfer process, while the *trans* conformer tends to undergo *trans*$\rightarrow$*cis* isomerization before also deactivating via the ring-N–H$\cdots$O=C proton-transfer process. The remaining trajectories for *trans* kynurenine deactivated via tail-N–H$\cdots$O=C proton transfer and via ring-N–H$\cdots$O=COH proton transfer (that is, involving the terminal carboxylic group). The calculated S_1 lifetimes of 2.8 and 0.96 ps for the *cis* and *trans* conformers, respectively, are of the same order of magnitude as the two shortest time constants determined by transient-absorption experiments of kynurenine in aqueous solution.[57] The dynamics simulations have not provided any evidence that the ring-puckering processes inherent to the phenyl moiety are of relevance in kynurenine. For 3-hydroxykynurenine O-β-D-glucoside, which is the predominant form of kynurenine in the ocular lens, we explored a deactivation process via proton transfer from the 6′-OH group of the glucose moiety to the ring-amino group of the phenyl moiety (that is, a 6′-O–H$\cdots$N2 proton transfer). This mechanism is very similar to the mechanism that we have identified for adenosine.[119] These results provide a new level of mechanistic in-

sight into the photochemical processes responsible for the efficient UV-filtering capacity of kynurenines.[128]

For eumelanin, we investigated—in collaboration with Anikó Udvarhelyi and Tatiana Domratcheva (Department of Biomolecular Mechanisms, Max-Planck-Institut für Medizinische Forschung, Heidelberg, Germany)—the effect of oligomerization and of π-stacking of 5,6-dihydroxyindole, one of the monomeric building blocks of eumelanin, on the onset of the electronic absorption spectra. For this, we considered a reasonable number of isomers of the monomers, dimers, trimers, tetramers, and pentamers, as well as stacked monomers, stacked dimers, stacked trimers, triply-stacked monomers, and triply-stacked dimers of 5,6-dihydroxyindole. While similar studies were conducted previously using semiempirical methods,[71–73] we performed such calculations with accurate *ab initio* methods. The calculations suggest that π-stacking of oligomers of 5,6-dihydroxyindole has a more profound effect on the red-shift of the absorption profile than increasing oligomerization.[129]

In the case of glucose, we computed the vertical singlet excitation energies, simulated the UV-absorption spectrum, and identified several photochemical mechanisms that can mediate radiationless deactivation or lead to the formation of photoproducts. The low-lying excited states are $n\sigma^*$ states of partial Rydberg character. We have identified two generic types of reaction processes: O–H hydrogen-detachment processes and C–O as well as C–C ring-opening processes. We optimized the conical intersections related to these processes and analyzed the branching-space vectors. These processes can mediate excited-state deactivation via an aborted photochemical reaction. The topography of the intersecting potential-energy surfaces in close proximity to the conical intersections suggests that the probability for aborted photoreactions is higher than for the generation of photoproducts. We compared our findings with the well-known photochemistry of methanol,[130–133] which as a "methylene-hydrate" can be regarded as the simplest building block of carbohydrates. The potential-energy profiles of the $n\sigma^*$ states as well as the apparent significance of O–H hydrogen-detachment processes in glucose show similarities to the characteristics of previously studied $\pi\sigma^*$ states for O–H and N–H hydrogen-detachment processes in aromatic molecules.[133,134] We suggest that our findings on glucose may be generic for the entire class of carbohydrates. The identified properties could have been a decisive factor for the widespread incorporation of carbohydrates into biological matter. Our results should stimulate future studies of the properties and photochemical mechanisms of more complex carbohydrates, such as disaccharides (for example, sucrose and cellobiose) or polysaccharides (for example, cellulose).[135]

We have shown by the *ab initio* studies of five biomolecules *in vacuo*

that the investigation of isolated molecules can provide a detailed level of insight into the intrinsic photophysical and photochemical properties of these biomolecules. The results suggest future studies which should aim at two major goals. First, it is desirable to study the reaction dynamics of the photoexcited molecular systems by performing nonadiabatic molecular-dynamics simulations. While we have performed such simulations of the photoinduced nonadiabatic dynamics for kynurenine, this is a pending task for the remaining molecules considered in this thesis. Another direction is the theoretical description of the photochemistry of these molecules in their natural environment, that is, in aqueous solution or in protein cavities. For example, urocanic acid and kynurenine are not found as neutral molecules in their natural environment, but as anions or zwitterions.[40,55,136,137] These future *in aquo* or *in situ* studies should comprise the exploration of the vertical excitation energies and the energy profiles of the photochemical reaction paths, as well as nonadiabatic dynamics simulations of these more complete systems.

The results presented in this thesis demonstrate the fruitful interplay between spectroscopy and computational chemistry.[19] On the one hand, some of the computational studies have been motivated by unexpected or peculiar findings obtained with spectroscopic means. On the other hand, we have presented several cases where our computational investigations have provided a rationalization of an unexpected spectroscopic result (for example, in adenosine and urocanic acid). Spectroscopic data may confront computational photochemistry with intriguing challenges. No less so, the insights gained from computational photochemistry may motivate spectroscopic investigations, which would not have been performed otherwise.

Bibliography

[1] M. Klessinger, J. Michl: *Excited States and Photochemistry of Organic Molecules*. VCH Publishers, Inc., New York, **1995**.

[2] P. Klán, J. Wirz: *Photochemistry of Organic Compounds*. Wiley, Hoboken, **2009**.

[3] M. Born, R. Oppenheimer: Zur Quantentheorie der Molekeln. *Ann. Phys.* **1927**, *84*, 457–484.

[4] C. Zener: Non-Adiabatic Crossing of Energy Levels. *Proc. R. Soc. Lond. A* **1932**, *137*, 696–702.

[5] E. Teller: The Crossing of Potential Surfaces. *J. Phys. Chem.* **1937**, *41*, 109–116.

[6] G. Herzberg, H. C. Longuet-Higgins: Intersection of Potential Energy Surfaces in Polyatomic Molecules. *Discuss. Faraday Soc.* **1963**, *35*, 77–82.

[7] G. J. Atchity, S. S. Xantheas, K. Ruedenberg: Potential Energy Surfaces Near Intersections. *J. Chem. Phys.* **1991**, *95*, 1862–1876.

[8] F. Bernardi, M. Olivucci, M. A. Robb: Potential Energy Surface Crossings in Organic Photochemistry. *Chem. Soc. Rev.* **1996**, *25*, 321–328.

[9] D. R. Yarkony: Conical Intersections: The New Conventional Wisdom. *J. Phys. Chem. A* **2001**, *105*, 6277–6293.

[10] W. Domcke, D. R. Yarkony, H. Köppel (Eds.): *Conical Intersections: Electronic Structure, Dynamics & Spectroscopy*. World Scientific Publishing, Singapore, **2004**.

[11] W. Domcke, D. R. Yarkony, H. Köppel (Eds.): *Conical Intersections: Theory, Computation and Experiment*. World Scientific Publishing, Singapore, **2011**.

[12] M. Olivucci (Ed.): *Computational Photochemistry*. Elsevier, Amsterdam, **2005**.

[13] Y. Helgaker, P. Jørgensen, J. Olsen: *Molecular Electronic-Structure Theory*. Wiley, Hoboken, **2000**.

[14] C. J. Cramer: *Essentials of Computational Chemistry, Second Edition*. John Wiley & Sons, Ltd, Chichester, **2004**.

[15] L. Serrano-Andrés, M. Merchán: Quantum Chemistry of the Excited State: 2005 Overview. *J. Mol. Struct.: THEOCHEM* **2005**, *729*, 99–108.

[16] F. Jensen: *Introduction to Computational Chemistry, Second Edition*. John Wiley & Sons, Ltd, Chichester, **2007**.

[17] L. González, D. Escudero, L. Serrano-Andrés: Progress and Challenges in the Calculation of Electronic Excited States. *ChemPhysChem* **2012**, *13*, 28–51.

[18] A. L. Sobolewski, W. Domcke: The Chemical Physics of the Photostability of Life. *Europhys. News* **2006**, *37*, 20–23.

[19] W. Domcke, A. L. Sobolewski: Peptide Deactivation: Spectroscopy Meets Theory. *Nature Chem.* **2013**, *5*, 257–258.

[20] E. Nir, C. Plützer, K. Kleinermanns, M. de Vries: Properties of Isolated DNA Bases, Base Pairs and Nucleosides Examined by Laser Spectroscopy. *Eur. Phys. J. D* **2002**, *20*, 317–329.

[21] C. E. Crespo-Hernández, B. Cohen, P. M. Hare, B. Kohler: Ultrafast Excited-State Dynamics in Nucleic Acids. *Chem. Rev.* **2004**, *104*, 1977–2019.

[22] H. Saigusa: Excited-State Dynamics of Isolated Nucleic Acid Bases and Their Clusters. *J. Photochem. Photobiol. C* **2006**, *7*, 197–210.

[23] M. Shukla, J. Leszczynski (Eds.): *Radiation Induced Molecular Phenomena in Nucleic Acids*. Springer, New York, **2008**.

[24] K. Kleinermanns, D. Nachtigallová, M. S. de Vries: Excited State Dynamics of DNA Bases. *Int. Rev. Phys. Chem.* **2013**, *32*, 308–342.

[25] A. L. Sobolewski, W. Domcke: *Ab Initio* Study of the Excited-State Coupled Electron-Proton-Transfer Process in the 2-Aminopyridine Dimer. *Chem. Phys.* **2003**, *294*, 73–83.

[26] T. Schultz, E. Samoylova, W. Radloff, I. V. Hertel, A. L. Sobolewski, W. Domcke: Efficient Deactivation of a Model Base Pair via Excited-State Hydrogen Transfer. *Science* **2004**, *306*, 1765–1768.

[27] A. L. Sobolewski, W. Domcke: *Ab Initio* Studies on the Photophysics of the Guanine–Cytosine Base Pair. *Phys. Chem. Chem. Phys.* **2004**, *6*, 2763–2771.

[28] A. L. Sobolewski, W. Domcke, C. Hättig: Tautomeric Selectivity of the Excited-State Lifetime of Guanine/Cytosine Base Pairs: The Role of Electron-Driven Proton-Transfer Processes. *Proc. Natl. Acad. Sci. U.S.A.* **2005**, *102*, 17903–17906.

[29] S. Perun, A. L. Sobolewski, W. Domcke: Role of Electron-Driven Proton-Transfer Processes in the Excited-State Deactivation of the Adenine–Thymine Base Pair. *J. Phys. Chem. A* **2006**, *110*, 9031–9038.

[30] A. L. Sobolewski, W. Domcke: Relevance of Electron-Driven Proton-Transfer Processes for the Photostability of Proteins. *ChemPhysChem* **2006**, *7*, 561–564.

[31] D. Shemesh, C. Hättig, W. Domcke: Photophysics of the Trp-Gly Dipeptide: Role of Electron and Proton Transfer Processes for Efficient Excited-State Deactivation. *Chem. Phys. Lett.* **2009**, *482*, 38–43.

[32] D. Shemesh, A. L. Sobolewski, W. Domcke: Efficient Excited-State Deactivation of the Gly-Phe-Ala Tripeptide via an Electron-Driven Proton-Transfer Process. *J. Am. Chem. Soc.* **2009**, *131*, 1374–1375.

[33] D. Voet, J. G. Voet: *Biochemistry, Fourth Edition.* Wiley, Hoboken, **2011**.

[34] E. Nir, P. Imhof, K. Kleinermanns, M. de Vries: REMPI Spectroscopy of Laser Desorbed Guanosines. *J. Am. Chem. Soc.* **2000**, *122*, 8091–8092.

[35] A. Hocquet, N. Leulliot, M. Ghomi: Ground-State Properties of Nucleic Acid Constituents Studied by Density Functional Calculations. 3. Role of Sugar Puckering and Base Orientation on the Energetics and Geometry of 2′-Deoxyribonucleosides and Ribonucleosides. *J. Phys. Chem. B* **2000**, *104*, 4560–4568.

[36] M. C. Alvarez-Ros, A. Palafox: Molecular Structure of the Nucleoside Analogue Inosine using DFT Methods: Conformational Analysis, Crystal Simulations and Possible Behaviour. *J. Mol. Struct.* **2013**, *1047*, 358–371.

[37] R. So, S. Alavi: Vertical Excitation Energies for Ribose and Deoxyribose Nucleosides. *J. Comput. Chem.* **2007**, *28*, 1776–1782.

[38] R. Improta, V. Barone: The Excited States of Adenine and Thymine Nucleoside and Nucleotide in Aqueous Solution: A Comparative Study by Time-Dependent DFT Calculations. *Theor. Chem. Acc.* **2008**, *120*, 491–497.

[39] H. Asami, K. Yagi, M. Ohba, S. Urashima, H. Saigusa: Stacked Base-Pair Structures of Adenine Nucleosides Stabilized by the Formation of Hydrogen-Bonding Network Involving the Two Sugar Groups. *Chem. Phys.* **2013**, *419*, 84–89.

[40] T. Mohammad, H. Morrison, H. HogenEsch: Urocanic Acid Photochemistry and Photobiology. *Photochem. Photobiol.* **1999**, *69*, 115–135.

[41] J. D. Simon: Spectroscopic and Dynamic Studies of the Epidermal Chromophores *trans*-Urocanic Acid and Eumelanin. *Acc. Chem. Res.* **2000**, *33*, 307–313.

[42] N. K. Gibbs, J. Tye, M. Norval: Recent Advances in Urocanic Acid Photochemistry, Photobiology and Photoimmunology. *Photochem. Photobiol. Sci.* **2008**, *7*, 655–667.

[43] H. Morrison, C. Bernasconi, G. Pandey: A Wavelength Effect on Urocanic Acid E/Z Photoisomerization. *Photochem. Photobiol.* **1984**, *40*, 549–550.

[44] K. M. Hanson, J. D. Simon: The Origin of the Wavelength-Dependent Photoreactivity of *trans*-Urocanic Acid. *Photochem. Photobiol.* **1998**, *67*, 538–540.

[45] A. Lahti, M. Hotokka, K. Neuvonen, P. Äyräs: A Theoretical Study of the Conformers of *trans*- and *cis*-Urocanic Acid. *J. Mol. Struct.: THEOCHEM* **1995**, *331*, 169–179.

[46] J. Danielsson, J. A. Söderhall, A. Laaksonen: Hydration Structure and Conformational Dynamics of Urocanic Acid: A Computer Simulation Study. *Mol. Phys.* **2002**, *100*, 1873–1886.

[47] M. K. Shukla, P. C. Mishra: Electronic Spectra, Structure and Photoisomerization of Urocanic Acid. *Spectrochim. Acta* **1995**, *51A*, 831–838.

[48] C. S. Page, M. Merchán, L. Serrano-Andrés, M. Olivucci: A Theoretical Study of the Low-Lying Excited States of *trans*- and *cis*-Urocanic Acid. *J. Phys. Chem. A* **1999**, *103*, 9864–9871.

[49] J. Danielsson, J. Uličný, A. Laaksonen: A TD-DFT Study of the Photochemistry of Urocanic Acid in Biologically Relevant Ionic, Rotameric, and Protomeric Forms. *J. Am. Chem. Soc.* **2001**, *123*, 9817–9821.

[50] O. Dmitrenko, W. Reischl, R. D. Bach, J. Spanget-Larsen: TD-DFT Computational Insight into the Origin of Wavelength-Dependent E/Z Photoisomerization of Urocanic Acid. *J. Phys. Chem. A* **2004**, *108*, 5662–5669.

[51] M. Barbatti: The Role of Tautomers in the UV Absorption of Urocanic Acid. *Phys. Chem. Chem. Phys.* **2011**, *13*, 4686–4692.

[52] A. M. Wood, R. J. W. Truscott: UV Filters in Human Lenses: Tryptophan Catabolism. *Exp. Eye Res.* **1993**, *56*, 317–325.

[53] A. Korlimbinis, R. J. W. Truscott: Identification of 3-Hydroxykynurenine Bound to Proteins in the Human Lens. A Possible Role in Age-Related Nuclear Cataract. *Biochemistry* **2006**, *45*, 1950–1960.

[54] L. Kessel, S. Kalinin, R. H. Nagaraj, M. Larsen, L. B.-Å. Johansson: Time-Resolved and Steady-State Fluorescence Spectroscopic Studies of the Human Lens with Comparison to Argpyrimidine, Pentosidine and 3-OH-Kynurenine. *Photochem. Photobiol.* **2002**, *76*, 549–554.

[55] Y. P. Tsentalovich, O. A. Snytnikova, P. S. Sherin, M. D. E. Forbes: Photochemistry of Kynurenine, a Tryptophan Metabolite: Properties of the Triplet State. *J. Phys. Chem. A* **2005**, *109*, 3565–3568.

[56] L. Kessel, I. B. Nielsen, A. V. Bochenkova, K. B. Bravaya, L. H. Andersen: Gas-Phase Spectroscopy of Protonated 3-OH Kynurenine and Argpyrimidine. Comparison of Experimental Results to Theoretical Modeling. *J. Phys. Chem. A* **2007**, *111*, 10537–10543.

[57] P. S. Sherin, J. Grilj, Y. P. Tsentalovich, E. Vauthey: Ultrafast Excited-State Dynamics of Kynurenine, a UV Filter of the Human Eye. *J. Phys. Chem. B* **2009**, *113*, 4953–4962.

[58] Y. P. Tsentalovich, P. S. Sherin, L. V. Kopylova, I. V. Cherepanov, J. Grilj, E. Vauthey: Photochemical Properties of UV Filter Molecules of the Human Eye. *Invest. Ophthalmol. Visual Sci.* **2011**, *10*, 7687–7696.

[59] E. Benassi, P. S. Sherin: Theoretical Study of Solvent Influence on the Electronic Absorption and Emission Spectra of Kynurenine. *Int. J. Quant. Chem.* **2011**, *111*, 3799–3804.

[60] M. d'Ischia, A. Napolitano, A. Pezzella, P. Meredith, T. Sarna: Chemical and Structural Diversity in Eumelanins: Unexplored Bio-Optoelectronic Materials. *Angew. Chem. Int. Ed.* **2009**, *48*, 3914–3921.

[61] J. D. Simon, D. N. Peles: The Red and the Black. *Acc. Chem. Res.* **2010**, *43*, 1452–1460.

[62] A. Huijser, A. Pezzella, V. Sundström: Functionality of Epidermal Melanin Pigments: Current Knowledge on UV-Dissipative Mechanisms and Research Perspectives. *Phys. Chem. Chem. Phys.* **2011**, *13*, 9119–9127.

[63] S. Olsen, J. Riesz, I. Mahadevan, A. Coutts, J. P. Bothma, B. J. Powell, R. H. McKenzie, S. C. Smith, P. Meredith: Convergent Proton-Transfer Photocycles Violate Mirror-Image Symmetry in a Key Melanin Monomer. *J. Am. Chem. Soc.* **2007**, *129*, 6672–6673.

[64] M. Gauden, A. Pezzella, K. Panzella, M. T. Neves-Petersen, E. Skovsen, S. B. Petersen, K. M. Mullen, A. Napolitano, M. d'Ischia, V. Sundström: Role of Solvent, pH, and Molecular Size in Excited-State Deactivation of Key Eumelanin Building Blocks: Implications for Melanin Pigment Photostability. *J. Am. Chem. Soc.* **2008**, *130*, 17038–17043.

[65] D. N. Peles, E. Lin, K. Wakamatsu, S. Ito, J. D. Simon: Ultraviolet Absorption Coefficients of Melanosomes Containing Eumelanin As Related to the Relative Content of DHI and DHICA. *J. Phys. Chem. Lett.* **2010**, *1*, 2391–2395.

[66] A. Huijser, M. F. Rode, A. Corani, A. L. Sobolewski, V. Sundström: Photophysics of Indole-2-Carboxylic Acid in an Aqueous Environment Studied by Fluorescence Spectroscopy in Combination with *Ab Initio* Calculations. *Phys. Chem. Chem. Phys.* **2012**, *14*, 2078–2086.

[67] A. Corani, A. Pezzella, T. Pascher, T. Gustavsson, D. Markovitsi, A. Huijser, M. d'Ischia, V. Sundström: Excited-State Proton-Transfer Processes of DHICA Resolved: From Sub-Picoseconds to Nanoseconds. *J. Phys. Chem. Lett.* **2013**, *4*, 1383–1388.

[68] Y. V. Il'ichev, J. D. Simon: Building Blocks of Eumelanin: Relative Stability and Excitation Energies of Tautomers of 5,6-Dihydroxyindole and 5,6-Indolequinone. *J. Phys. Chem. B* **2003**, *107*, 7162–7171.

[69] E. Kaxiras, A. Tsolakidis, G. Zonios, S. Meng: Structural Model of Eumelanin. *Phys. Rev. Lett.* **2006**, *97*, 218102.

[70] A. L. Sobolewski, W. Domcke: Photophysics of Eumelanin: *Ab Initio* Studies on the Electronic Spectroscopy and Photochemistry of 5,6-Dihydroxyindole. *ChemPhysChem* **2007**, *8*, 756–762.

[71] K. B. Stark, J. M. Gallas, G. W. Zajac, M. Eisner, J. T. Golab: Spectroscopic Study and Simulation from Recent Structural Models for Eumelanin: I. Monomer, Dimers. *J. Phys. Chem. B* **2003**, *107*, 3061–3067.

[72] K. B. Stark, J. M. Gallas, G. W. Zajac, M. Eisner, J. T. Golab: Spectroscopic Study and Simulation from Recent Structural Models for Eumelanin: II. Oligomers. *J. Phys. Chem. B* **2003**, *107*, 11558–11562.

[73] K. B. Stark, J. M. Gallas, G. W. Zajac, J. T. Golab, S. Gidanian, T. McIntire, P. J. Farmer: Effect of Stacking and Redox State on Optical Absorption Spectra of Melanins – Comparison of Theoretical and Experimental Results. *J. Phys. Chem. B* **2005**, *109*, 1970–1977.

[74] R. V. Stick, S. J. Williams: *Carbohydrates. The Essential Molecules of Life.* Elsevier, Amsterdam, The Netherlands, 2nd edn., **2009**.

[75] A. Imberty, S. Péres: Structure, Conformation, and Dynamics of Bioactive Oligosaccharides: Theoretical Approaches and Experimental Validations. *Chem. Rev.* **2000**, *100*, 4567–4588.

[76] J. P. Simons, R. A. Jockusch, P. Çarçabal, I. Hünig, R. T. Kroemer, N. A. Macleod, L. C. Snoek: Sugars in the Gas Phase. Spectroscopy, Conformation, Hydration, Co-operativity and Selectivity. *Int. Rev. Phys. Chem.* **2005**, *24*, 489–531.

[77] C. O. da Silva: Carbohydrates and Quantum Chemistry: How Useful is This Combination? *Theor. Chem. Acc.* **2006**, *116*, 137–147.

[78] P. L. Polavarapu, C. S. Ewig: *Ab Initio* Computed Molecular Structures and Energies of the Conformers of Glucose. *J. Comput. Chem.* **1992**, *13*, 1255–1261.

[79] C. J. Cramer, D. G. Truhlar: Quantum Chemical Conformational Analysis of Glucose in Aqueous Solution. *J. Am. Chem. Soc.* **1993**, *115*, 5745–5753.

[80] G. I. Csonka, I. Kolossváry, P. Császár, K. Éliás, I. G. Csizmadia: The Conformational Space of Selected Aldo-Pyrano-Hexoses. *J. Mol. Struct.: THEOCHEM* **1997**, *395–396*, 29–40.

[81] B. Ma, H. F. Schaefer III, N. L. Allinger: Theoretical Studies of the Potential Energy Surfaces and Compositions of the D-Aldo- and D-Ketohexoses. *J. Am. Chem. Soc.* **1998**, *120*, 3411–3422.

[82] S. E. Barrows, J. W. Storer, C. J. Cramer, A. D. French, D. G. Truhlar: Factors Controlling Relative Stability of Anomers and Hydroxymethyl Conformers of Glucopyranose. *J. Comput. Chem.* **1998**, *19*, 1111–1129.

[83] M. Appell, G. Strati, J. L. Willet, F. A. Momany: B3LYP/6-311++G** Study of α- and β-D-Glucopyranose and 1,5-Anhydro-D-Glucitol: $^4C_1$ and $^1C_4$ Chairs, $^{3,O}B$ and $B_{3,O}$ Boats, and Skew-Boat Conformations. *Carbohydr. Res.* **2004**, *339*, 537–551.

[84] J. C. Corchado, M. L. Sánchez, M. A. Aguilar: Theoretical Study of the Relative Stability of Rotational Conformers of α and β-D-Glucopyranose in Gas Phase and Aqueous Solution. *J. Am. Chem. Soc.* **2004**, *126*, 7311–7319.

[85] N. Miura, T. Taniguchi, K. Monde, S.-I. Nishimura: A Theoretical Study of α- and β-D-Glucopyranose Conformations by the Density Functional Theory. *Chem. Phys. Lett.* **2006**, *419*, 326–332.

[86] R. Weinkauf, J.-P. Schermann, M. S. de Vries, K. Kleinermanns: Molecular Physics of Building Blocks of Life Under Isolated or Defined Conditions. *Eur. Phys. J. D* **2002**, *20*, 309–316.

[87] I. N. Ragazos, M. A. Robb, F. Bernardi, M. Olivucci: Optimization and Characterization of the Lowest Energy Point on a Conical Intersection Using an MC-SCF Lagrangian. *Chem. Phys. Lett.* **1992**, *197*, 217–223.

[88] M. R. Manaa, D. R. Yarkony: On the Intersection of Two Potential Energy Surfaces of the Same Symmetry. Systematic Characterization Using a Lagrange Multiplier Constrained Procedure. *J. Chem. Phys.* **1993**, *99*, 5251–5258.

[89] M. J. Bearpark, M. A. Robb, H. B. Schlegel: A Direct Method for the Location of the Lowest Energy Point on a Potential Surface Crossing. *Chem. Phys. Lett.* **1994**, *223*, 269–274.

[90] H. Lischka, M. Dallos, P. G. Szalay, D. R. Yarkony, R. Shepard: Analytic Evaluation of Nonadiabatic Coupling Terms at the MR-CI Level. I. Formalism. *J. Chem. Phys.* **2004**, *120*, 7322–7329.

[91] M. Dallos, H. Lischka, R. Shepard, D. R. Yarkony, P. G. Szalay: Analytic Evaluation of Nonadiabatic Coupling Terms at the MR-CI Level. II. Minima on the Crossing Seam: Formaldehyde and the Photodimerization of Ethylene. *J. Chem. Phys.* **2004**, *120*, 7330–7339.

[92] D. R. Yarkony: Nuclear Dynamics Near Conical Intersections in the Adiabatic Representation: I. The Effects of Local Topography on Interstate Transitions. *J. Chem. Phys.* **2001**, *114*, 2601–2613.

[93] B. G. Levine, J. D. Coe, T. J. Martínez: Optimizing Conical Intersections without Derivative Coupling Vectors: Application to Multistate Multireference Second-Order Perturbation Theory (MS-CASPT2). *J. Phys. Chem. B* **2008**, *112*, 405–413.

[94] H. Lischka, R. Shepard, I. Shavitt, R. M. Pitzer, M. Dallos, T. Müller, P. G. Szalay, F. B. Brown, R. Ahlrichs, H. J. Böhm, A. Chang, D. C. Comeau, R. Gdanitz, H. Dachsel, C. Ehrhardt, M. Ernzerhof, P. Höchtl, S. Irle, G. Kedziora, T. Kovar, V. Parasuk, M. J. M. Pepper, P. Scharf, H. Schiffer, M. Schindler, M. Schüler, M. Seth, E. A. Stahlberg, J.-G. Zhao, S. Yabushita, Z. Zhang, M. Barbatti, S. Matsika, M. Schuurmann, D. R. Yarkony, S. R. Brozell, E. V. Beck, J.-P. Blaudeau, M. Ruckenbauer, B. Sellner, F. Plasser, J. J. Szymczak: COLUMBUS, an *Ab Initio* Electronic Structure Program, Release 7.0. **2012**.

[95] TURBOMOLE V6.3.1 2011, a Development of University of Karlsruhe and Forschungszentrum Karlsruhe GmbH, 1989-2007, TURBOMOLE GmbH, since 2007: Available from http://www.turbomole.com.

[96] P. Celani, M. A. Robb, M. Garavelli, F. Bernardi, M. Olivucci: Geometry Optimisation on a Hypersphere. Application to Finding Reaction Paths from a Conical Intersection. *Chem. Phys. Lett.* **1995**, *243*, 1–8.

[97] P.-O. Löwdin: Quantum Theory of Many-Particle Systems. III. Extension of the Hartree-Fock Scheme to Include Degenerate Systems and Correlation Effects. *Phys. Rev.* **1955**, *97*, 1509–1520.

[98] H.-J. Werner, W. Meyer: A Quadratically Convergent MCSCF Method for the Simultaneous Optimization of Several States. *J. Chem. Phys.* **1981**, *74*, 5794–5801.

[99] D. Roca-Sanjuán, F. Aquilante, R. Lindh: Multiconfiguration Second-Order Perturbation Theory Approach to Strong Electron Correlation in Chemistry and Photochemistry. *WIREs Comput. Mol. Sci.* **2012**, *2*, 585–603.

[100] F. Aquilante, L. D. Vico, N. Ferré, G. Ghigo, P.-Å. Malmqvist, P. Neogrády, T. B. Pedersen, M. Pitonak, M. Reiher, B. O. Roos, L. Serrano-Andrés, M. Urban, V. Veryazov, R. Lindh: MOLCAS 7: The Next Generation. *J. Comput. Chem.* **2010**, *31*, 224–247.

[101] H.-J. Werner, P. J. Knowles, R. Lindh, F. R. Manby, M. Schütz, P. Celani, T. Korona, G. Rauhut, R. D. Amos, A. Bernhardsson, A. Berning, D. L. Cooper, M. J. O. Deegan, A. J. Dobbyn, F. Eckert, C. Hampel, G. Hetzer, A. W. Lloyd, S. J. McNicholas, W. Meyer, M. E. Mura, A. Nicklass, P. Palmieri, R. Pitzer, U. Schumann, H. Stoll, A. J. Stone, R. Tarroni, T. Thorsteinsson: MOLPRO, Version 2006.1, a Package of *Ab Initio* Programs. See http://www.molpro.net.

[102] K. Andersson, P.-Å. Malmqvist, B. O. Roos, A. J. Sadlej, K. Wolinski: Second-Order Perturbation Theory with a CASSCF Reference Function. *J. Phys. Chem.* **1990**, *94*, 5483–5488.

[103] K. Andersson, P.-Å. Malmqvist, B. O. Roos: Second-Order Perturbation Theory with a Complete Active Space Self-Consistent Field Reference Function. *J. Chem. Phys.* **1992**, *96*, 1218–1226.

[104] J. Finley, P.-Å. Malmqvist, B. O. Roos, L. Serrano-Andrés: The Multi-State CASPT2 Method. *Chem. Phys. Lett.* **1998**, *288*, 299–306.

[105] B. O. Roos, K. Andersson: Multiconfigurational Perturbation Theory with Level Shift – the Cr_2 Potential Revisited. *Chem. Phys. Lett.* **1995**, *245*, 215–223.

[106] B. O. Roos, K. Andersson, M. P. Fülscher, L. Serrano-Andrés, K. Pierloot, M. Merchán, V. Molina: Applications of Level Shift Corrected Perturbation Theory in Electronic Spectroscopy. *J. Mol. Struct.: THEOCHEM* **1996**, *388*, 257–276.

[107] C. S. Page, M. Olivucci: Ground and Excited State CASPT2 Geometry Optimizations of Small Organic Molecules. *J. Comput. Chem.* **2003**, *24*, 298–309.

[108] O. Christiansen, H. Koch, P. Jørgensen: The Second-Order Approximate Coupled Cluster Singles and Doubles Model CC2. *Chem. Phys. Lett.* **1995**, *243*, 409418.

[109] C. Hättig: Structure Optimizations for Excited States with Correlated Second-Order Methods: CC2 and ADC(2). *Adv. Quant. Chem.* **2005**, *50*, 37–60.

[110] K. Snekov, O. Christiansen: Excited State Coupled Cluster Methods. *WIREs Comput. Mol. Sci.* **2012**, *2*, 566–584.

[111] M. Schreiber, M. R. Silva-Junior, S. P. A. Sauer, W. Thiel: Benchmarks for Electronically Excited States: CASPT2, CC2, CCSD, and CC3. *J. Chem. Phys.* **2008**, *128*, 134110.

[112] N. O. C. Winter, N. K. Graf, S. Leutwyler, C. Hättig: Benchmarks for 0–0 Transitions of Aromatic Organic Molecules: DFT/B3LYP, ADC(2), CC2, SOS-CC2 and SCS-CC2 Compared to High-Resolution Gas-Phase Data. *Phys. Chem. Chem. Phys.* **2013**, *15*, 6623–6630.

[113] A. Köhn, C. Hättig: Analytic Gradients for Excited States in the Coupled-Cluster Model CC2 Employing the Resolution-of-the-Identity Approximation. *J. Chem. Phys.* **2003**, *119*, 5021–5036.

[114] J. Schirmer: Beyond the Random-Phase Approximation: A New Approximation Scheme for the Polarization Propagator. *Phys. Rev. A* **1982**, *26*, 2395–2416.

[115] A. B. Trofimov, J. Schirmer: An Efficient Polarization Propagator Approach to Valence Electron Excitation Spectra. *J. Phys. B* **1995**, *28*, 2299–2324.

[116] S. Perun, A. L. Sobolewski, W. Domcke: *Ab Initio* Studies on the Radiationless Decay Mechanisms of the Lowest Excited Singlet States of 9H-Adenine. *J. Am. Chem. Soc.* **2005**, *127*, 6257–6265.

[117] C. M. Marian: A New Pathway for the Rapid Decay of Electronically Excited Adenine. *J. Chem. Phys.* **2005**, *122*, 104314.

[118] M. Barbatti, Z. Lan, R. Crespo-Otero, J. J. Szymczak, H. Lischka, W. Thiel: Critical Appraisal of Excited State Nonadiabatic Dynamics Simulations of 9H-Adenine. *J. Chem. Phys.* **2012**, *137*, 22A503.

[119] D. Tuna, A. L. Sobolewski, W. Domcke: Mechanisms of Ultrafast Excited-State Deactivation in Adenosine. *J. Phys. Chem. A* **2014**, *118*, 122–127.

[120] M. Barbatti, H. Lischka, S. Salzmann, C. M. Marian: UV Excitation and Radiationless Deactivation of Imidazole. *J. Chem. Phys.* **2009**, *130*, 034305.

[121] B. Sellner, M. Barbatti, T. Müller, W. Domcke, H. Lischka: Ultrafast Non-Adiabatic Dynamics of Ethylene Including Rydberg States. *Mol. Phys.* **2013**, *111*, 2439–2450.

[122] K. M. Hanson, B. Li, J. D. Simon: A Spectroscopic Study of the Epidermal Ultraviolet Chromophore *trans*-Urocanic Acid. *J. Am. Chem. Soc.* **1997**, *119*, 2715–2721.

[123] D. Tuna, A. L. Sobolewski, W. Domcke: Photochemical Mechanisms of Radiationless Deactivation Processes in Urocanic Acid. *J. Phys. Chem. B* **2014**, *118*, 976–985.

[124] I. J. Palmer, I. N. Ragazos, F. Bernardi, M. Olivucci, M. A. Robb: An MC-SCF Study of the S_1 and S_2 Photochemical Reactions of Benzene. *J. Am. Chem. Soc.* **1993**, *115*, 673–682.

[125] A. L. Sobolewski, C. Woywod, W. Domcke: *Ab Initio* Investigation of Potential-Energy Surfaces Involved in the Photophysics of Benzene and Pyrazine. *J. Chem. Phys.* **1993**, *98*, 5627–5641.

[126] Q. Li, D. Mendive-Tapia, M. J. Paterson, A. Migani, M. J. Bearpark, M. A. Robb, L. Blancafort: A Global Picture of the S_1/S_0 Conical Intersection Seam of Benzene. *Chem. Phys.* **2010**, *377*, 60–65.

[127] G. M. Roberts, C. A. Williams, J. D. Yound, S. Ullrich, M. J. Paterson, V. G. Stavros: Unraveling Ultrafast Dynamics in Photoexcited Aniline. *J. Am. Chem. Soc.* **2012**, *134*, 12578–12589.

[128] D. Tuna, N. Došlić, M. Mališ, A. L. Sobolewski, W. Domcke: How Kynurenines Protect the Retina from Sunburn: A Joint Electronic-Structure and Dynamics Study. *Submitted.*

[129] D. Tuna, A. Udvarhelyi, A. L. Sobolewski, W. Domcke, T. Domratcheva: *Ab Initio* Study of the Photophysics of Eumelanin: Onset of the Electronic Absorption Spectra of Isolated and π-Stacked Oligomers of 5,6-Dihydroxyindole. *In Preparation.*

[130] R. J. Buenker, G. Olbrich, H.-P. Schuchmann, B. L. Schürmann, C. von Sonntag: Photolysis of Methanol at 185 nm. Quantum Mechanical Calculations and Product Study. *J. Am. Chem. Soc.* **1984**, *106*, 4362–4368.

[131] J. B. Nee, M. Suto, L. C. Lee: Photoexcitation Processes of CH_3OH: Rydberg States and Photofragment Fluorescence. *Chem. Phys.* **1985**, *98*, 147–155.

[132] S. Harich, J. J. Lin, Y. T. Lee, X. Yang: Photodissociation Dynamics of Methanol at 157 nm. *J. Phys. Chem. A* **1999**, *103*, 10324–10332.

[133] M. N. R. Ashfold, G. A. King, D. Murdock, M. G. D. Nix, T. A. A. Oliver, A. G. Sage: $\pi\sigma^*$ Excited States in Molecular Photochemistry. *Phys. Chem. Chem. Phys.* **2010**, *12*, 1218–1238.

[134] A. L. Sobolewski, W. Domcke, C. Dedonder-Lardeux, C. Jouvet: Excited-State Hydrogen Detachment and Hydrogen Transfer Driven by Repulsive $^1\pi\sigma^*$ States: A New Paradigm for Nonradiative Decay in Aromatic Biomolecules. *Phys. Chem. Chem. Phys.* **2002**, *4*, 1093–1100.

[135] D. Tuna, A. L. Sobolewski, W. Domcke: Electronically Excited States and Photochemical Reaction Mechanisms of β-Glucose. *Phys. Chem. Chem. Phys.* **2014**, *16*, 38–47.

[136] A. H. Mehler, H. Tabor: Deamination of Histidine to Form Urocanic Acid in Liver. *J. Biol. Chem.* **1953**, *201*, 775–784.

[137] A. Lahti, M. Hotokka, K. Neuvonen, P. Äyräs: Quantum-Chemical Gas-Phase Calculations on the Protonation Forms of *trans*- and *cis*-Urocanic Acid. *Struct. Chem.* **1997**, *8*, 331–342.

List of Publications

7 ***Ab Initio* Study of the Photophysics of Eumelanin: Onset of the Electronic Absorption Spectra of Isolated and π-Stacked Oligomers of 5,6-Dihydroxyindole.** Deniz Tuna, Anikó Udvarhelyi, Andrzej L. Sobolewski, Wolfgang Domcke, and Tatiana Domratcheva: *in preparation.*

6 **How Kynurenines Protect the Retina from Sunburn: A Joint Electronic-Structure and Dynamics Study.** Deniz Tuna, Nađa Došlić, Momir Mališ, Andrzej L. Sobolewski, and Wolfgang Domcke: *submitted.*

5 **Photochemical Mechanisms of Radiationless Deactivation Processes in Urocanic Acid.** Deniz Tuna, Andrzej L. Sobolewski, and Wolfgang Domcke: *J. Phys. Chem. B* **2014**, *118*, 976–985.

4 **Mechanisms of Ultrafast Excited-State Deactivation in Adenosine.** Deniz Tuna, Andrzej L. Sobolewski, and Wolfgang Domcke: *J. Phys. Chem. A* **2014**, *118*, 122–127.

3 **Electronically excited states and photochemical reaction mechanisms of β-glucose.** Deniz Tuna, Andrzej L. Sobolewski, and Wolfgang Domcke: *Phys. Chem. Chem. Phys.* **2014**, *16*, 38–47. *Featured on the cover of issue 1.*

2 **Photochemistry of 2-Aminooxazole, a Hypothetical Prebiotic Precursor of RNA Nucleotides.** Rafał Szabla, Deniz Tuna, Robert W. Góra, Jiří Šponer, Andrzej L. Sobolewski, and Wolfgang Domcke: *J. Phys. Chem. Lett.* **2013**, *4*, 2785–2788.

1 **Computational Study of the Mechanism of Cyclic Acetal Formation via the Iridium(I)-Catalyzed Double Hydroalkoxylation of 4-Pentyn-1-ol with Methanol.** Torstein Fjermestad, Joanne H. H. Ho, Stuart A. Macgregor, Barbara A. Messerle, and Deniz Tuna: *Organometallics* **2011**, *30*, 618–626.

Paper #1

Electronically excited states and photochemical reaction mechanisms of β-glucose. D. Tuna, A. L. Sobolewski, W. Domcke, *Phys. Chem. Chem. Phys.* **2014**, *16*, 38—47. — Reproduced by permission of the PCCP Owner Societies.

Volume 16 | Number 1 | 7 January 2014 | Pages 1–364

PCCP

Physical Chemistry Chemical Physics

www.rsc.org/pccp

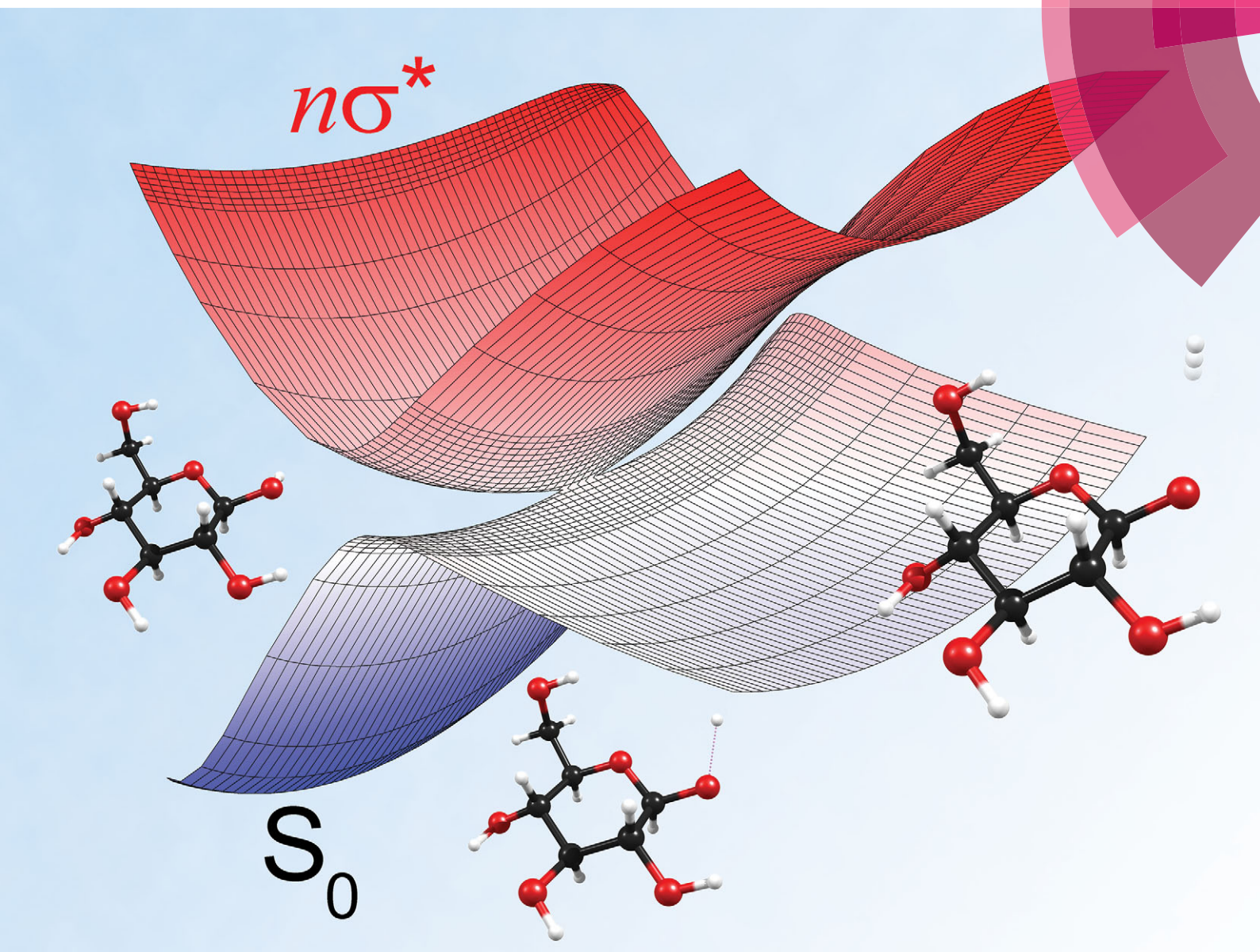

ISSN 1463-9076

ROYAL SOCIETY OF CHEMISTRY

PAPER

Deniz Tuna *et al.*

Electronically excited states and photochemical reaction mechanisms of β-glucose

PCCP

PAPER

View Article Online
View Journal | View Issue

Electronically excited states and photochemical reaction mechanisms of β-glucose†

Cite this: *Phys. Chem. Chem. Phys.*, 2014, **16**, 38

Deniz Tuna,*[a] Andrzej L. Sobolewski[b] and Wolfgang Domcke[a]

Carbohydrates are important molecular components of living matter. While spectroscopic and computational studies have been performed on carbohydrates in the electronic ground state, the lack of a chromophore complicates the elucidation of the excited-state properties and the photochemistry of this class of compounds. Herein, we report on the first computational investigation of the singlet photochemistry of β-glucose. It is shown that low-lying singlet excited states are of nσ* nature. Our computations of the singlet vertical excitation energies predict absorption from 6.0 eV onward. Owing to a dense manifold of weakly-absorbing states, a sizable and broad absorption in the ultraviolet-C range arises. We have explored two types of photochemical reaction mechanisms: hydrogen-detachment processes for each of the five O–H groups and a C–O ring-opening process. Both types of reactions are driven by repulsive nσ* states that are readily accessible from the Franck–Condon region and lead to conical intersections in a barrierless fashion. We have optimized the geometries of the conical intersections involved in these photochemical processes and found that these intersections are located around 5.0 eV for the O–H hydrogen-detachment reactions and around 4.0 eV for the C–O ring-opening reaction. The energies of all conical intersections are well below the computed absorption edge. The calculations were performed using linear-response methods for the computation of the vertical excitation energies and multiconfigurational methods for the optimization of conical intersections and the computation of energy profiles.

Received 6th June 2013,
Accepted 24th July 2013

DOI: 10.1039/c3cp52359d

www.rsc.org/pccp

1 Introduction

Glucose is a constituent of many forms of biological matter found in nature, for example, sucrose (table sugar), lactose (milk sugar), amylose (starch), and cellulose, the biopolymer found in the cell walls of green plants and the most abundant organic material on earth. Carbohydrates (also known as saccharides or sugars) fulfill a multitude of biological functions. They are part of nucleic acids (DNA and RNA), glycoproteins, proteoglycans, glycolipids, glycoside hydrolases, and glycosyltransferases.[1]

For decades, carbohydrates have been the focus of many experimental, spectroscopic, and computational investigations. Studies include the exploration of the conformational space and structural properties of mono-,[2–12] di-,[13–16] oligo-, and polysaccharides,[17–20] chemical reactions (condensation and isomerization,[21–26] hydrogen abstraction[27] and (photo-)fragmentation[28–31]) and the computation of vibrational spectra.[32–34] Progress has also been made in the computational simulation of the structure of biopolymers such as cellulose[35,36] as well as computations of their physical and chemical properties.[37–39]

Computational and experimental studies of carbohydrates were reviewed by Imberty and Péres.[40] A review on joint spectroscopic and computational studies of carbohydrates in the gas phase was given by Simons *et al.*,[41] and a review on the merits of using quantum chemistry to investigate various aspects of carbohydrate chemistry by da Silva.[42] Considerable efforts were put into the development and evaluation of suitable force-field,[43,44] semi-empirical,[45] and *ab initio* methods[46–48] for the study of carbohydrates.

Despite a number of computational studies published to date, we are not aware of any computational study on the

[a] *Department of Chemistry, Technische Universität München, 85747 Garching, Germany. E-mail: deniz.tuna@ch.tum.de; Fax: +49 8928913622; Tel: +49 8928913610*

[b] *Institute of Physics, Polish Academy of Sciences, 02668 Warsaw, Poland*

† Electronic supplementary information (ESI) available: Differences in the electron densities of the excited states and the ground state. Comparison of scans along the C1–C2 elongation and the C2–C1–O1 bending coordinate originating from the conical intersection for the O1–H hydrogen-detachment process shown in Fig. 3. Linearly interpolated reaction paths between the ground-state equilibrium geometry and the conical intersections for the remaining four O–H groups (O2–H, O3–H, O4–H, O6–H). Nuclear-displacement vectors of the branching-space vectors of the four remaining conical intersections. Linear approximation of the potential-energy surfaces of the ground state and the nσ* state in the branching space of the conical intersection for the C1–O5 ring-opening process shown in Fig. 7. Potential energies of the ground state and the nσ* state in the vicinity of a conical intersection along the C2–C3 ring-opening reaction coordinate. Cartesian coordinates of the ground-state equilibrium geometry and all conical intersections. See DOI: 10.1039/c3cp52359d

excited states and photochemical reaction mechanisms of carbohydrates. Herein, we report on results for the singlet vertical excitation energies, the absorption spectrum and photochemical reaction mechanisms of β-glucose (more precisely, β-D-glucopyranose), which we chose as a representative of this huge class of biomolecules. The present investigation is the first of its kind for a carbohydrate. Previous research on the possible conformations of β-glucose in the ground state[2–9] was helpful for the present work.

The study of the photochemical and photophysical properties of the "molecules of life"—bioorganic molecules that constitute living matter—has been a very active and fruitful field of research for more than a decade. The combination of gentle laser evaporation of biomolecules with sophisticated double-resonance spectroscopic techniques in supersonic jets or molecular traps allows highly precise spectroscopic investigations of biomolecules with aromatic chromophores, for example, the DNA bases and the aromatic amino acids.[49–52] The electronic and vibrational spectra can be assigned to specific conformers or tautomers of these flexible biomolecules by matching the experimental spectra to first-principles calculations.[52] Extensive spectroscopic and computational studies have been performed for the five nucleobases[53–57] and the nucleosides and nucleotides,[50,53,57] as well as hydrogen-bonded base pairs.[58,59] The determination of the conformational preferences of aromatic amino acids and of peptides with aromatic chromophores is of relevance for the understanding of protein folding.[60–62] While excited-state lifetimes of biomolecules or supramolecular complexes could be measured only in exceptional cases,[63] the excited-state lifetime is implicit in the observed spectra. A sufficiently long excited-state lifetime is required for the detection of resonant two-photon ionization or laser-induced fluorescence. The fact that the spectra of the energetically most stable conformers or tautomers are often not observed is a clear indication that ultrafast (sub-picosecond) radiationless excited-state deactivation processes prevail.[50–53,63] It has been argued that these ultrafast excited-state quenching processes provide biological matter with a particularly high degree of UV photostability.[52,53,64–66]

Carbohydrates, like non-aromatic amino acids, lack a chromophore and therefore do not exhibit sharp, intense and sparse UV spectra suitable for double-resonance spectroscopy. Simons and co-workers tagged carbohydrates with a phenyl chromophore, which allowed them to obtain structural information on monomeric and oligomeric carbohydrates in the gas phase.[10,14,41] Owing to their flexible nature and the lack of any symmetry, carbohydrates also are a challenge for computational investigations. For these reasons, very little is known on the mechanistic details of the photochemistry of even the simplest carbohydrates. In the present work, we aim at closing this gap of knowledge by computational investigations of the photochemistry of glucose.

It is a widely accepted paradigm that photochemical reactions are governed by critical points on the excited-state potential-energy surfaces, so-called conical intersections or photochemical funnels.[67,68] These photochemical funnels are believed to be of comparable significance for excited-state chemistry as are transition states for ground-state chemistry.[67,69] The unique features of conical intersections are a complete breakdown of the Born–Oppenheimer approximation and an exceptionally strong local anharmonicity of the potential-energy surfaces, which leads to a very efficient energy exchange between vibrational degrees of freedom.[68] The conical intersection can act as a funnel that directs the photochemical reaction to specific photoproducts.[70] The analysis of the topography of the lower adiabatic energy surface near a conical intersection can provide qualitative predictions of the relative yields of photoproducts. Photochemical reactions that are aborted at conical intersections of the S_1 and S_0 energy surfaces are a very efficient mechanism for ultrafast internal conversion, that is, recovery of the reactant after photoexcitation.[67–71] The quenching of deleterious photochemical reactions by ultrafast internal conversion is believed to be decisive for a high intrinsic photostability of DNA bases as well as amino acids and peptides with aromatic chromophores.[64–66]

2 Results

2.1 Vertical excitation energies and absorption spectra

We consider in the present work a conformer of β-D-glucopyranose (for simplicity called β-glucose in the following) that is, according to calculations,[2–9] one of the most stable conformers in the gas phase. This conformer is characterized by the following structural properties (*cf.* Fig. 3 for the numbering of atoms): (1) a $^4C_1$ chair conformation, that is, all OH groups and the CH_2OH group occupying an equatorial position; (2) a counterclockwise orientation of the four OH groups connected to carbon atoms C1 to C4; (3) a *gauche–gauche* orientation of the CH_2OH group with respect to the C4–C5 and C5–O5 bonds; and (4) a *syn*-orientation of the C6–OH group with respect to the C5–C6 bond.

While glucose can be found in numerous conformations regarding the torsion angles of the OH groups, the barriers for the conversion of the conformation described in the previous paragraph into rotamers range from around 9 to 20 kJ mol^{-1} (at the DFT level). For comparison, the harmonic vibrational frequencies of the OH torsional modes of this conformer are found in the range 400–600 cm^{-1} (4.8–7.2 kJ mol^{-1}). It is therefore reasonable to assume that the OH torsional angles can be considered as fixed for a given conformer. Herein, we investigate the photochemistry of the lowest-energy conformer with respect to the OH torsional angles.

According to the Franck–Condon principle, excitation of a molecule by absorption of a photon proceeds in a vertical manner, that is, without a change of the nuclear geometry during the electronic transition. The trajectory of nuclear motion on the excited-state potential-energy surface starts in the Franck–Condon region vertically above the minimum of the ground-state potential well. The calculation of the vertical electronic excitation energies of the ground-state equilibrium geometry is the starting point for the computational simulation of the absorption spectrum as well as the photochemical reaction dynamics.

To our knowledge, neither the vertical excitation energies nor the absorption spectra of any carbohydrate have been

calculated using *ab initio* methods so far. The most popular method for the computation of excitation energies of organic molecules is the time-dependent density functional theory (TDDFT) method. We compared the performance of this method with the CC2 method, which is an approximate second-order coupled cluster method (*cf.* Computational methods). The vertical excitation energies (*cf.* Table 1) predict the location of the lowest singlet excited state at 6.52 eV (CC2) or at 6.22 eV (TDDFT). Glucose thus absorbs only in the UV-C range of the electromagnetic spectrum. The oscillator strengths of all individual excitations are lower than 0.09 (*cf.* Fig. 2), which reflects the lack of a chromophore. Although the individual excitations possess only low oscillator strengths, the latter add up to a sizable magnitude: summation of the oscillator strengths for the first 50 excited states yields 0.4164 (CC2) or 0.3066 (TDDFT).

The dipole moment of the ground state is 3.42 D at the CC2 level. The dipole moments of the first 50 excited states range from as low as 0.94 to as high as 9.91 D.

Fig. 1 shows the self-consistent-field (SCF) orbitals at the HOMO–LUMO frontier. The HOMO − 1 and the HOMO are mainly lone-pair orbitals of the oxygen atoms O5 and O6 with some σ-bonding contributions. The LUMO and LUMO + 1 are σ* orbitals of partial Rydberg character of the O–H bonds connected to the carbon atoms C1 and to C2 and C3, respectively (*cf.* Fig. 3 for the numbering of atoms). These SCF orbitals look very similar to the Kohn–Sham orbitals used in the TDDFT computation. Basically, all low-lying excited states are generated by excitation of electrons from lone-pair orbitals of one or several oxygen atoms to diffuse antibonding σ* orbitals of one or several O–H or C–H bonds (the σ* orbitals of the O–H bonds are lower in energy than the σ* orbitals of the C–H bonds). Therefore, all these low-lying excited states can be classified as nσ* states of partial Rydberg character. This nσ* nature is further illustrated by the differences in the electron densities of the excited states and the ground state shown in Fig. S1 in the ESI.†

The absorption spectra computed at the CC2 and the TDDFT levels obtained by convolution of the stick spectra with Gaussian envelopes are shown in Fig. 2. Despite the low oscillator strengths of individual transitions, a sizable absorption occurs due to the high density of excited electronic states. The absorption edge is located around 6.1 eV (CC2) or 5.9 eV (TDDFT), a local peak is located around 7.8 eV (CC2) or 7.5 eV (TDDFT), and a shoulder is located near 7.0 eV (CC2) or 6.8 eV (TDDFT). The absorption profiles continue to increase toward higher energies. We cannot

Table 1 Singlet vertical excitation energies (in eV) and oscillator strengths (*f*) computed with the CC2 and TDDFT methods. The states are listed in ascending order of energy. (For details, consult the section Computational methods.)

State	CC2/eV	*f*	TDDFT/eV	*f*
2 ^{1}A	6.52	0.0087	6.22	0.0047
3 ^{1}A	6.88	0.0028	6.44	0.0035
4 ^{1}A	6.90	0.0151	6.58	0.0007
5 ^{1}A	7.04	0.0119	6.65	0.0124
6 ^{1}A	7.05	0.0094	6.70	0.0027
7 ^{1}A	7.18	0.0080	6.72	0.0089
8 ^{1}A	7.30	0.0344	6.77	0.0015

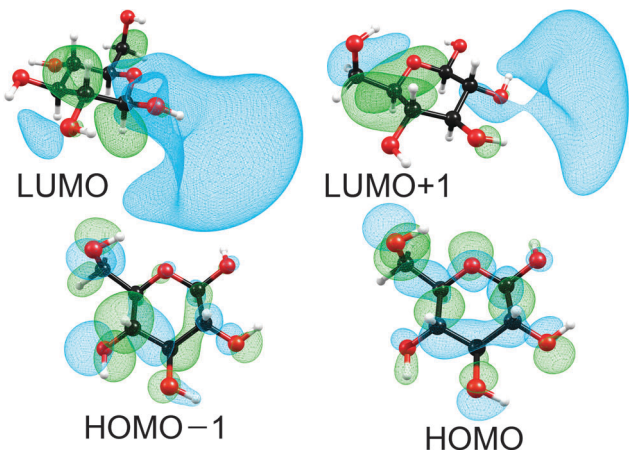

Fig. 1 Self-consistent-field orbitals at the HOMO–LUMO frontier. For the HOMOs an isosurface value of 0.03 was used, while for the LUMOs a value of 0.015 was used.

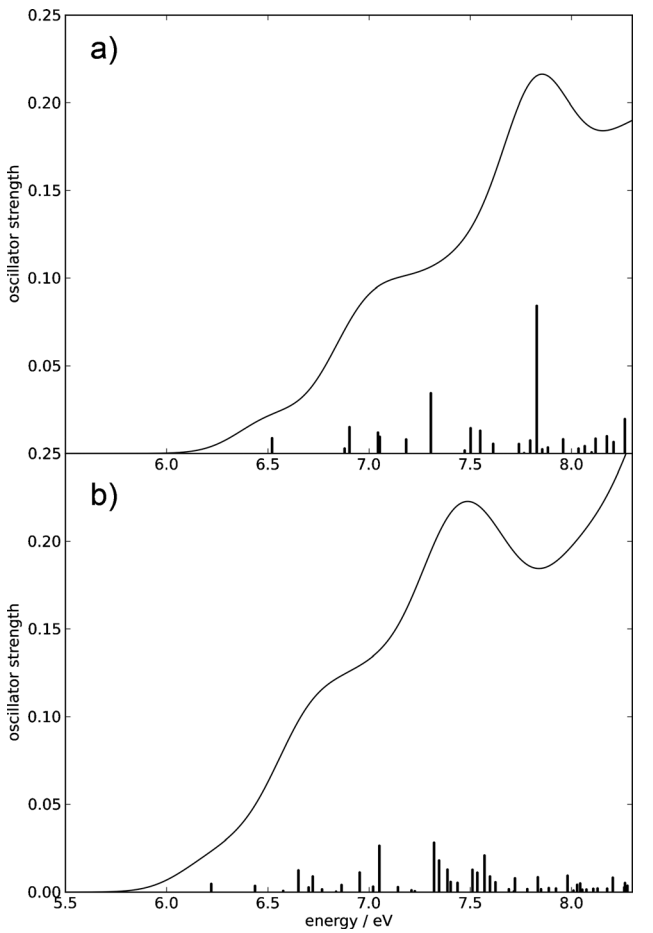

Fig. 2 Absorption spectra of β-glucose computed using the CC2 method (a) and the TDDFT method (b) up to 8.3 eV. The spectral envelopes were obtained by convolution of the stick spectra using Gaussian functions of 0.4 eV FWHM. (For details, consult the section Computational methods.)

compare our computed spectra to spectroscopic results, since we were unable to find an experimentally recorded gas-phase absorption spectrum of glucose.

2.2 Potential-energy surfaces and conical intersections: hydrogen-detachment reactions

The exploration of the lowest singlet excited-state potential-energy surface (S_1) from the Franck–Condon region to the conical intersection with the electronic ground state (S_0), at which the system can convert its excess electronic energy into vibrational energy and deactivate to the electronic ground state, is required for the understanding of the kinetic feasibility of a particular deactivation pathway. In order to describe a photochemical reaction one has to explore the reaction path from the Franck–Condon region to the relevant conical intersection connecting the excited state with the ground state.[72–75] This strategy was dubbed the "pathway approach" by Fuß *et al.*[76]

Fig. 3 shows the potential-energy profiles of the ground state and the nσ* excited state obtained for the linearly interpolated reaction path (*cf.* Computational methods) from the ground-state equilibrium geometry (full black circle at the lower left) to the conical intersection (full black and red circles on the right) for the hydrogen-detachment process of the O–H group located at the carbon atom C1. Clearly, the reaction path on the nσ* potential-energy surface is barrierless from the Franck–Condon region to the conical intersection. The conical intersection is located at around 5.0 eV, about 1.5 eV below the lowest vertical excitation energy.

As one can see from the molecular orbitals shown in the insets, the nσ* state corresponds to the excitation of an electron from the lone-pair orbital of the oxygen atom to the antibonding σ* orbital of the O–H bond. At short O–H distances, the σ* orbital exhibits a partial Rydberg character. As the distance between the two nuclei is increased, this orbital contracts and at longer distances collapses to the 1s orbital of the hydrogen atom.

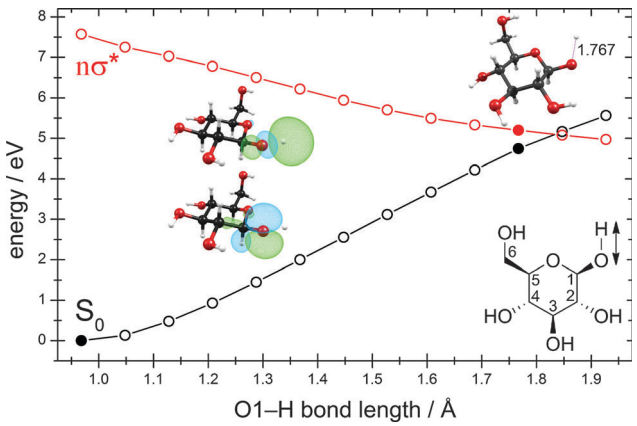

Fig. 3 Energy profiles of the ground state and the nσ* state along the stretching coordinate of the O–H group located at the carbon atom C1. The profiles were obtained by linear interpolation between the ground-state equilibrium geometry (full black circle at the lower left) and the conical intersection (full black and red circles at the right). The last two geometries were obtained by rigid scan originating from the conical intersection. The insets show the lone-pair orbital of the oxygen atom and the σ* orbital of the O–H bond. Also shown is the structure of the conical intersection with the value of the O–H internuclear distance and the structural formula with the numbering of the C atoms. (For details, consult the section Computational methods.)

At a point of degeneracy of two potential-energy surfaces of like multiplicity, that is, a point of conical intersection, only two nuclear degrees of freedom, the so-called branching-space vectors, are able to lift the degeneracy. The other $3N - 8$ degrees of freedom describe the motion of the system along the multi-dimensional intersection seam, along which degeneracy is preserved.[68] Fig. 4 shows the nuclear displacements of the orthogonalized branching-space vectors of the conical intersection shown in Fig. 3, namely, the gradient-difference vector ***g*** and the non-adiabatic-coupling vector ***h***. The gradient-difference vector ***g*** describes the molecular distortion of maximal splitting of the two intersecting potential-energy surfaces. The non-adiabatic-coupling vector ***h*** describes the molecular distortion that leads to the strongest non-adiabatic coupling between the two adiabatic electronic states.[68] Fig. 4 shows that the effective reaction coordinate depicted in Fig. 3, the elongation of the O–H bond length, corresponds to the nuclear displacements of the non-adiabatic-coupling vector ***h***. The gradient-difference vector ***g***, on the other hand, is a combination of bond-length and bond-angle alterations involving mainly the nuclei O1, C1 and C2 (*cf.* Fig. 3 for the numbering of atoms). The two most pronounced distortions are the C1–C2 elongation and the C2–C1–O1 bending.

A linear approximation of the potentials in the branching space,[77] that is, the shape of the intersecting potential-energy surfaces in close proximity to the conical intersection, is shown in Fig. 5. The slope of the ground-state potential-energy surface towards the negative direction of the ***h*** vector (which corresponds to the recombination of the hydrogen atom and the glucosyl radical and thus to an aborted photochemical reaction), is steeper than the slope towards the positive direction (which corresponds to the fragmentation yielding a glucosyl radical and a hydrogen atom). This topography classifies this conical intersection, according to Atchity *et al.*,[78] as a sloped one, that is, the gradient of the ground-state potential-energy surface towards the O–H recombination is steep, whereas towards the fragmentation products it is only weakly sloped. The topography of the conical intersection thus suggests that the probability of an aborted photoreaction regenerating the reactant could be substantial.

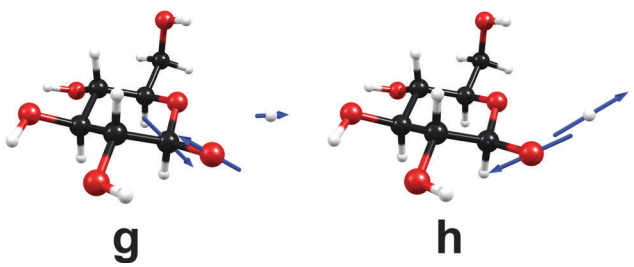

Fig. 4 Nuclear-displacement vectors of the gradient-difference vector ***g*** and the non-adiabatic-coupling vector ***h*** of the conical intersection shown in Fig. 3. (For details, consult the section Computational methods.)

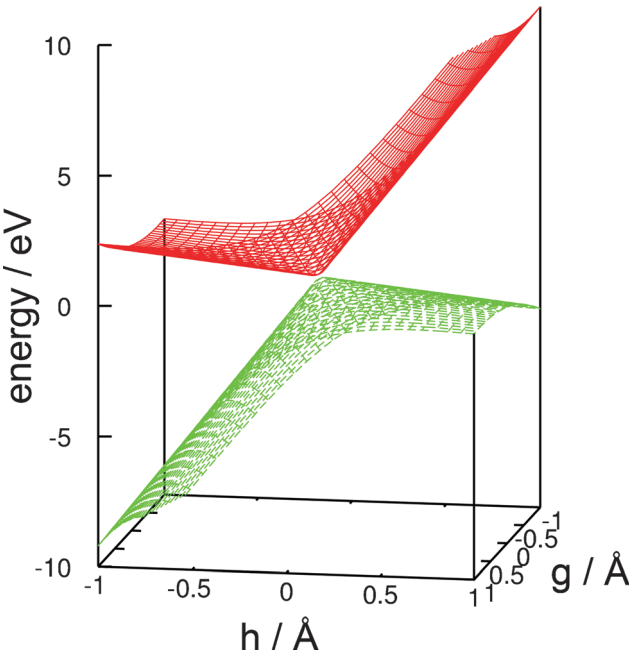

Fig. 5 Linear approximation of the potential-energy surfaces of the ground state and the nσ* state in the branching space of the conical intersection shown in Fig. 3. (For details, consult the section Computational methods.)

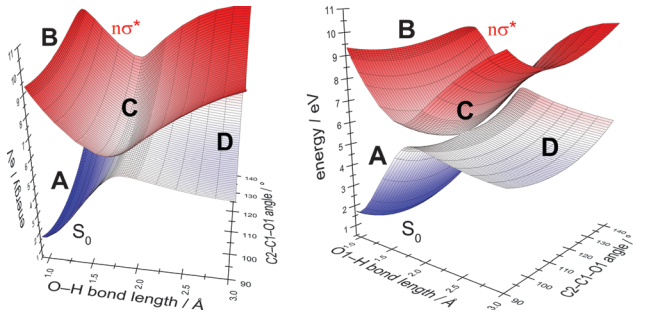

Fig. 6 Two-dimensional adiabatic potential-energy surfaces of the ground state and the nσ* excited state for the O1–H elongation and the C2–C1–O1 bending coordinate of the C1–OH group (shown from two perspectives). Four distinct regions of the energy surfaces are shown: the ground-state equilibrium geometry (A), the Franck–Condon region on the excited-state potential-energy surface (B), the conical intersection (C) and the photoproducts (D). In the case of an aborted photoreaction, the reactant (A) is regenerated after passage through the conical intersection.

In order to determine the most suitable second internal coordinate for a more extended two-dimensional scan of the potential-energy surfaces of the ground state and the nσ* state (the first coordinate is the O–H bond length), we computed the extent of the splitting of the energy between the intersecting states for several internal coordinates approximating the nuclear displacements of the gradient-difference vector ***g*** (*cf.* Fig. 4) of the conical intersection shown in Fig. 3. Fig. S2 in the ESI† shows the extent of the splitting of the energy of the ground-state and nσ* potential-energy surfaces near the point of conical intersection. The figure shows that the splitting of the energy along the C2–C1–O1 bending coordinate is more pronounced than the splitting along the C1–C2 elongation coordinate. We therefore chose the C2–C1–O1 bending coordinate as an approximation for the nuclear displacements of the gradient-difference vector ***g*** for the computation of the extended potential-energy surfaces shown in Fig. 6.

In Fig. 6, we highlight four distinct regions. The first region, (A), is the ground-state equilibrium region. The second region, (B), is the excited-state Franck–Condon region that the molecule is promoted to by absorption of a photon. The third region, (C), is the region of conical intersection between the potential-energy surfaces of the ground state and the nσ* state. As mentioned before, the system can move from the Franck–Condon region along the potential-energy surface of the nσ* state towards this conical intersection without having to overcome any barriers. At the conical intersection, (C), the photoreaction can proceed along at least two routes. One route is the regeneration of the reactant (A). In this case, the process is an aborted photochemical reaction and the outcome is radiationless deactivation of the excited state (also known as internal conversion). The other possible route is dissociation towards the photoproducts (region D), which correspond to a glucosyl radical and a hydrogen atom.

The reaction paths, conical intersections and branching-space vectors for the hydrogen-detachment reactions of the other four O–H groups of β-glucose are shown in Fig. S3–S7 in the ESI.†

2.3 Potential-energy surfaces and conical intersections: ring-opening reactions

We were able to optimize the conical intersection between the electronic ground state and the lowest nσ* state for the ring-opening reaction breaking the C1–O5 bond. Given the ground-state equilibrium geometry and the conical intersection, a linearly interpolated reaction path (*cf.* Computational methods) was constructed between these two structures. The resulting energy profiles are shown in Fig. 7. Interestingly, this conical intersection is located at around 4.0 eV with respect to the ground-state equilibrium geometry and is thus about 1.0 eV lower than the conical intersection for the hydrogen-detachment reactions of the O–H groups (*cf.* Fig. 3 and Fig. S3–S6 in the ESI†).

The nuclear-displacement vectors of the gradient-difference vector ***g*** and the non-adiabatic-coupling vector ***h*** of the conical intersection related to C1–O5 bond-breaking are shown in Fig. 8. In this case, the gradient-difference vector ***g*** is the effective reaction coordinate shown in Fig. 7, that is, the ring-opening/ring-closing motion. The non-adiabatic-coupling vector ***h*** is a combination of bending coordinates mainly involving the nuclei C5, C4 and C1.

The linear approximation of the potentials in the branching space in close proximity to the conical intersection is shown in Fig. S8 in the ESI.† Again, the ground-state potential-energy surface exhibits the steeper slope for the ring-closing reaction than for the direction leading to a biradical open-chain sugar, which classifies this conical intersection as a sloped one.[78] The topography of this conical intersection seems to favor the aborted photochemical reaction in which the reactant (the cyclic form of

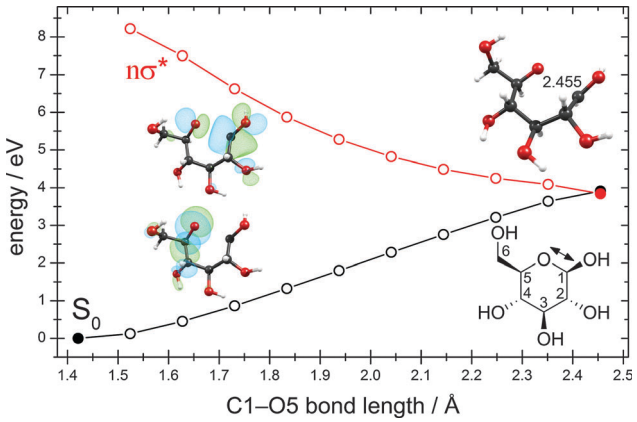

Fig. 7 Energy profiles of the ground state and the nσ* state along the C1–O5 ring-opening coordinate. The profiles were obtained by linear interpolation between the ground-state equilibrium geometry (full black circle at the lower left) and the optimized conical intersection (full black and red circles at the right). The insets show the lone-pair orbital of the oxygen atom and the σ* orbital of the C1–O5 bond. Also shown is the structure of the conical intersection with the value of the C1–O5 internuclear distance and the structural formula with the numbering of the C atoms. (For details, consult the section Computational methods.)

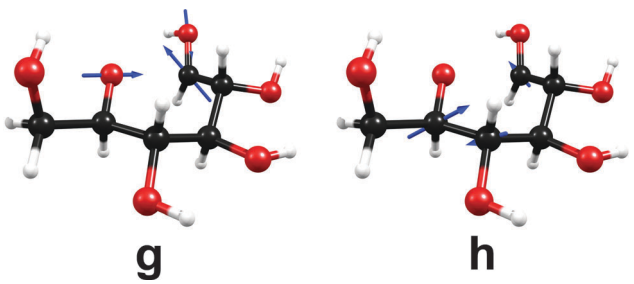

Fig. 8 Nuclear-displacement vectors of the gradient-difference vector ***g*** and the non-adiabatic-coupling vector ***h*** of the conical intersection shown in Fig. 7. (For details, consult the section Computational methods.)

β-glucose) is regenerated. The successful photoreaction yielding the biradical open-chain sugar appears less favorable due to the small gradient of the ground-state potential-energy surface in the direction leading to this photoproduct.

While the optimization of the conical intersection for the C1–O5 ring-opening process was unproblematic, this was not the case for the four possible C–C ring-opening reactions. We were unsuccessful in optimizing the conical intersection for any of these ring-opening processes. In principle, conical intersections should exist for these reactions. This is shown by Fig. S9 in the ESI.† In a series of calculations we were able to obtain two points of the reaction path for the C2–C3 ring-opening reaction, one with a C2–C3 distance of 2.49 Å, the other with a distance of 2.75 Å. Although the energies of the points are too high due to the use of geometries optimized for the ground state, this figure nevertheless reveals that between these two geometries a crossing of the energies of the ground state and the ring-opening nσ* state must exist. From this figure, the (non-optimized) energy of this conical intersection can be estimated to be about 6.0 eV.

3 Discussion and conclusions

We have performed the first detailed computational investigation of the singlet vertical excitation energies, the absorption spectrum and possible photochemical reaction pathways of β-glucose in the gas phase. We have shown that the lowest excited electronic states are of nσ* character, originating from excitation of lone-pair electrons of oxygen into O–H antibonding σ* orbitals of partial Rydberg character. The estimated absorption profile shows an onset at around 6.0 eV and a local peak near 7.5 or 7.8 eV. Although individual excitations exhibit only very low oscillator strengths, the sum of all oscillator strengths leads to a sizable absorption in the UV-C region.

Our results on photochemical pathways indicate that two generic types of reaction processes dominate the photochemistry of β-glucose: hydrogen-detachment processes, which have been known for many systems of aromatic and non-aromatic character, and ring-opening processes. Both are potential photochemical reactions (which means they may yield photoproducts, namely, a glucosyl radical and a hydrogen atom in the case of a hydrogen-detachment reaction, and a biradical open-chain sugar in the case of a ring-opening reaction), but are also potential radiationless deactivation channels regenerating the reactant. We have shown that the relevant conical intersections are readily accessible *via* barrierless reaction paths from the Franck–Condon region. The topography of the involved conical intersections indicates that the probability of aborted photoreactions could be higher than the probability of the generation of photoproducts. The conical intersections appear to be highly efficient channels for internal conversion. The one- and two-dimensional energy profiles of the ground-state and nσ* potential-energy surfaces for the hydrogen-detachment channels (*cf.* Fig. 3 and 6) show the typical behavior of an X–H detachment reaction (X being an oxygen, nitrogen or sulfur atom) as previously reported for the πσ* and nσ* states of phenol,[79–81] pyrrole[80–83] and several other aromatic and non-aromatic molecules.[80,81,83–85]

While the conical intersections for the hydrogen-detachment reactions are located around 5.0 eV (*cf.* Fig. 3 and Fig. S3–S6 in the ESI†), the conical intersection for the C–O ring-opening reaction is located near 4.0 eV (*cf.* Fig. 7). The energies of both types of conical intersections are well below the computed absorption edge of glucose and should thus be readily accessible for radiationless deactivation of electronically excited molecules. Although the conical intersection for the C–O ring-opening reaction is about 1.0 eV lower in energy than the conical intersections for the hydrogen-detachment processes, we expect the latter to prevail due to the faster motion of the light hydrogen atom. This hypothesis, however, can only be proven by photofragmentation spectroscopy[81,84,85] or by computational studies of the non-adiabatic nuclear-wavepacket or mixed quantum-classical surface-hopping dynamics.[63,79,86–94]

Although we were unable to optimize the conical intersections for the C–C ring-opening reactions, we can confirm based

on the results of test calculations that they exist and are located below 6.0 eV (*cf.* Fig. S9 in the ESI†). Our results indicate that the C–O ring-opening channel should be energetically favored compared to the C–C ring-opening channel.

While no photodissociation experiments have been performed on carbohydrates so far, numerous experiments have been performed on methanol. Methanol can be regarded as a "methylene-hydrate", and as such, as the simplest building block of carbohydrates. The absorption spectrum of methanol reveals the lowest-lying excited states to be of n → 3s and n → 3p Rydberg character.[95] We predict a UV absorption for glucose with an onset of around 200 nm which is also very similar to the UV absorption behavior of methanol.[95] It has been concluded that a transition to a state of valence nσ* character occurs upon elongation of the C–O or the O–H bonds of methanol.[81,96] A study of the photodissociation dynamics of methanol revealed that the hydrogen-detachment process occurs on a repulsive excited-state potential-energy surface[96] and exhibits a higher energy threshold than the C–O bond fission,[97] but is, nevertheless, the dominating channel due to the lower mass of the hydrogen atom.[96] For glucose, we have found that the conical intersections for the hydrogen-detachment reactions are located higher in energy than the intersections for the C–O ring-opening reaction, which seems to be analogous to the theoretical findings on methanol.[81] Nevertheless, it can be expected that the hydrogen-detachment reactions will dominate over the C–O ring-opening processes due to the lower mass of the hydrogen atom.

It is likely that other carbohydrates will exhibit the same photochemical reaction mechanisms that we have analyzed for glucose in this work. The hydrogen-detachment channels for O–H groups and the ring-opening channels for C–O and C–C ring-opening should be generic for the entire class of compounds.

The present study could be the starting point for further investigations of the excited-state chemistry of carbohydrates. It remains to be explored what kind of photophysical and photochemical properties of carbohydrates are the underlying cause for the diversity with which nature has incorporated this class of compounds into a multitude of molecular systems in the course of biological evolution. It also remains to be investigated how these photochemical reaction mechanisms of carbohydrates are modified when they are bound to typical chromophores, for example, in nucleosides and nucleotides. Furthermore, it is possible that the conversion of carbohydrates from cyclic forms, that is, hemiacetals or hemiketals, into open-chain forms, that is, hydroxy-aldehydes or hydroxy-ketons, could also be accomplished *via* a photochemical mechanism.

Another challenge is the understanding of the excited-state deactivation mechanisms in carbohydrate oligomers and polymers, for example, cellobiose (the glucose dimer) or cellulose (the glucose polymer). The vast number of hydrogen bonds in these structures may offer a multitude of radiationless deactivation channels *via* intramolecular proton-transfer reactions along hydrogen bonds.

4 Computational methods

The ground-state equilibrium geometry of the conformer of β-glucose described in Section 2.1 was optimized at the MP2 level (Møller–Plesset perturbation theory of second order) using the correlation-consistent split-valence polarized double-zeta basis set (cc-pVDZ)[98] and the resolution-of-the-identity (RI) approximation. The energy of the ground-state equilibrium geometry at the respective levels of theory served as the reference energy for the determination of vertical excitation energies and relative energies of potential-energy surfaces. The barriers for the conversion of the conformer into rotamers and the harmonic vibrational frequencies were determined at the DFT level using the hybrid functional B3LYP[99,100] and the basis sets cc-pVDZ and aug-cc-pVTZ,[98] respectively.

For the computation of vertical excitation energies and excited-state properties we used three linear-response methods: the CC2 (approximate second-order coupled cluster) method,[101] the ADC(2) (algebraic diagrammatic construction of second order) method,[102] and the LR-TDDFT (linear-response time-dependent density functional theory) method.[103] The RI approximation was employed in the CC2 and ADC(2) calculations.[104] For the TDDFT calculations we used the hybrid functional B3LYP.[99,100] For the calculation of vertical excitation energies we used the augmented cc-pVTZ basis set (aug-cc-pVTZ).[98] All of these calculations, as well as the MP2 geometry optimization mentioned in the previous paragraph, were carried out using the Turbomole 6.3.1 program package.[105]

Linear-response methods are particularly suitable for the computation of the absorption spectrum of carbohydrates due to the distribution of the oscillator strength over a dense manifold of excited states. When using standard linear-response methods, one has to pay attention to the limitations of single-configuration methods, that is, a potential multiconfigurational character of the ground state and the weight of doubly excited configurations. The D_1 diagnostic of 0.0464 at the CC2 level shows that the multiconfigurational character of the ground state is negligible.[106] The contributions of doubly excited configurations to the excited states range from 8.94 to 10.84% for the first 50 excited states at the CC2 level, which is also within the acceptable range. At the ADC(2) level, we obtained practically the same results for the excitation energies, oscillator strengths and convoluted spectrum as at the CC2 level.

For the geometry optimization of minimum-energy conical intersections (minima on the conical intersection seam), the calculation of the nuclear displacements of the orthogonalized branching-space vectors, and linear approximations of potentials in the branching space we used the state-averaged complete-active-space self-consistent-field wavefunction (SA-CASSCF) method with the cc-pVDZ[98] basis set. These calculations were carried out using Columbus 7.0.[107]

The reaction paths for hydrogen-detachment processes and for the ring-opening process were constructed by linear interpolation of internal coordinates between the initial geometry (the ground-state equilibrium geometry) and the final geometry (the respective optimized conical intersection). The energy profiles of the reaction paths were obtained by single-point energy calculations along the interpolated path, using single-state second-order perturbation theory on top of an SA-CASSCF wavefunction (SS-CASPT2//SA-CASSCF) with a level-shift of 0.2. The two-dimensional scan shown in Fig. 6 was obtained by a

rigid scan. For the computation of the hydrogen-detachment reaction paths we used a partially-augmented basis set that we denote as ''aug(2)-cc-pVDZ''. The cc-pVDZ basis was employed for all atoms except for the oxygen and hydrogen atoms of the O–H group involved in the hydrogen-detachment process (the ''2'' in aug(2)-cc-pVDZ indicates the use of the augmented basis on only two atoms of the molecule). The use of this partial augmentation helps to describe the short bond-length regions of the reaction paths (where Rydberg-valence mixing is important). The partial augmentation lowers the energy of the nσ* state belonging to the O–H group under investigation. The SS-CASPT2//SA-CASSCF single-point calculations were carried out using Molpro 2006.1.[108]

It is also possible to use an aug(1)-cc-pVDZ basis, that is, augmenting only the oxygen atom of the O–H group with diffuse basis functions. Test calculations showed that using diffuse basis functions on both the oxygen and the hydrogen atom leads to a better and smoother description of short bond-length regions of the potential-energy profiles of the nσ* states. For the computation of reaction paths of ring-opening processes we used the cc-pVDZ[98] basis for all atoms, since a partial augmentation is not helpful in this case.

For the computation of photochemical hydrogen-detachment and ring-opening energy profiles as well as for the optimization of conical intersections we used a compact active space of two electrons in two active orbitals. The averaging of the energy included only the electronic ground state and the nσ* state of interest. This recipe is denoted as SA2-CASSCF(2,2). We found that this (2,2) active space works well for a qualitative description of the reactions under investigation. The use of a larger active space (*e.g.*, four electrons in four orbitals) introduces active electrons and orbitals that barely contribute to the wavefunction of the lowest nσ* state.

Acknowledgements

D.T. is grateful for a PhD fellowship granted by the International Max Planck Research School of Advanced Photon Science (IMPRS-APS) and for support by the TUM Graduate School. This work was partially supported by a research grant of the Deutsche Forschungsgemeinschaft (DFG) and by the DFG Cluster of Excellence ''Munich-Centre for Advanced Photonics''.

References

1 R. V. Stick and S. J. Williams, *Carbohydrates. The Essential Molecules of Life*, Elsevier, Amsterdam, The Netherlands, 2nd edn, 2009.
2 P. L. Polavarapu and C. S. Ewig, *J. Comput. Chem.*, 1992, **13**, 1255–1261.
3 C. J. Cramer and D. G. Truhlar, *J. Am. Chem. Soc.*, 1993, **115**, 5745–5753.
4 G. I. Csonka, I. Kolossváry, P. Császár, K. Éliás and I. G. Csizmadia, *THEOCHEM*, 1997, **395–396**, 29–40.
5 B. Ma, H. F. Schaefer III and N. L. Allinger, *J. Am. Chem. Soc.*, 1998, **120**, 3411–3422.
6 S. E. Barrows, J. W. Storer, C. J. Cramer, A. D. French and D. G. Truhlar, *J. Comput. Chem.*, 1998, **19**, 1111–1129.
7 M. Appell, G. Strati, J. L. Willet and F. A. Momany, *Carbohydr. Res.*, 2004, **339**, 537–551.
8 J. C. Corchado, M. L. Sánchez and M. A. Aguilar, *J. Am. Chem. Soc.*, 2004, **126**, 7311–7319.
9 N. Miura, T. Taniguchi, K. Monde and S.-I. Nishimura, *Chem. Phys. Lett.*, 2006, **419**, 326–332.
10 P. Çarçabal, R. A. Jockusch, I. Hünig, L. C. Snoek, R. T. Kroemer, B. G. Davis, D. P. Gamblin, I. Compagnon, J. Oomens and J. P. Simons, *J. Am. Chem. Soc.*, 2005, **127**, 11414–11425.
11 A. F. Jalbout, L. Adamowicz and L. M. Ziurys, *Chem. Phys.*, 2006, **328**, 1–7.
12 E. J. Cocinero, A. Lesarri, P. Écija, F. J. Basterretxea, J.-U. Grabow, J. A. Fernández and F. Castaño, *Angew. Chem., Int. Ed.*, 2012, **51**, 3119–3124.
13 G. L. Strati, J. L. Willett and F. A. Momany, *Carbohydr. Res.*, 2002, **337**, 1833–1849.
14 E. J. Cocinero, D. P. Gamblin, B. G. Davis and J. P. Simons, *J. Am. Chem. Soc.*, 2009, **131**, 11117–11123.
15 F. A. Momany and U. Schnupf, *Carbohydr. Res.*, 2011, **346**, 619–630.
16 A. D. French, G. P. Johnson, C. J. Cramer and G. I. Csonka, *Carbohydr. Res.*, 2012, **350**, 68–76.
17 Y. Nishiyama, P. Langan and H. Chanzy, *J. Am. Chem. Soc.*, 2002, **124**, 9074–9082.
18 K. Mazeau and L. Heux, *J. Phys. Chem. B*, 2003, **107**, 2394–2403.
19 S. Queyroy, F. Müller-Plathe and D. Brown, *Macromol. Theory Simul.*, 2004, **13**, 427–440.
20 Y. Nishiyama, G. P. Johnson, A. D. French, V. T. Forsyth and P. Langan, *Biomacromolecules*, 2008, **9**, 3133–3140.
21 A. M. Silva, E. C. da Silva and C. O. da Silva, *Carbohydr. Res.*, 2006, **341**, 1029–1040.
22 D. Liu, M. R. Nimlos, D. K. Johnson, M. E. Himmel and X. Qian, *J. Phys. Chem. A*, 2010, **114**, 12936–12944.
23 X. Qian and X. Wei, *J. Phys. Chem. B*, 2012, **116**, 10898–10904.
24 G. Yang, E. A. Pidko and E. J. M. Hensen, *J. Catal.*, 2012, **295**, 122–132.
25 R. S. Assary and L. A. Curtiss, *Energy Fuels*, 2012, **26**, 1344–1352.
26 V. Seshadri and P. R. Westmoreland, *J. Phys. Chem. A*, 2012, **116**, 11997–12013.
27 N. Luo, A. Litvin and R. Osman, *J. Phys. Chem. A*, 1999, **103**, 592–600.
28 I. Baccarelli, F. A. Gianturco, A. Grandi, N. Sanna, R. R. Lucchese, I. Bald, J. Kopyra and E. Illenberger, *J. Am. Chem. Soc.*, 2007, **129**, 6269–6277.
29 G. Vall-Ilosera, M. A. Huels, M. Coreno, A. Kivimäki, K. Jakubowska, M. Stankiewicz and E. Rachlew, *ChemPhysChem*, 2008, **9**, 1020–1029.
30 J.-W. Shin, F. Dong, M. E. Grisham, J. J. Rocca and E. R. Bernstein, *Chem. Phys. Lett.*, 2011, **506**, 161–166.
31 D. Ghosh, A. Golan, L. K. Takahashi, A. I. Krylov and M. Ahmed, *J. Phys. Chem. Lett.*, 2012, **3**, 97–101.

32 W. B. Bosma, U. Schnupf, J. L. Willet and F. A. Momany, *THEOCHEM*, 2009, **905**, 59–69.
33 B. Brauer, M. Pincu, V. Buch, I. Bar, J. P. Simons and R. B. Gerber, *J. Phys. Chem. A*, 2011, **115**, 5859–5872.
34 L. Jin, J. P. Simons and R. B. Gerber, *J. Phys. Chem. A*, 2012, **116**, 11088–11094.
35 X. Qian, S.-Y. Ding, M. R. Nimlos, D. K. Johnson and M. E. Himmel, *Macromolecules*, 2005, **38**, 10580–10589.
36 Y. Li, M. Lin and J. W. Davenport, *J. Phys. Chem. C*, 2011, **115**, 11533–11539.
37 M. Bergenstråhle, L. A. Berglund and K. Mazeau, *J. Phys. Chem. B*, 2007, **111**, 9138–9145.
38 T. Shen, P. Langan, A. D. French, G. P. Johnson and S. Gnanakaran, *J. Am. Chem. Soc.*, 2009, **131**, 14786–14794.
39 S. Barsberg, *J. Phys. Chem. B*, 2010, **114**, 11703–11708.
40 A. Imberty and S. Péres, *Chem. Rev.*, 2000, **100**, 4567–4588.
41 J. P. Simons, R. A. Jockusch, P. Çarçabal, I. Hünig, R. T. Kroemer, N. A. Macleod and L. C. Snoek, *Int. Rev. Phys. Chem.*, 2005, **24**, 489–531.
42 C. O. da Silva, *Theor. Chem. Acc.*, 2006, **116**, 137–147.
43 S. Pérez, A. Imberty, S. B. Engelsen, J. Gruza, K. Mazeau, J. Jimenez-Barbero, A. Poveda, J.-F. Espinosa, B. P. van Eyck, G. Johnson, A. D. French, M. L. C. E. Kouwijzer, P. D. J. Grootenuis, A. Bernardi, L. Raimondi, H. Senderowitz, V. Durier, G. Vergoten and K. Rasmussen, *Carbohydr. Res.*, 1998, **314**, 141–155.
44 C. A. Stortz, G. P. Johnson, A. D. French and G. I. Csonka, *Carbohydr. Res.*, 2009, **344**, 2217–2228.
45 J. Y. Mane and M. Klobukowski, *Chem. Phys. Lett.*, 2010, **500**, 140–143.
46 J.-H. Lii, B. Ma and N. L. Allinger, *J. Comput. Chem.*, 1999, **20**, 1593–1603.
47 G. I. Csonka, A. D. French, G. P. Johnson and C. A. Stortz, *J. Chem. Theory Comput.*, 2009, **5**, 679–692.
48 W. M. C. Sameera and D. A. Pantazis, *J. Chem. Theory Comput.*, 2012, **8**, 2630–2645.
49 E. G. Robertson and J. P. Simons, *Phys. Chem. Chem. Phys.*, 2001, **3**, 1–18.
50 E. Nir, C. Plützer, K. Kleinermanns and M. de Vries, *Eur. Phys. J. D*, 2002, **20**, 317–329.
51 H. Saigusa, *J. Photochem. Photobiol., C*, 2006, **7**, 197–210.
52 M. S. de Vries and P. Hobza, *Annu. Rev. Phys. Chem.*, 2007, **58**, 585–612.
53 C. E. Crespo-Hernández, B. Cohen, P. M. Hare and B. Kohler, *Chem. Rev.*, 2004, **104**, 1977–2019.
54 S. Perun, A. L. Sobolewski and W. Domcke, *J. Am. Chem. Soc.*, 2005, **127**, 6257–6265.
55 L. Blancafort, *J. Am. Chem. Soc.*, 2006, **128**, 210–219.
56 L. Serrano-Andrés, M. Merchán and A. C. Borin, *J. Am. Chem. Soc.*, 2008, **130**, 2473–2484.
57 *Radiation Induced Molecular Phenomena in Nucleic Acids*, ed. M. Shukla and J. Leszczynski, Springer, New York, 2008.
58 A. Abo-Riziq, L. Grace, E. Nir, M. Kabelac, P. Hobza and M. S. de Vries, *Proc. Natl. Acad. Sci. U. S. A.*, 2005, **102**, 20–23.
59 A. L. Sobolewski and W. Domcke, *Phys. Chem. Chem. Phys.*, 2004, **6**, 2763–2771.
60 H. Valdes, V. Spiwok, J. Rezac, D. Reha, A. G. Abo-Riziq, M. S. de Vries and P. Hobza, *Chem.–Eur. J.*, 2008, **14**, 4886–4898.
61 D. Shemesh, A. L. Sobolewski and W. Domcke, *J. Am. Chem. Soc.*, 2009, **131**, 1374–1375.
62 E. Gloaguen, B. de Courcy, J.-P. Piquemal, J. Pilmé, O. Parisel, R. Pollet, H. S. Biswal, F. Piuzzi, B. Tardivel, M. Broquier and M. Mons, *J. Am. Chem. Soc.*, 2010, **132**, 11860–11863.
63 M. Mališ, Y. Loquais, E. Gloaguen, H. S. Biswal, F. Piuzzi, B. Tardivel, V. Brenner, M. Broquier, C. Jouvet, M. Mons, N. Došlić and I. Ljubić, *J. Am. Chem. Soc.*, 2012, **134**, 20340–20351.
64 A. L. Sobolewski and W. Domcke, *Europhys. News*, 2006, **37**, 20–23.
65 A. L. Sobolewski and W. Domcke, *Phys. Chem. Chem. Phys.*, 2010, **12**, 4897–4898.
66 W. Domcke and A. L. Sobolewski, *Nature Chem.*, 2013, **5**, 257–258.
67 M. Klessinger and J. Michl, *Excited States and Photochemistry of Organic Molecules*, VCH Publishers, New York, 1995.
68 *Conical Intersections: Electronic Structure, Dynamics & Spectroscopy*, ed. W. Domcke, D. R. Yarkony and H. Köppel, World Scientific Publishing, Toh Tuck Link, Singapore, 2004.
69 I. Schapiro, F. Melaccio, E. N. Laricheva and M. Olivucci, *Photochem. Photobiol. Sci.*, 2011, **10**, 867–886.
70 F. Bernardi, M. Olivucci and M. A. Robb, *Chem. Soc. Rev.*, 1996, **25**, 321–328.
71 T. J. Martínez, *Nature*, 2010, **467**, 412–413.
72 S. Kato, *J. Chem. Phys.*, 1988, **88**, 3045–3056.
73 A. L. Sobolewski, C. Woywod and W. Domcke, *J. Chem. Phys.*, 1993, **98**, 5627–5641.
74 I. J. Palmer, I. N. Ragazos, F. Bernardi, M. Olivucci and M. A. Robb, *J. Am. Chem. Soc.*, 1993, **115**, 673–682.
75 J. Dreyer and M. Klessinger, *J. Chem. Phys.*, 1994, **101**, 10655–10665.
76 W. Fuß, S. Lochbrunner, A. M. Müller, T. Schikarski, W. E. Schmid and S. A. Trushin, *Chem. Phys.*, 1998, **232**, 161–174.
77 D. R. Yarkony, *J. Chem. Phys.*, 2001, **114**, 2601–2613.
78 G. J. Atchity, S. S. Xantheas and K. Ruedenberg, *J. Chem. Phys.*, 1991, **95**, 1862–1876.
79 Z. Lan, W. Domcke, V. Vallet, A. L. Sobolewski and S. Mahapatra, *J. Chem. Phys.*, 2005, **122**, 224315.
80 A. L. Sobolewski, W. Domcke, C. Dedonder-Lardeux and C. Jouvet, *Phys. Chem. Chem. Phys.*, 2002, **4**, 1093–1100.
81 M. N. R. Ashfold, G. A. King, D. Murdock, M. G. D. Nix, T. A. A. Oliver and A. G. Sage, *Phys. Chem. Chem. Phys.*, 2010, **12**, 1218–1238.
82 V. Vallet, Z. Lan, S. Mahapatra, A. L. Sobolewski and W. Domcke, *J. Chem. Phys.*, 2005, **123**, 144307.
83 A. L. Sobolewski and W. Domcke, *Chem. Phys.*, 2000, **259**, 181–191.
84 T. A. A. Oliver, G. A. King and M. N. R. Ashfold, *Chem. Sci.*, 2010, **1**, 89–96.

85 T. A. A. Oliver, G. A. King and M. N. R. Ashfold, *J. Chem. Phys.*, 2010, **133**, 194303.
86 M. Barbatti and H. Lischka, *J. Am. Chem. Soc.*, 2008, **130**, 6831–6839.
87 G. Groenhof, L. V. Schäfer, M. Boggio-Pasqua, M. Goette, H. Grubmüller and M. A. Robb, *J. Am. Chem. Soc.*, 2007, **129**, 6812–6819.
88 G. Tomasello, M. Wohlgemuth, J. Petersen and R. Mitrić, *J. Phys. Chem. B*, 2012, **116**, 8762–8770.
89 T. S. Venkatesan, S. G. Ramesh, Z. Lan and W. Domcke, *J. Chem. Phys.*, 2012, **136**, 174312.
90 P. R. L. Markwick and N. L. Doltsinis, *J. Chem. Phys.*, 2007, **126**, 175102.
91 E. Fabiano and W. Thiel, *J. Phys. Chem. A*, 2008, **112**, 6859–6863.
92 H. R. Hudock and T. J. Martínez, *ChemPhysChem*, 2008, **9**, 2486–2490.
93 F. Plasser, M. Barbatti, A. J. A. Aquino and H. Lischka, *Theor. Chem. Acc.*, 2012, **131**, 1073–1087.
94 M. Barbatti, Z. Lan, R. Crespo-Otero, J. J. Szymczak, H. Lischka and W. Thiel, *J. Chem. Phys.*, 2012, **137**, 22A503.
95 J. B. Nee, M. Suto and L. C. Lee, *Chem. Phys.*, 1985, **98**, 147–155.
96 R. J. Buenker, G. Olbrich, H.-P. Schuchmann, B. L. Schürmann and C. von Sonntag, *J. Am. Chem. Soc.*, 1984, **106**, 4362–4368.
97 S. Harich, J. J. Lin, Y. T. Lee and X. Yang, *J. Phys. Chem. A*, 1999, **103**, 10324–10332.
98 T. H. Dunning, *J. Chem. Phys.*, 1989, **90**, 1007–1023.
99 C. Lee, W. Yang and R. G. Parr, *Phys. Rev. B: Condens. Matter Mater. Phys.*, 1988, **37**, 785–789.
100 A. D. Becke, *J. Chem. Phys.*, 1993, **98**, 5648–5652.
101 O. Christiansen, H. Koch and P. Jørgensen, *Chem. Phys. Lett.*, 1995, **243**, 409–418.
102 J. Schirmer, *Phys. Rev. A*, 1982, **26**, 2395–2416.
103 R. Bauernschmitt and R. Ahlrichs, *Chem. Phys. Lett.*, 1996, **256**, 454–464.
104 C. Hättig and F. Weigend, *J. Chem. Phys.*, 2000, **113**, 5154–5161.
105 TURBOMOLE V6.3.1 2011, a development of University of Karlsruhe and Forschungszentrum Karlsruhe GmbH, 1989–2007, TURBOMOLE GmbH, since 2007, available from http://www.turbomole.com.
106 C. L. Janssen and I. M. B. Nielsen, *Chem. Phys. Lett.*, 1998, **290**, 423–430.
107 H. Lischka, R. Shepard, I. Shavitt, R. M. Pitzer, M. Dallos, T. Müller, P. G. Szalay, F. B. Brown, R. Ahlrichs, H. J. Böhm, A. Chang, D. C. Comeau, R. Gdanitz, H. Dachsel, C. Ehrhardt, M. Ernzerhof, P. Höchtl, S. Irle, G. Kedziora, T. Kovar, V. Parasuk, M. J. M. Pepper, P. Scharf, H. Schiffer, M. Schindler, M. Schüler, M. Seth, E. A. Stahlberg, J.-G. Zhao, S. Yabushita, Z. Zhang, M. Barbatti, S. Matsika, M. Schuurmann, D. R. Yarkony, S. R. Brozell, E. V. Beck, J.-P. Blaudeau, M. Ruckenbauer, B. Sellner, F. Plasser and J. J. Szymczak, *COLUMBUS, an ab initio* electronic structure program, release 7.0, 2012.
108 H.-J. Werner, P. J. Knowles, R. Lindh, F. R. Manby, M. Schütz, P. Celani, T. Korona, G. Rauhut, R. D. Amos, A. Bernhardsson, A. Berning, D. L. Cooper, M. J. O. Deegan, A. J. Dobbyn, F. Eckert, C. Hampel, G. Hetzer, A. W. Lloyd, S. J. McNicholas, W. Meyer, M. E. Mura, A. Nicklass, P. Palmieri, R. Pitzer, U. Schumann, H. Stoll, A. J. Stone, R. Tarroni and T. Thorsteinsson, *MOLPRO, version 2006.1, a package of ab initio programs*, see http://www.molpro.net.

Paper #2

Mechanisms of Ultrafast Excited-State Deactivation in Adenosine. *Reprinted with permission from* D. Tuna, A. L. Sobolewski, W. Domcke, *J. Phys. Chem. A* **2014**, *118*, 122—127.

THE JOURNAL OF PHYSICAL CHEMISTRY A

Article

pubs.acs.org/JPCA

Mechanisms of Ultrafast Excited-State Deactivation in Adenosine

Deniz Tuna,[†,*] Andrzej L. Sobolewski,[‡] and Wolfgang Domcke[†]

[†]Department of Chemistry, Technische Universität München, 85747 Garching, Germany

[‡]Institute of Physics, Polish Academy of Sciences, 02668 Warsaw, Poland

Supporting Information

ABSTRACT: Recently, resonant two-photon ionization experiments on isolated adenine and adenosine suggested that adenosine exhibits a significantly shorter excited-state lifetime than adenine, which indicates the existence of an efficient excited-state deactivation mechanism in adenosine that is not existent in adenine. We report on ab initio investigations on a syn and an anti conformer of adenosine exhibiting an intramolecular O−H···N3 hydrogen bond. For both conformers, we have identified the existence of a barrierless excited-state deactivation mechanism that involves the forward−backward transfer of a proton along the intramolecular hydrogen bond and ultrafast radiationless deactivation through conical intersections. The S_1/S_0 conical intersection associated with the proton-transfer process is lower in energy than the known S_1/S_0 conical intersections associated with the excited-state deactivation processes inherent to the adenine moiety. These results support the conjecture that the photochemistry of hydrogen bonds plays a decisive role for the photostability of the molecular building blocks of RNA and DNA, which have been selected at the earliest stages of the chemical evolution of life.

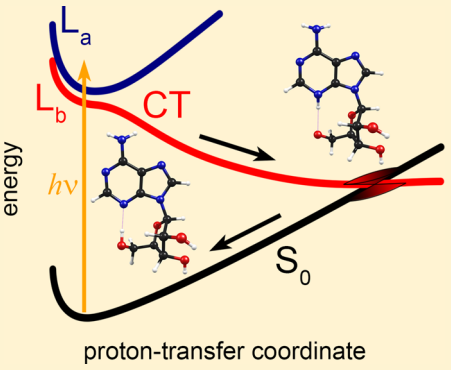

INTRODUCTION

Ribonucleosides and deoxyribonucleosides are the building blocks of RNA and DNA. In these polymers the nucleosides are connected by phosphodiester bonds.[1] The nucleobases adenine, guanine, cytosine, thymine and uracil, as well as several nucleosides and nucleotides, have been the focus of spectroscopic and quantum-chemical investigations in the past decade.[2−7] Probing such biomolecules under isolated conditions in the gas phase allows one to explore their intrinsic photophysical and photochemical properties without the interference of perturbative effects originating from the environment.[8] De Vries and co-workers have performed the first resonant two-photon ionization mass-spectrometry experiments on a jet-cooled nucleoside, guanosine, in 2000,[9] which was followed by several spectroscopic studies on nucleosides in the gas phase.[10−15] Computational studies on nucleosides have also been performed: these include, among others, the exploration of the stable conformers[16,17] and of the vertical excitation energies.[18,19]

Saigusa and co-workers recently performed resonant two-photon ionization mass-spectrometry experiments on laser-desorbed samples of jet-cooled adenosine and adenosine dimers.[15] Surprisingly, upon excitation with UV laser pulses of 6 ns temporal width at 266 nm wavelength, adenosine does not produce a resonant two-photon ionization signal in the mass spectrum,[15] in contrast to adenine under the same conditions,[20] confirming an earlier result of Nir and de Vries from 2001.[10] The authors concluded that the excited-state lifetime of adenosine must be significantly shorter than the lifetime of adenine,[15] which is of the order of a few picoseconds after excitation to the bright $\pi\pi^*$ state (the L_a state in Platt's notation[21]).[2,15,20] This finding indicates the existence of an ultrafast radiationless deactivation process that is able to effectively quench photoexcited adenosine before a second photon can be absorbed. The coupling of the nucleobase with the carbohydrate appears to provide the nucleoside with an efficient mechanism for excited-state deactivation that is not present in the isolated nucleobase. This finding motivated us to search for a mechanism for radiationless excited-state deactivation in adenosine that is introduced by the N-glycosidic bond between adenine and β-D-ribofuranose (from hereon called ribose). Although this is not a joint experimental and theoretical study, a spectroscopic experiment motivated us to perform this investigation.

On the basis of previous results obtained for DNA base pairs and small peptides, we anticipate an excited-state deactivation mechanism via proton transfer, which is mediated by an excited singlet state of charge-transfer character.[22,23] Therefore, we focus on a syn and an anti conformer of adenosine[1] that exhibit an intramolecular hydrogen bond between an OH proton of the ribose moiety and the N3 heteroatom of the adenine moiety (cf. Figures 1 and S1 (Supporting Information) for the structures). We describe the suggested mechanistic picture for the syn conformer in detail in this article, whereas the corresponding material for the anti conformer is presented in the Supporting Information.

It is a well-established fact that ultrafast (subpicosecond) radiationless deactivation processes are mediated by conical

Received: October 11, 2013
Revised: December 6, 2013
Published: December 9, 2013

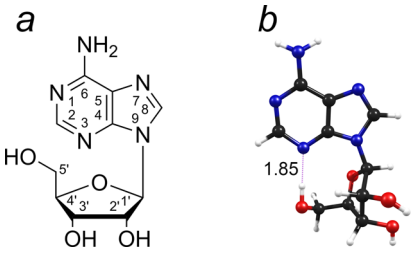

Figure 1. Structural formula of adenosine with the conventional numbering of atoms for purine nucleosides (a) and molecular structure of the ground-state equilibrium geometry of the 5′-O−H···N3 intramolecularly hydrogen-bonded syn conformer (b). The length of the intramolecular hydrogen bond is indicated (Å).

intersections of Born−Oppenheimer potential-energy surfaces.[24,25] At a conical intersection two (or more) surfaces of the same multiplicity are degenerate in energy. These critical points are of comparable significance for chemical reactions proceeding on potential-energy surfaces of electronically excited states as are transition states for reactions proceeding on the potential-energy surface of the electronic ground state.[26] The dynamics at a conical intersection is characterized by a complete breakdown of the Born−Oppenheimer approximation, which allows an efficient conversion of electronic energy into vibrational energy (known as internal conversion). The determination of the energy and the geometry of conical intersections between the S_1 and S_0 states is therefore essential for the characterization of photochemical reactions and radiationless deactivation processes.[6,24−27]

To describe radiationless deactivation processes, one has to explore the reaction paths connecting the Franck−Condon region (vertically above the potential well of the ground-state equilibrium geometry) of the initially populated excited state with the accessible S_1/S_0 conical intersections, where the system can relax back to the electronic ground state.[21,26,28]

RESULTS

We consider in this work two conformers of adenosine that exhibit an intramolecular hydrogen bond between an O−H proton of the ribose moiety and the N3 heteroatom of the adenine moiety. The first is a syn conformer with respect to the mutual orientation of the ribose and the adenine moieties[1] and exhibits an intramolecular hydrogen bond between the 5′-O−H proton of the ribose moiety and the N3 heteroatom of the adenine moiety. The second conformer exhibits an anti orientation between the ribose and the adenine moieties[1] and an intramolecular hydrogen bond between the 2′-O−H proton of the ribose moiety and the N3 heteroatom of the adenine moiety. The structures of these two conformers are shown in Figures 1 and S1 (Supporting Information), respectively.

To our knowledge, no comprehensive conformational analysis using ab initio methods has been performed for adenosine to date. However, a detailed investigation by de Vries and co-workers of the possible conformers of guanosine using spectroscopic techniques and ab initio calculations showed that a 5′-O−H···N3 intramolecularly hydrogen-bonded syn conformer and a 2′-O−H···N3 intramolecularly hydrogen-bonded anti conformer are the most stable conformers.[11,12] Saigusa and co-workers have shown that the 5′-O−H···N3 hydrogen-bonded syn conformer is also found in hydrated clusters of guanosine,[13] and that capping the 5′−OH group of guanosine with an ethyl group leads preferably to the formation of the 2′-O−H···N3 hydrogen-bonded anti conformer.[14] A very recent study presents an extensive ab initio investigation of the stable conformers of inosine. Alvarez-Ros and Palafox found that among 69 optimized conformers the two most stable conformers of inosine are the syn 5′-O−H···N3 and the anti 2′-O−H···N3 hydrogen-bonded conformers. These two conformers also exhibit the strongest among the many possible intramolecular hydrogen bonds.[17] For these reasons, there is strong evidence that the two intramolecularly hydrogen-bonded conformers of adenosine considered in this work are the—or at least among the—most stable conformers of adenosine.

Figure 2a shows the potential-energy profiles of the electronic ground state, the weakly absorbing $\pi\pi^*$ state (L_b in Platt's notation[21]), the optically bright $\pi\pi^*$ state (L_a), and the lowest $n\pi^*$ state of the adenine moiety, as well as the lowest-lying charge-transfer (CT) state along the reaction coordinate defined as the internuclear distance between the oxygen and the hydrogen atom of the 5′-O−H group of the ribose moiety of the 5′-O−H···N3 intramolecularly hydrogen-bonded syn conformer of adenosine. This reaction coordinate describes the movement of the proton from the 5′-O−H group of the ribose moiety to the N3 heteroatom of the adenine moiety. The full black circles represent the potential-energy function of the electronic ground state along the proton-transfer coordinate obtained by a relaxed scan (cf. Computational Methods section). The vertical excitation energies of the L_b, the $n\pi^*$,

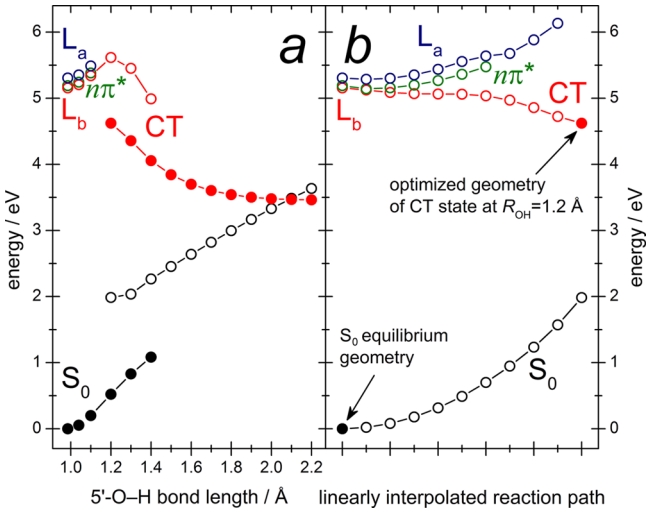

Figure 2. Energy profiles (eV) of the electronic ground state (S_0), the lowest $\pi\pi^*$ state (L_b), the $n\pi^*$ state, and the optically bright $\pi\pi^*$ state (L_a) of the adenine moiety as well as the charge-transfer state (CT) for the 5′-O−H···N3 intramolecularly hydrogen-bonded syn conformer of adenosine. (a) Energy profiles obtained by a relaxed scan along the 5′-O−H internuclear distance in the electronic ground state (full black circles) with vertical excitation energies of the L_b/CT state (empty red circles), the $n\pi^*$ state (empty green circles), and the L_a state (empty blue circles). The energy profile of the charge-transfer state for the reaction path optimized in the charge-transfer state is shown by full red circles. The energy of the ground state at the same geometries is given by empty black circles. (b) Energy profiles for the linear interpolation between the ground-state equilibrium geometry (full black circle at the lower left) and the optimized geometry of the charge-transfer state at a fixed O−H bond length of 1.2 Å (full red circle at the right). The L_b state correlates adiabatically and barrierlessly with the charge-transfer state at large O−H distances. For details, consult the Computational Methods section.

dx.doi.org/10.1021/jp410121h | J. Phys. Chem. A 2014, 118, 122−127

and the L_a states (empty red, green, and blue circles) are given as well. One can see that the energies of the L_b, the $n\pi^*$, and the L_a states rise with increasing O−H internuclear distance. The L_b state correlates adiabatically with the charge-transfer state at large O−H distances. The energy of the L_b state initially rises along the proton-transfer coordinate. Once the charge-transfer character of the lowest singlet state outweighs the $\pi\pi^*$ character (at an O−H distance of ∼1.2 Å), the L_b/CT energy begins to drop. The energy profile shown by the full red circles in Figure 2a represents the potential-energy function of the lowest charge-transfer state obtained by a relaxed scan for this state. The energy of the ground state at the same geometries is given by the empty black circles. It can be seen that the energy of the charge-transfer state decreases significantly with increasing distance between the oxygen atom and the proton. In other words, in the charge-transfer state the proton is driven from the 5′-O−H group of the ribose moiety toward the N3 heteroatom of the adenine moiety. This pronounced effect can be understood by the fact that the charge-transfer state is characterized by a substantial translocation of electron density from the 5′-OH group to the π-orbital system of the adenine moiety (in comparison to the electron density in the electronic ground state).

To elucidate the radiationless transition of the system from the initially populated L_a state to the reactive charge-transfer state, Figure 2b shows the energy profiles of the relevant electronic states obtained by a linear interpolation (cf. Computational Methods section) between the ground-state equilibrium geometry and the optimized geometry of the lowest charge-transfer state at an internuclear distance of 1.2 Å (it is not possible to optimize the geometry of the first charge-transfer state for internuclear O−H distances shorter than 1.2 Å because it steeply rises in energy and mixes with various other electronic states at shorter distances). The ground state, the $n\pi^*$ state, and the L_a state gradually rise in energy along this reaction path. On the other hand, the Lb state, which correlates adiabatically with the lowest-lying charge-transfer state, decreases in energy along the linearly interpolated reaction path (cf. Figure. 2b). After population of the L_a state the system can easily populate the nearby L_b state via vibronic interactions. Overall, the pathway from the Franck−Condon region of the L_a state to the reactive charge-transfer state is completely barrierless. For the sake of completeness, we mention that the $n\pi^*$ state correlates adiabatically with a slightly higher-lying charge-transfer state, which is described by the excitation of an electron from the second lone-pair orbital of the oxygen atom of the 5′-OH group. This second charge-transfer state also drops in energy along the interpolated reaction path once the charge-transfer character outweighs the $n\pi^*$ character (this part of the profile is not shown in Figure 2b for clarity).

Figure 3 depicts the molecular orbitals involved in the description of the relevant excited states. The L_a state is characterized mainly by excitation of an electron from the highest occupied π orbital to the lowest unoccupied π^* orbital. The lowest-lying charge-transfer state is characterized by the excitation of an electron from a lone-pair orbital of the oxygen atom of the 5′-OH group of the ribose moiety to the π^* orbital of the adenine moiety. Therefore, Figure 3 illustrates the translocation of electron density from the 5′-OH group of the ribose moiety to the aromatic system of the adenine moiety in the charge-transfer state.

In the charge-transfer state, the 5′-OH group becomes more acidic, whereas the nucleobase becomes more basic, which

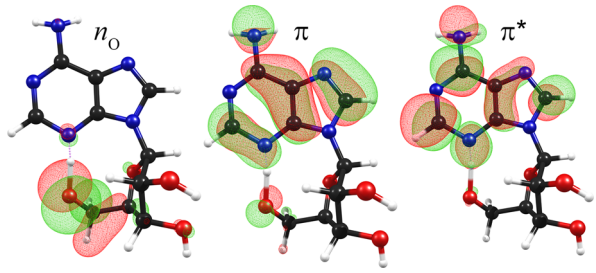

Figure 3. Molecular orbitals of the 5′-O−H···N3 intramolecularly hydrogen-bonded syn conformer of adenosine involved in the electronic states shown in Figure 2. Shown are the lone-pair orbital located at the oxygen atom of the 5′-OH group (involved in the description of the lowest charge-transfer state) as well as the π and π^* orbitals (involved in the description of the L_a state). For details, consult the Computational Methods section.

drives the proton from the ribose moiety to the adenine moiety. This process has been termed electron-driven proton transfer.[22,23,29] Due to the fact that the energy of the ground state rises with increasing O−H distance, whereas the energy of the charge-transfer state drops, the potential-energy surfaces of the charge-transfer state and the ground state intersect at an internuclear distance of ∼2.1 Å (cf. Figure 2a). The crossing of the potential-energy profile of the charge-transfer state (full red circles) and the energy profile of the ground state at the same geometries (empty black circles) is a conical intersection. This conical intersection gives rise to a radiationless transition between the two electronic states (i.e., internal conversion).

Figure 4 shows three conical intersections of the syn conformer of adenosine: the proton-transfer conical inter-

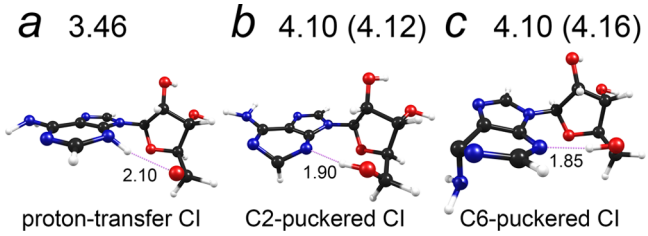

Figure 4. Optimized geometries of the S_1/S_0 conical intersections of the 5′-O−H···N3 intramolecularly hydrogen-bonded syn conformer of adenosine: (a) conical intersection (CI) for the electron-driven proton-transfer process; (b) C2-puckered conical intersection; (c) C6-puckered conical intersection. The relative energies (eV) of the conical intersections with respect to the ground-state equilibrium geometry are also given. The values in parentheses are the energies of the corresponding conical intersections in adenine. The length of the hydrogen bond is indicated (Å). For details, consult the Computational Methods section.

section (Figure 4a), the C2-puckered conical intersection of the adenine moiety (Figure 4b), and the C6-puckered conical intersection of the adenine moiety (Figure 4c). It is nowadays well established by extensive ab initio electronic-structure and semiclassical trajectory-surface-hopping dynamics studies that the excited-state deactivation of 9H-adenine proceeds primarily via two S_1/S_0 conical intersections involving a puckering of the six-membered ring: the C2-puckered intersection and the C6-puckered intersection.[30−32] The optimized geometries of these two conical intersections for the syn conformer of adenosine are shown in Figures 4b,c. For comparison, the optimized geometry of the S_1/S_0 conical intersection involved in the

dx.doi.org/10.1021/jp410121h | J. Phys. Chem. A 2014, 118, 122−127

electron-driven proton-transfer process is shown in Figure 4a. The proton-transfer intersection is located 0.64 eV lower in energy than the C2- and the C6-puckered conical intersections. All three conical intersections are located well below the vertical excitation energy of the L_a state of this conformer of adenosine (5.3 eV). The relative energies of the two ring-puckered conical intersections of adenosine are almost equal to the relative energies of these intersections in adenine (cf. values in parentheses in Figure 4b,c). These intersections, which are inherent to the adenine chromophore, are thus barely influenced by the coupling with the ribose moiety.

The molecular structure of the ground-state equilibrium geometry, the potential-energy profiles, the relevant molecular orbitals, and the conical intersections for the anti conformer of adenosine exhibiting a 2′-O−H···N3 intramolecular hydrogen bond are presented in Figures S1−S4 in the Supporting Information. The qualitative picture is exactly the same as we have presented above for the syn conformer: the initially populated L_a state is higher in energy than, although very close to, the L_b state that correlates adiabatically with the lowest-lying charge-transfer state (cf. Figure S2, Supporting Information). The conical intersection between the charge-transfer state and the ground state is located at an energy of 3.43 eV, again well below the energy of the C2- and C6-puckered conical intersections inherent to the adenine moiety, and the relative energies of the ring-puckered conical intersections are very close to the relative energies of these intersections in adenine (cf. Figure S4, Supporting Information). It should be noted that due to the more strained structure of the hydrogen-bonded anti conformer the O−H distance of the proton-transfer conical intersection is significantly longer (2.39 Å, cf. Figure S4a (Supporting Information)) than that of the corresponding conical intersection of the syn conformer (2.10 Å, cf. Figure 4a).

DISCUSSION AND CONCLUSIONS

This work is motivated by gas-phase laser-spectroscopic experiments suggesting that adenosine exhibits a significantly shorter excited-state lifetime than adenine, to an extent that resonant two-photon ionization processes are quenched in adenosine as opposed to adenine.[15] Our computational investigations provide a mechanistic explanation of this observation. We have shown that in the intramolecularly 5′-O−H···N3 hydrogen-bonded syn and in the 2′-O−H···N3 hydrogen-bonded anti conformers of adenosine a mechanism for ultrafast excited-state deactivation exists via an electron-driven proton-transfer process that is mediated by an excited state of charge-transfer character (cf. Figures 2 and S2 (Supporting Information)). This mechanism involving ultrafast (i.e., proceeding on a femtosecond time scale) forward−backward motion of the proton complements the excited-state deactivation mechanisms inherent to the adenine moiety (the ring-puckering processes). The relevant conical intersection for the proton-transfer process in adenosine (cf. Figures 4a and S4a (Supporting Information)) is significantly lower in energy than the ring-puckered conical intersections inherent to the adenine moiety (cf. Figures 4b,c and S4b,c (Supporting Information)). Moreover, the relevant conical intersection between the lowest charge-transfer state and the ground state can be reached on a completely barrierless pathway starting from the Franck−Condon region of the initially populated L_a state (cf. Figures 2 and S2 (Supporting Information)). This process can explain the quenching of the electronic excitation energy in adenosine before a second photon can be absorbed and, thus, a signal in the mass spectrum be generated. We have also shown that the ring-puckered conical intersections inherent to the adenine moiety are barely influenced by the coupling with ribose. This is in agreement with earlier findings of Zgierski and Alavi on cytidine, who showed that the deactivation mechanisms inherent to the cytosine moiety of cytidine did not change significantly compared to isolated cytosine.[33] These results indicate that the ring-puckered conical intersections inherent to the adenine moiety cannot be responsible for the experimental observation that adenosine exhibits a shorter excited-state lifetime than adenine. We can thus rule out that changes in the electronic structure introduced by the coupling of the nucleobase with the carbohydrate by the N-glycosidic bond are responsible for the observed behavior. We suggest that it is rather the favorable energetic location and the barrierless reaction path leading to the proton-transfer conical intersection that is the reason for the shortened lifetime of adenosine. It is plausible that deactivation via the proton-transfer conical intersection occurs on a faster time scale than the processes mediated by the ring-puckered conical intersections of the adenine moiety, because the former involves primarily a movement of the light hydrogen atom, and the latter involve the movement of carbon atoms, nitrogen atoms, and amino groups. Though we did not explicitly treat the dynamics of the radiationless transitions, the exploration of the relevant reaction coordinates and their energy profiles is an essential prerequisite for future simulations of the dynamics of these photoinduced reactions. Future trajectory-surface-hopping dynamics simulations employing an accurate electronic-structure method could provide definitive computational proof that the mechanism proposed here is indeed the dominating excited-state deactivation process in intramolecularly hydrogen-bonded conformers of adenosine.

The involvement of the charge-transfer states translocating electron density from an OH group of the ribose moiety to the π system of the adenine moiety is why this deactivation mechanism is only available for intramolecularly hydrogen-bonded conformers involving an OH proton of the ribose moiety as the hydrogen-bond donor atom, in contrast to conformers exhibiting a "reverse type" of hydrogen bond, for example, a C8−H···O5′ hydrogen-bonded anti conformer, which is also one of the most stable conformers of adenosine and constitutes, in fact, the hydrogen-bonding motif found in many nucleic acid helices.[16]

We propose a simple experimental test that may validate our prediction that the electron-driven proton-transfer process is responsible for the nonexistence of a signal in the resonant two-photon ionization mass spectrum of adenosine. Capping all three OH groups of the ribose moiety by alcohol-protecting groups (e.g., three methyl, ethyl, or isopropyl groups, or one methyl and one 2′O,3′O-isopropylidene group; cf. compounds **1**−**4** in Figure S5 (Supporting Information)), thereby obtaining an adenosine triether, prohibits the molecule from forming intramolecular hydrogen bonds between the ribose and the adenine moieties involving OH protons of the ribose moiety. These derivatives of adenosine should exhibit a significantly longer excited-state lifetime than adenosine and thus should give a signal in the resonant two-photon ionization mass spectrum. Two-photon ionization spectra of conformers of guanosine with partially capped OH groups of the ribose moiety have been reported by de Vries and co-workers[11] and Saigusa and co-workers.[14] In these experiments, the partial

dx.doi.org/10.1021/jp410121h | J. Phys. Chem. A 2014, 118, 122−127

capping was used to facilitate the assignment of vibrational spectra,[11] and to force the molecule into forming a particular intramolecularly hydrogen-bonded conformer.[14] However, completely capped derivatives have not been considered so far.

The ability of the nucleobases of efficient quenching of the energy of absorbed UV photons by radiationless deactivation, thus converting electronic energy into vibrational motion and, ultimately, dissipating the absorbed energy into heat by energy transfer to the surrounding solvent, is believed to be the underlying cause for the high photostability of these molecules.[3,34] The inherent photostability of nucleobases toward UV irradiation might have been a dominating selection criterion during the early stages of the chemical evolution of life and may have been the reason for their incorporation into a wide range of biological systems. The photoprotective mechanism outlined in the present work for adenosine may have had significant relevance in the chemical evolution of life. The enhanced photostability of adenosine may have been a decisive factor when the first nucleosides evolved. Specifically, the first nucleosides, being more photostable than the nucleobases themselves, may have prevailed in the competition with alternate molecular structures. Excited-state deactivation via proton-transfer processes mediated by charge-transfer states appears to be a ubiquitous photoprotective mechanism in the molecular building blocks of life.[22,23,29,34]

The intramolecular hydrogen bond between the ribose and the nucleobase moieties will have to compete with solvent-mediated intermolecular hydrogen bonds in aqueous solution, which was most likely the environment for the evolution of life on primordial earth. In this context, it is noteworthy that Saigusa and co-workers have confirmed the existence of the 5′-OH···N3 hydrogen-bonded syn conformer of guanosine in hydrated clusters.[13] Moreover, molecular-dynamics simulations of adenosine in aqueous solution[35,36] have shown that intramolecularly hydrogen-bonded syn and anti conformers persist in aqueous solution, although the intramolecular hydrogen bond is in competition with solvent-mediated intermolecular hydrogen bonds. These results support the hypothesis that the enhanced photostability of adenosine provided by the intramolecular hydrogen bond may have been of relevance in the chemical evolution of life.

■ COMPUTATIONAL METHODS

The second-order Møller−Plesset (MP2) method was used for optimizing ground-state equilibrium geometries (shown in Figures 1b and S1b (Supporting Information)) and for performing calculations of ground-state potential-energy profiles. The ADC(2) method (algebraic diagrammatic construction of second order)[37] was used for excited-state calculations. This methodology offers a description of electronically excited states that is of similar quality as is the MP2 level for the electronic ground state. The potential-energy profiles of the electronic ground state (depicted by full black circles in Figures 2a and S2a (Supporting Information)) were obtained by constrained optimization at the MP2 level, that is, by fixing the distance between the oxygen and hydrogen nuclei of the 5′-O−H and the 2′-O−H group of the ribose moiety of the syn and anti conformer, respectively, at a given value and relaxing all remaining internal degrees of freedom. Single-point calculations of excitation energies were performed for the obtained relaxed geometries at the ADC(2) level. The potential-energy profile of the lowest-lying charge-transfer state (depicted by full red circles in Figures 2a and S2a (Supporting Information)) was obtained by constrained optimization at the ADC(2) level. Single-point energy calculations were performed for the obtained geometries at the MP2 level to obtain the corresponding energies of the ground state. The approximate reaction path from the ground-state equilibrium geometry to the relaxed geometry of the charge-transfer state shown in Figures 2b and S2b (Supporting Information) was constructed by linear interpolation of internal coordinates between the initial geometry (the ground-state equilibrium geometry) and the final geometry (the relaxed geometry of the charge-transfer state at an O−H distance of 1.2 or 1.3 Å for the syn and anti conformers, respectively). The energy profiles for the approximated reaction path were obtained by single-point energy computations along the interpolated path. The molecular orbitals shown in Figures 3 and S3 (Supporting Information) are self-consistent-field orbitals. All these calculations, which employed the cc-pVDZ basis set throughout, were performed with the Turbomole 6.3.1 program package.[38]

Minimum-energy conical intersections (shown in Figures 4 and S4 (Supporting Information)) were optimized using the program package CIOpt devoloped by Levine, Coe, and Martínez.[39] The underlying algorithm allows the optimization of conical intersections without the need of evaluating nonadiabatic couplings between the intersecting states. This allows the use of electronic-structure methods for which nonadiabatic couplings between adiabatic states are not available, such as the ADC(2) method. The program CIOpt was linked to Turbomole 6.3.1[38] and the S_1/S_0 conical intersections were optimized at the mixed ADC(2)/MP2 level. To construct the starting geometries for the optimization of the C2- and the C6-puckered conical intersections, which are well-known for 9H-adenine,[30] in adenosine, we attached the structure of the ribose moiety (obtained by the optimization of the ground-state equilibrium geometry of the syn and anti conformers of adenosine) to these structures of adenine. To obtain relative energies of the C2- and C6-puckered conical intersections of adenine, we reoptimized these intersections of adenine using the same procedure and level of theory.

■ ASSOCIATED CONTENT

Supporting Information

Molecular structure corresponding to Figure 1, potential-energy profiles corresponding to Figure 2, molecular orbitals corresponding to Figure 3, and conical intersections corresponding to Figure 4 for the 2′-O−H···N3 intramolecularly hydrogen-bonded anti conformer of adenosine; structural formulas of compounds **1**−**4** proposed for the spectroscopic validation of our prediction; Cartesian coordinates of the ground-state equilibrium geometry of the syn and anti conformers and of three optimized conical intersections of adenosine each, as well as the ground-state equilibrium geometry, the C2- and the C6-puckered conical intersections of adenine. This material is available free of charge via the Internet at http://pubs.acs.org/.

■ AUTHOR INFORMATION

Corresponding Author

*D. Tuna: e-mail, deniz.tuna@ch.tum.de; phone, +49 89 289 13610.

Notes

The authors declare no competing financial interest.

■ ACKNOWLEDGMENTS

D.T. is grateful for a Ph.D. fellowship granted by the International Max Planck Research School of Advanced Photon Science (IMPRS-APS) and for support by the TUM Graduate School. This work was partially supported by a research grant of the Deutsche Forschungsgemeinschaft (DFG) and by the DFG Cluster of Excellence "Munich-Centre for Advanced Photonics".

■ REFERENCES

(1) Voet, D.; Voet, J. G. *Biochemistry*, 4th ed.; Wiley: Hoboken, NJ, 2011.
(2) Nir, E.; Plützer, C.; Kleinermanns, K.; de Vries, M. Properties of Isolated DNA Bases, Base Pairs and Nucleosides Examined by Laser Spectroscopy. *Eur. Phys. J. D* **2002**, *20*, 317−329.
(3) Crespo-Hernández, C. E.; Cohen, B.; Hare, P. M.; Kohler, B. Ultrafast Excited-State Dynamics in Nucleic Acids. *Chem. Rev.* **2004**, *104*, 1977−2019.
(4) Saigusa, H. Excited-State Dynamics of Isolated Nucleic Acid Bases and Their Clusters. *J. Photochem. Photobiol. C* **2006**, *7*, 197−210.
(5) Shukla, M., Leszczynski, J., Eds. *Radiation Induced Molecular Phenomena in Nucleic Acids*; Springer: New York, 2008.
(6) Barbatti, M.; Aquino, A. J. A.; Szymczak, J. J.; Nachtigallová, D.; Hobza, P.; Lischka, H. Relaxation Mechanisms of UV-Photoexcited DNA and RNA Nucleobases. *Proc. Natl. Acad. Sci. U. S. A.* **2010**, *107*, 21453−21458.
(7) Kleinermanns, K.; Nachtigallová, D.; de Vries, M. S. Excited State Dynamics of DNA Bases. *Int. Rev. Phys. Chem.* **2013**, *32*, 308−342.
(8) Weinkauf, R.; Schermann, J.-P.; de Vries, M. S.; Kleinermanns, K. Molecular Physics of Building Blocks of Life Under Isolated or Defined Conditions. *Eur. Phys. J. D* **2002**, *20*, 309−316.
(9) Nir, E.; Imhof, P.; Kleinermanns, K.; de Vries, M. REMPI Spectroscopy of Laser Desorbed Guanosines. *J. Am. Chem. Soc.* **2000**, *122*, 8091−8092.
(10) Nir, E.; de Vries, M. S. Fragmentation of Laser-Desorbed 9-Substituted Adenines. *Int. J. Mass Spectrom.* **2002**, *219*, 133−138.
(11) Nir, E.; Hünig, I.; Kleinermanns, K.; de Vries, M. S. Conformers of Guanosines and their Vibrations in the Electronic Ground and Excited States, as Revealed by Double-Resonance Spectroscopy and *Ab Initio* Calculations. *ChemPhysChem* **2004**, *5*, 131−137.
(12) Abo-Riziq, A.; Crews, B. O.; Compagnon, I.; Oomens, J.; Meijer, G.; Von Helden, G.; Kabeláč, M.; Hobza, P.; de Vries, M. S. The Mid-IR Spectra of 9-Ethyl Guanine, Guanosine, and 2-Deoxyguanosine. *J. Phys. Chem. A* **2007**, *111*, 7529−7536.
(13) Saigusa, H.; Urashima, S.; Asami, H. IR-UV Double Resonance Spectroscopy of the Hydrated Clusters of Guanosine and 9-Methylguanine: Evidence for Hydration Structures Involving the Sugar Group. *J. Phys. Chem. A* **2009**, *113*, 3455−3462.
(14) Asami, H.; Urashima, S.; Tsukamoto, M.; Motoda, A.; Hayakawa, Y.; Saigusa, H. Controlling Glycosyl Bond Conformation of Guanine Nucleosides: Stabilization of the *Anti* Conformer in 5′-O-Ethylguanosine. *J. Phys. Chem. Lett.* **2012**, *3*, 571−575.
(15) Asami, H.; Yagi, K.; Ohba, M.; Urashima, S.; Saigusa, H. Stacked Base-Pair Structures of Adenine Nucleosides Stabilized by the Formation of Hydrogen-Bonding Network Involving the Two Sugar Groups. *Chem. Phys.* **2013**, *419*, 84−89.
(16) Hocquet, A.; Leulliot, N.; Ghomi, M. Ground-State Properties of Nucleic Acid Constituents Studied by Density Functional Calculations. 3. Role of Sugar Puckering and Base Orientation on the Energetics and Geometry of 2′-Deoxyribonucleosides and Ribonucleosides. *J. Phys. Chem. B* **2000**, *104*, 4560−4568.
(17) Alvarez-Ros, M. C.; Palafox, A. Molecular Structure of the Nucleoside Analogue Inosine using DFT Methods: Conformational Analysis, Crystal Simulations and Possible Behaviour. *J. Mol. Struct.* **2013**, *1047*, 358−371.
(18) So, R.; Alavi, S. Vertical Excitation Energies for Ribose and Deoxyribose Nucleosides. *J. Comput. Chem.* **2007**, *28*, 1776−1782.
(19) Improta, R.; Barone, V. The Excited States of Adenine and Thymine Nucleoside and Nucleotide in Aqueous Solution: a Comparative Study by Time-Dependent DFT Calculations. *Theor. Chem. Acc.* **2008**, *120*, 491−497.
(20) Kang, H.; Chang, J.; Lee, S. H.; Ahn, T. K.; Kim, N. J.; Kim, S. K. Excited-State Lifetime of Adenine near the first Electronic Band Origin. *J. Chem. Phys.* **2010**, *133*, 154311.
(21) Klessinger, M.; Michl, J. *Excited States and Photochemistry of Organic Molecules*; VCH Publishers: New York, 1995.
(22) Sobolewski, A. L.; Domcke, W. *Ab Initio* Studies on the Photophysics of the Guanine-Cytosine Base Pair. *Phys. Chem. Chem. Phys.* **2004**, *6*, 2763−2771.
(23) Sobolewski, A. L.; Domcke, W. Relevance of Electron-Driven Proton-Transfer Processes for the Photostability of Proteins. *ChemPhysChem* **2006**, *7*, 561−564.
(24) Domcke, W., Yarkony, D. R., Köppel, H., Eds. *Conical Intersections: Electronic Structure, Dynamics & Spectroscopy*; World Scientific Publishing: Toh Tuck Link, 2004.
(25) Domcke, W., Yarkony, D. R., Köppel, H., Eds. *Conical Intersections: Theory, Computation and Experiment*; World Scientific Publishing: Toh Tuck Link, 2011.
(26) Bernardi, F.; Olivucci, M.; Robb, M. A. Potential Energy Surface Crossings in Organic Photochemistry. *Chem. Soc. Rev.* **1996**, *25*, 321−328.
(27) Martínez, T. J. Seaming is Believing. *Nature* **2010**, *467*, 412−413.
(28) Olivucci, M., Ed. *Computational Photochemistry*; Elsevier: Amsterdam, 2005.
(29) Domcke, W.; Sobolewski, A. L. Peptide Deactivation: Spectroscopy Meets Theory. *Nat. Chem.* **2013**, *5*, 257−258.
(30) Perun, S.; Sobolewski, A. L.; Domcke, W. *Ab Initio* Studies on the Radiationless Decay Mechanisms of the Lowest Excited Singlet States of 9H-Adenine. *J. Am. Chem. Soc.* **2005**, *127*, 6257−6265.
(31) Marian, C. M. A New Pathway for the Rapid Decay of Electronically Excited Adenine. *J. Chem. Phys.* **2005**, *122*, 104314.
(32) Barbatti, M.; Lan, Z.; Crespo-Otero, R.; Szymczak, J. J.; Lischka, H.; Thiel, W. Critical Appraisal of Excited State Nonadiabatic Dynamics Simulations of 9H-Adenine. *J. Chem. Phys.* **2012**, *137*, 22A503.
(33) Zgierski, M. Z.; Alavi, S. Quantum Chemical Study of Biradical Decay Channels in Cytidine Nucleosides. *Chem. Phys. Lett.* **2006**, *426*, 398−404.
(34) Sobolewski, A. L.; Domcke, W. The Chemical Physics of the Photostability of Life. *Europhys. News* **2006**, *37*, 20−23.
(35) Foloppe, N.; Nilsson, L. Toward a Full Characterization of Nucleic Acid Components in Aqueous Solution: Simulations of Nucleosides. *J. Phys. Chem. B* **2005**, *109*, 9119−9131.
(36) Murugan, N. A.; Hugosson, H. W. Solvent Dependence of Conformational Distribution, Molecular Geometry, and Electronic Structure in Adenosine. *J. Phys. Chem. B* **2009**, *113*, 1012−1021.
(37) Schirmer, J. Beyond the Random-Phase Approximation: A New Approximation Scheme for the Polarization Propagator. *Phys. Rev. A* **1982**, *26*, 2395−2416.
(38) *TURBOMOLE* V6.3.1 2011, a development of University of Karlsruhe and Forschungszentrum Karlsruhe GmbH, 1989−2007, TURBOMOLE GmbH, since 2007, available from http://www.turbomole.com.
(39) Levine, B. G.; Coe, J. D.; Martínez, T. J. Optimizing Conical Intersections without Derivative Coupling Vectors: Application to Multistate Multireference Second-Order Perturbation Theory (MS-CASPT2). *J. Phys. Chem. B* **2008**, *112*, 405−413.

Paper #3

Photochemical Mechanisms of Radiationless Deactivation Processes in Urocanic Acid. *Reprinted with permission from* D. Tuna, A. L. Sobolewski, W. Domcke, *J. Phys. Chem. B* **2014**, *118*, 976—985. Copyright 2014, American Chemical Society.

THE JOURNAL OF PHYSICAL CHEMISTRY B

Article

pubs.acs.org/JPCB

Photochemical Mechanisms of Radiationless Deactivation Processes in Urocanic Acid

Deniz Tuna,*[,†] Andrzej L. Sobolewski,[‡] and Wolfgang Domcke[†]

[†]Department of Chemistry, Technische Universität München, Lichtenbergstr. 4, 85747 Garching, Germany

[‡]Institute of Physics, Polish Academy of Sciences, Al. Lotników 32/46, 02668 Warsaw, Poland

Supporting Information

ABSTRACT: Urocanic acid is a UV filter found in human skin that protects the skin from UV damage but has also been linked to the onset of skin cancer and to photoimmunosuppression. We report on ab initio investigations of two rotameric forms of each of the two tautomers of neutral (*E*)- and (*Z*)-urocanic acid. We have computed the vertical singlet excitation energies of eight isomers and have explored the singlet excited-state reaction paths of several photochemical processes for radiationless excited-state deactivation: the *E*/*Z* photoisomerization, an electron-driven proton transfer for an intramolecularly hydrogen-bonded *Z* isomer, as well as the hydrogen-atom detachment process and the ring-puckering process involving the NH group inherent to the imidazole moiety. We have optimized the S_1/S_0 conical intersections for each of these processes and located additional $\pi\pi^*/n\pi^*$ conical intersections. Because of the reversed energetic order of the $n\pi^*$ and $\pi\pi^*$ states in the N3H and N1H tautomers, an energy window exists where the N3H tautomers can be excited to the $n\pi^*$ state, from which only the photoisomerization process is accessible, while the N1H tautomers can be excited to the $\pi\pi^*$ state, from which several deexcitation processes compete from the onset of the absorption. These results explain the unusual dependence of the quantum yield for *E*→*Z* photoisomerization on the excitation wavelength. The present work provides novel insight into the complex photochemistry of this biomolecule and paves the way for future computational studies of the photoinduced excited-state dynamics of urocanic acid.

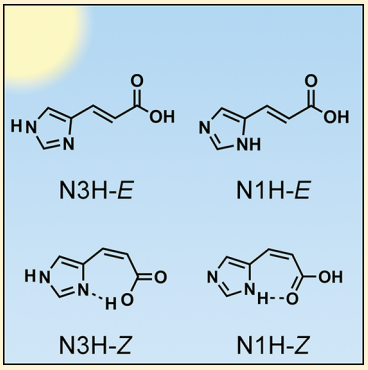

1. INTRODUCTION

Urocanic acid is a UV chromophore found in the *stratum corneum* (the uppermost layer) of the epidermis of human skin. Its *E* isomer is produced from histidine by the enzyme histidine ammonia-lyase. Upon UV irradiation, (*E*)-urocanic acid can undergo *E*→*Z* photoisomerization, which leads to an accumulation of (*Z*)-urocanic acid in the upper layers of skin. While urocanic acid acts as a natural sunscreen (a UV filter), it is nowadays believed that the *Z* isomer constitutes a health risk due to its ability to suppress the immune system and facilitate the onset of skin cancer.[1]

Urocanic acid is a remarkable subject of study in the sense that it has attracted attention from researchers of a large number of disciplines. Among these disciplines are photochemistry, photobiology, spectroscopy, immunology, dermatology, biochemistry, and bacteriology. The three most recent reviews on the various aspects of urocanic acid were given by Mohammad, Morrison, and HogenEsch in 1999,[1] Simon in 2000,[2] and Gibbs, Tye, and Norval in 2008.[3] A recent comment on the "two faces"—the beneficial and detrimental effects—of naturally occurring urocanic acid in skin was given by Gibbs and Norval in 2011.[4]

Numerous spectroscopic and kinetic studies on urocanic acid in aqueous solution have been performed.[5−17] An important result of these studies, which has been the topic of controversial discussions, is the determination of the unusual wavelength-dependent quantum yield for *E*/*Z* photoisomerization.[5,9] Only a single study on urocanic acid in a supersonic jet has been reported so far.[18]

A number of publications have reported on the results of computational investigations.[19−32] Various protonated forms of (*E*)- and (*Z*)-urocanic acid have been considered,[21] and a detailed investigation of an intramolecularly hydrogen-bonded *Z* isomer has been performed.[22] Molecular-dynamics simulations of the conformational dynamics in aqueous solution were reported.[27] A number of studies reported on the vertical excitation energies of the neutral species of urocanic acid,[19,23,24,26,32] while two studies reported on the vertical excitation energies of ionic forms.[25,26] Further studies dealt with the photosensitization mechanism (the ability of triplet-excited urocanic acid to react with molecular oxygen to produce singlet molecular oxygen)[30] and with the hydroxyl-radical-scavenging ability of urocanic acid.[31] The reaction paths for the photoisomerization process have been investigated.[28] One study dealt with the exploration of the potential-energy functions of various singlet and triplet states along the C6−C7−C8−O9 torsion angle (cf. Figure 1) and determined the locations of two singlet−triplet crossings.[29]

Received: December 2, 2013
Revised: January 6, 2014
Published: January 7, 2014

   dx.doi.org/10.1021/jp411818j | *J. Phys. Chem. B* 2014, 118, 976−985

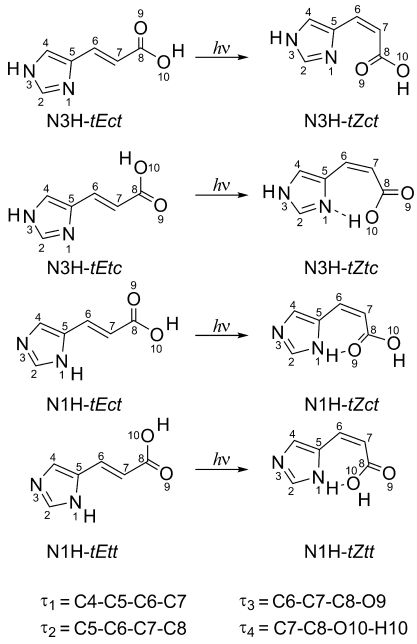

Figure 1. Structural formulas of the four isomers of urocanic acid considered in this work and their photoisomerization products. The designations of the isomers used in this work are given below the respective structures. The definition of the four torsion angles defining the isomers is given at the bottom.

Herein, we report on a systematic analysis of photochemical reaction paths in several rotamers and isomers of two tautomers of urocanic acid: the $E \rightarrow Z$ photoisomerization process of four E isomers, a radiationless deactivation process via proton transfer in an intramolecularly hydrogen-bonded Z isomer, a radiationless deactivation process via N−H bond elongation, and a radiationless deactivation process via ring-puckering of the imidazole moiety. We show that urocanic acid possesses the intrinsic ability to quench the energy of absorbed UV photons and dissipate this energy into heat. For each of the explored processes, we have located, optimized, and analyzed the relevant conical intersections and explored the reaction paths along the relevant singlet excited states. The systematic analysis of both tautomeric forms of neutral urocanic acid and of two rotamers of each of these tautomers sets our study apart from the majority of the previous less comprehensive computational studies on this system.

It is an established fact that ultrafast, that is, subpicosecond, photochemical reactions in the singlet manifold are mediated by critical points on the potential-energy surfaces, so-called conical intersections. These points are characterized by a complete breakdown of the Born−Oppenheimer approximation, which allows efficient energy transfer of electronic energy into vibrational energy. Exploring the structures of these conical intersections and the nuclear-displacement vectors of the so-called branching-space vectors—two nuclear-displacement vectors along which the degeneracy between the potential-energy surfaces is lifted in first order—is a necessary step to understand the photochemical reaction under study. Furthermore, the exploration of the topography of the lower potential-energy surface of a conical intersection can provide clues of the possible photoproducts that may be generated after the system has passed through the intersection.[33−36]

Triplet states may be of significance for the photochemical reactivity of urocanic acid in two respects. First, the existence of $n\pi^*$ and $\pi\pi^*$ excited states might allow an efficient intersystem crossing according to El-Sayed's rule.[33] Second, in its natural environment, urocanic acid is in contact with molecular oxygen and is thus able to undergo triplet-singlet energy-transfer and photosensitization reactions with triplet oxygen to form reactive oxygen species.[11] Dmitrenko et al. have suggested several mechanistic scenarios for the photoisomerization process involving intersystem crossings.[29] While aspects of the triplet photochemistry of this molecule are not yet resolved, we do not consider the role of triplet states in this work. It is a reasonable assumption that in the isolated system intersystem crossing to the triplet manifold cannot compete with the ultrafast processes occurring in the singlet manifold, which are the focus of this work. However, only quantitative calculations of the intersystem-crossing rates can definitively prove or disprove this assumption.

To map the photochemical reaction paths, one has to explore the relevant excited-state potential-energy surfaces from the Franck−Condon region vertically above the ground-state equilibrium geometry to the relevant conical intersections with the electronic ground state.[35]

2. RESULTS

2.1. Isomers and Conformers. We consider in this work four E isomers (cf. left column in Figure 1) that have been shown by Barbatti to contribute most significantly to the absorption spectrum of a mixture of eight E isomers.[32] The designations of the different isomers used in this work are described in the following. The protonation site of the imidazole moiety is specified by the prefix, either N3H or N1H. The torsion angles of four bonds are specified by the suffix, three of which are formally single bonds and are specified by the descriptors "*t*" for "trans" and "*c*" for "cis". The torsion angle of the isomerizing C=C bond is specified by the descriptors "*E*" and "*Z*". For example, the isomer N3H-*tEtc* is protonated at the N3 position of the imidazole moiety and exhibits a C4−C5−C6−C7 torsion angle of ∼180° (*t*), a C5−C6−C7−C8 torsion angle of ∼180° (*E*), a C6−C7−C8−O9 torsion angle of ∼180° (*t*), and a C7−C8−O10−H10 torsion angle of ∼0° (*c*). The photoisomerization of this isomer generates the N3H-*tZtc* isomer. The four isomers considered in this work and their photoisomerization products are given in Figure 1.

2.2. Vertical Excitation Energies. The vertical excitation energies and oscillator strengths of the lowest five singlet excited valence states computed at the MS-CASPT2 and the CC2 levels (cf. Computational Methods section) are given in Table 1. Vertical excitation energies of urocanic acid have been computed in the past using a number of electronic-structure methods.[19,23,24,26,28,29,32]

The results obtained at the CASPT2 and the CC2 levels agree surprisingly well. At both levels, the lowest $\pi\pi^*$ state, which in all cases is the HOMO→LUMO transition, possesses the largest oscillator strength. This is the spectroscopically absorbing state (the "bright" state) that accounts for the peak in the absorption spectrum. Barbatti found at the TDDFT level that the bright state of the N1H tautomers is red-shifted in comparison with the bright state of the N3H tautomers.[32] The present results confirm this pattern at both levels of theory.

The energetic order of the lowest $n\pi^*$ and $\pi\pi^*$ states shows a distinct pattern. At the CC2 level, the S_1 state of all N3H tautomers is an $n\pi^*$ state, while the S_2 state is a $\pi\pi^*$ state. For the N1H tautomers, this order is reversed. This pattern is also

dx.doi.org/10.1021/jp411818j | J. Phys. Chem. B 2014, 118, 976−985

Table 1. Vertical Excitation Energies (in eV) and Oscillator Strengths (in parentheses) of the Lowest Five Singlet Excited Valence States of Each of the Eight *E* and *Z* Isomers Considered in This Work[a]

	MS-CASPT2				
isomer	S_1	S_2	S_3	S_4	S_5
N3H-*tEct*	4.83 (0.3526)	5.14 (0.0006)	6.06 (0.0639)	6.47 (0.0012)	6.95 (0.0174)
N3H-*tEtc*	4.75 (0.0006)	4.99 (0.6985)	6.25 (0.0681)	6.42 (0.0010)	6.93 (0.0175)
N1H-*tEct*	4.39 (0.3761)	5.09 (0.0005)	6.09 (0.0044)	6.21 (0.1207)	6.45 (0.2532)
N1H-*tEtt*	4.48 (0.4928)	5.02 (0.0006)	6.10 (0.0045)	6.25 (0.1391)	6.47 (0.1779)
N3H-*tZct*	4.72 (0.0011)	4.78 (0.2858)	6.09 (0.0009)	6.10 (0.0606)	6.61 (0.0162)
N3H-*tZtc*	4.50 (0.0004)	5.75 (0.1401)	6.84 (0.0463)	7.02 (0.0133)	7.14 (0.0122)
N1H-*tZct*	4.05 (0.2798)	5.20 (0.0004)	5.72 (0.0013)	6.16 (0.1371)	6.26 (0.1702)
N1H-*tZtt*	4.31 (0.4416)	5.07 (0.0006)	5.92 (0.0024)	6.22 (0.1043)	6.37 (0.2589)
	CC2				
isomer	S_1	S_2	S_3	S_4	S_5
N3H-*tEct*	5.05 (0.0001)	5.18 (0.6547)	6.22 (0.0938)	6.24 (0.0010)	6.83 (0.1360)
N3H-*tEtc*	4.69 (0.0002)	5.25 (0.6130)	6.22 (0.0011)	6.27 (0.1236)	6.87 (0.0919)
N1H-*tEct*	4.80 (0.7309)	5.02 (0.0001)	5.64 (0.0001)	6.03 (0.0066)	6.78 (0.0008)
N1H-*tEtt*	4.83 (0.7504)	4.95 (0.0001)	5.66 (0.0001)	6.03 (0.0051)	6.81 (0.0008)
N3H-*tZct*	4.63 (0.0002)	5.16 (0.5578)	5.89 (0.0008)	6.24 (0.1051)	6.68 (0.0050)
N3H-*tZtc*	4.39 (0.0001)	5.51 (0.5244)	6.21 (0.1582)	6.37 (0.0335)	6.46 (0.0001)
N1H-*tZct*	4.39 (0.5209)	5.05 (0.0000)	5.41 (0.0000)	5.66 (0.0062)	6.78 (0.0368)
N1H-*tZtt*	4.62 (0.6221)	5.04 (0.0001)	5.46 (0.0000)	5.86 (0.0054)	6.85 (0.0888)

[a]Excitation energies were computed at the MS-CASPT2 and the CC2 levels. The color represents the physical nature of each excited state: red color denotes $n\pi^*$ states, and blue color denotes $\pi\pi^*$ states. For details, consult the Computational Methods section.

recognizable at the CASPT2 level, although one outlier exists. Higher-lying $n\pi^*$ states are found from 5.4 eV onward. Higher-lying $\pi\pi^*$ states are found from 6.0 eV onward and exhibit moderately large oscillator strengths at both levels of theory.

The agreement between the present CASPT2 results with the results on two specific isomers computed by Olivucci and coworkers is moderate, but this can be understood by technical differences between the calculations.[24] The present CC2 results are almost identical to the CC2 results on two specific isomers obtained by Barbatti (the only difference is the employed basis set).[32]

2.3. *E/Z*-Photoisomerization and $\pi\pi^*/S_0$ Conical Intersection. We explored the *E*/*Z* photoisomerization process for two rotamers of each of the N3H and N1H tautomers. These four species have been identified by Barbatti as the four species contributing most significantly to the UV absorption spectrum of (*E*)-urocanic acid in the gas phase.[32]

Figure 2 shows the potential-energy profiles of the electronic ground state, the lowest $n\pi^*$ state, and the lowest $\pi\pi^*$ state for the photoisomerization of the N3H-*tEtc*/*tZtc* isomers, computed along the linearly interpolated reaction path (cf. Computational Methods) from the ground-state equilibrium geometry of the *E* isomer via the $\pi\pi^*/S_0$ conical intersection to the ground-state equilibrium geometry of the *Z* isomer. In the Franck–Condon region of the *E* isomer, the S_1 state exhibits $n\pi^*$ character and the S_2 state exhibits $\pi\pi^*$ character. Along the reaction path for the photoisomerization process, the $n\pi^*$ state rises in energy, whereas the $\pi\pi^*$ state drops in energy and eventually reaches the conical intersection with the ground state. In this isomer, the $n\pi^*$ state drops again in energy below the lowest $\pi\pi^*$ state in the region of the *Z* isomer. (This is not the case in other isomers.) The *Z* isomer is slightly more stable in the ground state than the *E* isomer due to the formation of an intramolecular hydrogen bond between the imidazole and the carboxyl moieties. The topography of the $\pi\pi^*$ surface in urocanic acid will be compared with the potential-energy surface of the *V* state in ethylene in the Discussion and

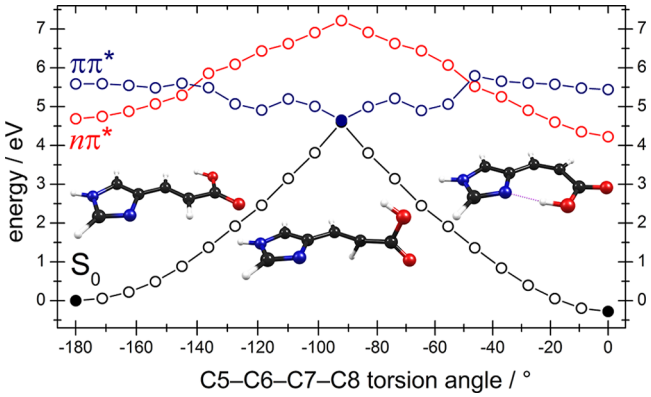

Figure 2. Energy profiles of the ground state, the $n\pi^*$ state, and the $\pi\pi^*$ state of the N3H-*tEtc* isomer along the photoisomerization reaction path computed at the MS-CASPT2 level. The profiles were obtained by two linear interpolations: the first interpolation was performed between the ground-state equilibrium geometry of the *E* isomer (full black circle at the lower left) and the optimized $\pi\pi^*/S_0$ conical intersection (full blue and black circles in the center); the second interpolation was performed between the conical intersection (center) and the ground-state equilibrium geometry of the *Z* isomer (full black circle at the lower right). The structures shown as insets are the ground-state equilibrium geometry of the *E* isomer (left), the $\pi\pi^*/S_0$ conical intersection for the *E*/*Z* photoisomerization process (center), and the ground-state equilibrium geometry of the *Z* isomer (right). For details, consult the Computational Methods section.

Conclusions section. It is seen in Figure 2 that a conical intersection between the $\pi\pi^*$ and $n\pi^*$ states exists approximately midway between the Franck–Condon region of the *E* and *Z* isomers and the $\pi\pi^*/S_0$ conical intersection. We were unsuccessful in optimizing this $\pi\pi^*/n\pi^*$ conical intersection. The energy profiles show that a barrier of ~0.8 eV separates the Franck–Condon region of the $n\pi^*$ state from the $\pi\pi^*/S_0$ conical intersection. Because of the use of a linearly interpolated reaction path, this value is an upper bound for the true barrier height.

The nuclear-displacement vectors of the branching-space vectors of the $\pi\pi^*/S_0$ conical intersection[34] for the N3H-*tEtc*/*tZtc* photoisomerization process are shown in Figure 3. The

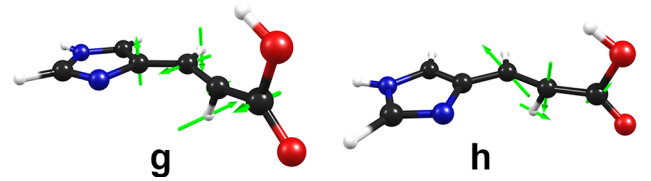

Figure 3. Nuclear-displacement vectors of the gradient-difference vector **g** and the nonadiabatic-coupling vector **h** of the $\pi\pi^*/S_0$ conical intersection for the *E*/*Z* photoisomerization process of the N3H-*tEtc* isomer shown in Figure 2. For details, consult the Computational Methods section.

gradient-difference vector **g** shows a clear isomerization displacement, while the nonadiabatic-coupling vector **h** shows skeletal-deformation displacements that primarily separate the atoms C6 and C7 and also includes a displacement of the C7–H atom that may lead to hydrogen migration. We were unable to obtain a geometry of this $\pi\pi^*/S_0$ conical intersection that did not exhibit this hydrogen-migration character.

A linear approximation of the potential-energy surfaces in the branching space in close proximity of the $\pi\pi^*/S_0$ conical

dx.doi.org/10.1021/jp411818j | J. Phys. Chem. B 2014, 118, 976–985

intersection is shown in Figure 4. The potential-energy surfaces of the ground state and the $\pi\pi^*$ state split symmetrically along the positive and the negative directions of the gradient-difference vector **g**, and the slope of the ground state is virtually equal along the two directions (cf. left part of Figure 4). This suggests that at this conical intersection the *E* and *Z* isomers are formed with equal probability. Along the second branching-space vector, the nonadiabatic-coupling vector **h**, the conical intersection is strongly tilted (cf. right part of Figure 4). These properties classify this conical intersection as a sloped intersection.[37] This topography is qualitatively similar to the topography of the corresponding $\pi\pi^*/S_0$ conical intersection in stilbene.[38]

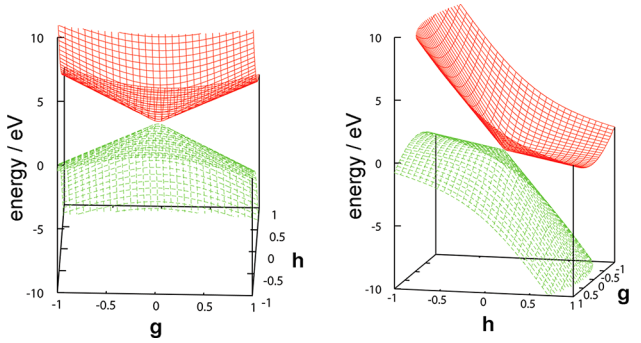

Figure 4. Linear approximation of the potential-energy surfaces of the ground state and the $\pi\pi^*$ state in the branching space of the $\pi\pi^*/S_0$ conical intersection shown in Figure 2 (shown from two perspectives) computed at the SA-CASSCF level. The gradient-difference vector **g** corresponds to the isomerization displacement, and the nonadiabatic-coupling vector **h** corresponds to a combination of skeletal-deformation displacements (cf. nuclear-displacement vectors of the branching-space vectors in Figure 3). For details, consult the Computational Methods section.

Figure 5 shows the potential-energy profiles of the electronic ground state, the lowest $n\pi^*$ state, and the lowest $\pi\pi^*$ state for the photoisomerization of the N1H-*tEct*/*tZct* isomers, computed along the linearly interpolated reaction path (cf. Computational Methods) from the ground-state equilibrium geometry of the *E* isomer via the $\pi\pi^*/S_0$ conical intersection to the ground-state equilibrium geometry of the *Z* isomer. Because of the intramolecular hydrogen bond in the *Z* isomer, which perturbs the lone-pair orbital of the oxygen atom of the carbonyl moiety, the $n\pi^*$ state, which originates from the excitation of an electron from the lone-pair orbital of the carbonyl oxygen atom to the π system (the $n\pi^*$ state originating from the lone-pair orbital of the imidazole nitrogen atom is higher in energy for all isomers), remains the S_2 state in the Franck−Condon region of the *Z* isomer, in contrast with the Franck−Condon region of the *E* isomer. The $\pi\pi^*/S_0$ conical intersection exhibits a distinct pyramidalization in the H7−C7−C8 group. The nuclear-displacement vectors of the branching-space vectors of this $\pi\pi^*/S_0$ conical intersection are shown in Figure S1 in the Supporting Information. Here the nonadiabatic-coupling vector **h** shows a clear isomerization displacement. In the Franck−Condon region of the *E* isomer, the $n\pi^*$ and $\pi\pi^*$ states are nearly degenerate (cf. Figure 5), and the conical intersection of the $\pi\pi^*$ and $n\pi^*$ states occurs rather early on the interpolated path.

The energy profiles along the photoisomerization reaction path of another rotamer of each of the N3H and N1H

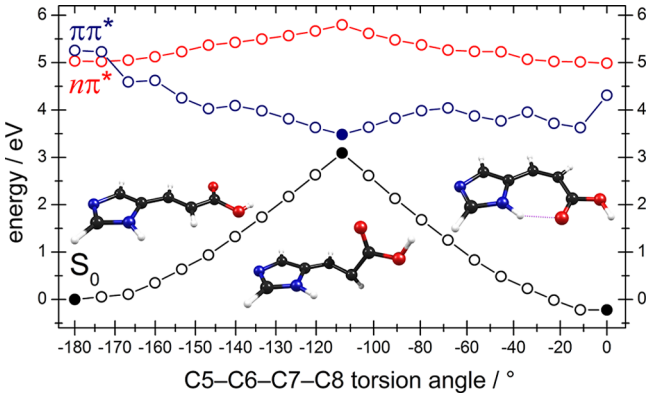

Figure 5. Energy profiles of the ground state, the $n\pi^*$ state, and the $\pi\pi^*$ state of the N1H-*tEct* isomer along the photoisomerization reaction path computed at the MS-CASPT2 level. The profiles were obtained by two linear interpolations: the first interpolation was performed between the ground-state equilibrium geometry of the *E* isomer (full black circle at the lower left) and the optimized $\pi\pi^*/S_0$ conical intersection (full blue and black circles in the center); the second interpolation was performed between the conical intersection (center) and the ground-state equilibrium geometry of the *Z* isomer (full black circle at the lower right). The structures shown as insets are the ground-state equilibrium geometry of the *E* isomer (left), the $\pi\pi^*/S_0$ conical intersection for the *E*/*Z* photoisomerization process (center), and the ground-state equilibrium geometry of the *Z* isomer (right). For details, consult the Computational Methods section.

tautomers along with the nuclear-displacement vectors of the branching-space vectors of the $\pi\pi^*/S_0$ conical intersections are given in Figures S2−S5 in the Supporting Information.

2.4. $\pi\pi^*/n\pi^*$ Conical Intersections of Planar *E* Isomers. We also optimized the geometry of the conical intersection of planar structure between the lowest $\pi\pi^*$ and $n\pi^*$ states for each of the four *E* isomers. We emphasize that these intersections are different from the ones previously mentioned, where the $\pi\pi^*/n\pi^*$ intersection occurs along the photoisomerization reaction path. At the latter intersections, the structures are not planar but exhibit a moderate twist about the central C=C double bond. The geometry of the planar $\pi\pi^*/n\pi^*$ conical intersection for the N3H-*tEct* isomer is shown in Figure 6, where the nuclear-displacement vectors of the

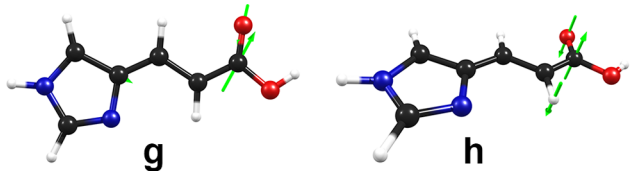

Figure 6. Nuclear-displacement vectors of the gradient-difference vector **g** and the nonadiabatic-coupling vector **h** of the planar conical intersection between the $\pi\pi^*$ state and the $n\pi^*$ state of the N3H-*tEct* isomer. For details, consult the Computational Methods section.

branching-space vectors are indicated. The corresponding intersections for the other three *E* isomers are shown in Figures S6−S8 in the Supporting Information. These intersections differ from the ground-state equilibrium geometries mainly in the bond lengths along the C4−C5−C6−C7−C8 chain. Along these four bonds, a distinct bond-length alternation pattern can be recognized: C−C bonds that are formally a single bond in the ground state are ∼0.1 Å shorter, and C=C bonds that are formally a double bond in the ground

dx.doi.org/10.1021/jp411818j | J. Phys. Chem. B 2014, 118, 976−985

state are ~0.1 Å longer. This can be understood by the fact that in the $\pi\pi^*$ state a π^* orbital is occupied that exhibits an inverse bonding/antibonding pattern compared with the highest occupied π orbital in the ground state. The nuclear-displacement vectors of the branching-space vectors of these four $\pi\pi^*/n\pi^*$ conical intersections (cf. Figure 6 and Figures S6–S8 in the SI) show that the gradient-difference vector **g** exhibits in all cases in-plane nuclear displacements that preserve the C_s symmetry of the molecule, while the nonadiabatic-coupling vector **h** exhibits out-of-plane nuclear displacements that break the C_s symmetry. Symmetry requires an out-of-plane displacement for an A' state (the $\pi\pi^*$ state) to couple with an A'' state (the $n\pi^*$ state).[34] A comparison of the geometrical parameters of the $\pi\pi^*/n\pi^*$ conical intersection shown in Figure 6 with the parameters of the equilibrium geometry of the lowest $\pi\pi^*$ state of the N3H-*tEct* isomer optimized by Olivucci and coworkers at the CASSCF level[24] shows that the conical intersection is structurally very similar to the $\pi\pi^*$ minimum, which also exhibits a very clear bond-length alternation pattern compared with the ground-state equilibrium geometry. We expect this similarity to hold for the other isomers as well. This suggests that very close to the $\pi\pi^*$ minima an extended intersection seam between the $\pi\pi^*$ and $n\pi^*$ states exists. Because of these reasons, it can be expected that after photoexcitation of any *E* isomer to the bright $\pi\pi^*$ state the system can convert to the $n\pi^*$ state in an ultrafast manner (i.e., on a femtosecond time scale). We expect that analogous intersections exist for the *Z* isomers.

2.5. Excited-State Proton Transfer in an Intramolecularly Hydrogen-Bonded *Z* Isomer. The N3H-*tZtc* isomer exhibits a strong intramolecular hydrogen bond,[21,22] where the carboxyl moiety acts as the hydrogen-bond donor. Figure 7 shows the potential-energy profiles of the ground state, the $n\pi^*$ state, and the $\pi\pi^*$ state for the linearly interpolated reaction path from the ground-state equilibrium geometry of the N3H-*tZtc* isomer to the $n\pi^*/S_0$ conical intersection. The intramolecular hydrogen bond can dissipate excess electronic energy via an electron-driven proton transfer. Upon absorption of a photon, the system is excited to the $\pi\pi^*$ state from which it can reach the potential-energy surface of the $n\pi^*$ state via internal conversion, as discussed in the previous subsection. In the $n\pi^*$ state, an electron is excited from the lone-pair orbital of the oxygen atom of the carbonyl moiety to the π system, which is partially located on the imidazole moiety. Therefore, the $n\pi^*$ state exhibits a clear charge-transfer character. A graphical representation of the molecular orbitals involved in the description of the $n\pi^*$ state as well as the weight of the two dominant configurations is given in Figure 8. Upon population of the $n\pi^*$ state, the carboxyl moiety becomes more acidic and the imidazole moiety becomes more basic than in the ground state (due to the translocation of electron density from the carboxyl to the imidazole moiety, cf. Figure 8). Therefore, the proton of the carboxyl moiety may follow the electron. The resulting stabilization of the $n\pi^*$ state combined with an elongation of the C=O bond length leads to an $n\pi^*/S_0$ conical intersection. The structure of the conical intersection shown as an inset in Figure 7 exhibits an elongated C=O bond. One can see that the energy of the $n\pi^*$ state along the reaction path from the ground-state equilibrium geometry to the $n\pi^*/S_0$ conical intersection does not involve a barrier but passes through a local minimum. This minimum indicates that in the $n\pi^*$ state a zwitterionic structure, where the proton is attached to the imidazole moiety, is more stable than the neutral form (again due to the translocation of electron density). Because the energy of the $n\pi^*/S_0$ conical intersection is well below the vertical excitation energy of the $\pi\pi^*$ state, the system should possess sufficient internal energy to reach the $n\pi^*/S_0$ conical intersection. The nuclear-displacement vectors of the branching-space vectors of the $n\pi^*/S_0$ conical intersection are shown in Figure S9 in the Supporting Information. It is noteworthy that the gradient-difference vector **g** is C_s-symmetric, that is, it does not break the planar symmetry of the molecule, while the nonadiabatic-coupling vector **h** does break the C_s symmetry and exhibits an out-of-plane displacement mainly located at the carboxyl moiety. The **g** vector shows a clear opposing

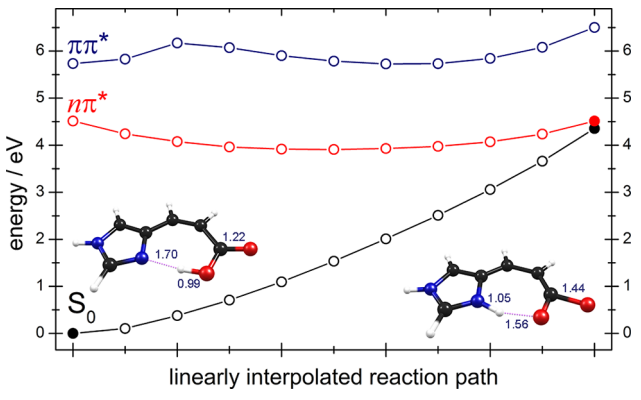

Figure 7. Energy profiles of the ground state, the $n\pi^*$ state, and the $\pi\pi^*$ state of the N3H-*tZtc* isomer along the reaction path for radiationless deactivation via electron-driven proton transfer computed at the MS-CASPT2 level. The profiles were obtained by linear interpolation between the ground-state equilibrium geometry of the *Z* isomer (full black circle at the lower left) and the optimized $n\pi^*/S_0$ conical intersection (full red and black circles at the right). The structures shown as insets are the ground-state equilibrium geometry (left) and the $n\pi^*/S_0$ conical intersection (right) with selected bond lengths (in angstroms). For details, consult the Computational Methods section.

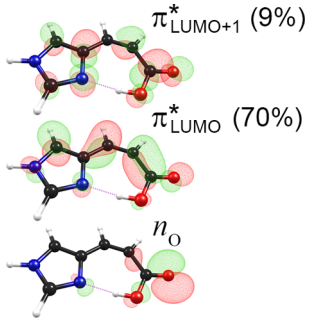

Figure 8. Molecular orbitals of the intramolecularly hydrogen-bonded N3H-*tZtc* isomer involved in the description of the lowest $n\pi^*$ state. Shown are the lone-pair orbital of the carbonyl oxygen atom (n_O) and two π^* orbitals (the LUMO and the LUMO+1). The values in parentheses specify the weight of the excited configurations $n_O \rightarrow$ LUMO and $n_O \rightarrow$ LUMO+1 in the MS-CASPT2 wave function for the computation of the vertical excitation energies for this isomer (which are given in Table 1). The translocation of electron density from the lone-pair orbital to the π-orbital system rationalizes the charge-transfer character of the $n\pi^*$ state and the existence of an electron-driven proton-transfer process. For details, consult the Computational Methods section.

dx.doi.org/10.1021/jp411818j | J. Phys. Chem. B 2014, 118, 976–985

displacement of the C8 and O9 atoms, which indicates that this conical intersection mediates the deactivation by transferring electronic energy into vibrational modes involving the carboxyl moiety.

2.6. Deactivation Mechanisms Inherent to the Imidazole Moiety. We also considered the deactivation mechanisms inherent to the imidazole moiety. Imidazole itself mainly deactivates via two mechanisms: the N−H stretching and ring-puckering processes. These processes have been found to be the dominating deactivation channels in imidazole.[39−42]

Figure 9 shows the potential-energy profiles of the ground state, the $\pi\pi^*$ state, and the $\pi\sigma^*_{NH}$ state of the N3H-*tEct* isomer

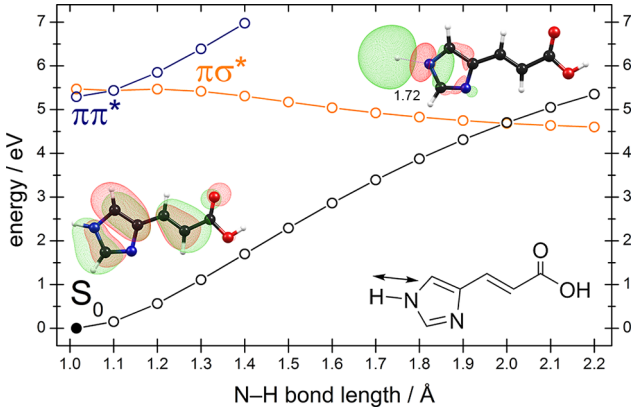

Figure 9. Energy profiles of the ground state, the $\pi\pi^*$ state, and the $\pi\sigma^*_{NH}$ state of the N3H-*tEct* isomer along the N−H stretching coordinate computed at the MS-CASPT2 level. The profiles were obtained by a rigid scan originating from the ground-state equilibrium geometry (full black circle at the lower left). The structures shown as insets are the ground-state equilibrium geometry with the highest-occupied π orbital and the structure of the $\pi\sigma^*_{NH}/S_0$ conical intersection with the value of the N−H internuclear distance (in angstroms) and the σ^*_{NH} orbital. The two orbitals shown are the active orbitals used for the optimization of the conical intersection at the SA2-CASSCF(2,2) level. For details, consult the Computational Methods section.

along the N−H stretching coordinate obtained by a rigid scan starting from the ground-state equilibrium geometry (cf. Computational Methods). The reaction path from the Franck−Condon region of the $\pi\pi^*$ state to the conical intersection between the $\pi\sigma^*$ state and the ground state is essentially barrierless. The two orbitals shown as insets are the two active orbitals used in the optimization of the conical intersection at the SA2-CASSCF(2,2) level: the highest occupied π orbital and the σ^*_{NH} orbital. This mechanism can mediate radiationless deactivation or hydrogen detachment. In the former case, the electronic energy is converted into vibrational motion mainly of the N−H stretching vibration. In the latter case, the electronic energy is converted into kinetic energy of the ejected hydrogen atom.

In the CASPT2 energy profiles, the crossing between the $\pi\sigma^*$ state and the ground state occurs at 2.0 Å. The optimized σ^*_{NH}/S_0 conical intersection (optimized at the CASSCF level) exhibits an N−H nuclear distance of 1.72 Å. Because dynamic electron correlation is not included at the CASSCF level, the location of conical intersections associated with hydrogen-detachment processes is usually found at shorter X−H distances than suggested by the CASPT2 energy profiles. The reason for this is the differential correlation effect, that is, the second-order perturbation correction affects the two electronic states in a different manner.[43]

The nuclear-displacement vectors of the branching-space vectors for the $\pi\sigma^*_{NH}/S_0$ conical intersection shown in Figure 9 are shown in Figure S10 in the Supporting Information. The gradient-difference vector **g** shows an opposing displacement of the nitrogen and hydrogen atoms, while the nonadiabatic-coupling vector **h** is an out-of-plane displacement involving mainly the imidazole moiety.

Inspection of the energetic order of the virtual Hartree−Fock orbitals suggests the existence of additional channels for X−H dissociation: the C4−H σ^* orbital is the second lowest σ^* orbital, and the O−H σ^* orbital is the third lowest. Therefore, photodissociation of hydrogen atoms originating from O−H and C−H bond dissociation can be expected for excitation energies above 6 eV.

Figure 10 shows the potential-energy profiles of the ground state and the $\pi\pi^*$ state for the linearly interpolated reaction

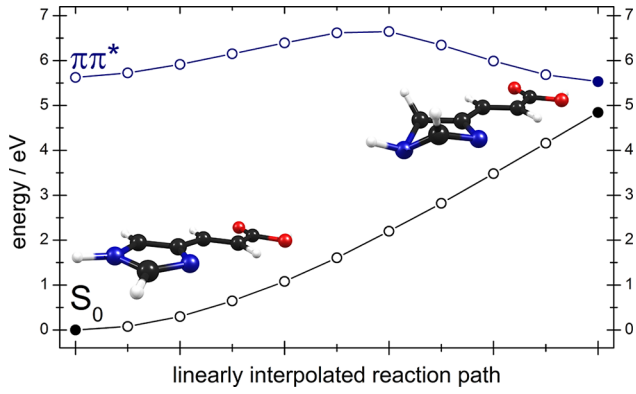

Figure 10. Energy profiles of the ground state and the $\pi\pi^*$ state of the N3H-*tEct* isomer along the reaction path for the NH ring-puckering deactivation process, computed at the MS-CASPT2 level. The profiles were obtained by linear interpolation between the ground-state equilibrium geometry of the *E* isomer (full black circle at the lower left) and the optimized $\pi\pi^*/S_0$ conical intersection (full blue and black circles at the right). The structures shown as insets are the ground-state equilibrium geometry (left) and the structure of the conical intersection for the NH ring-puckering process (right). For details, consult the Computational Methods section.

path from the ground-state equilibrium geometry of the N3H-*tEct* isomer to the $\pi\pi^*/S_0$ conical intersection for the NH ring-puckering deactivation process inherent to the imidazole moiety. The energy profile of the linearly interpolated reaction path exhibits a barrier of ~1.0 eV, which may be absent in the energy profile of the minimum-energy path. The energetic location of this $\pi\pi^*/S_0$ conical intersection with respect to the energy of the ground-state equilibrium geometry is roughly the same as that in imidazole.[39] The branching-space vectors of the $\pi\pi^*/S_0$ conical intersection are shown in Figure S11 in the Supporting Information. Both vectors show displacements located on the imidazole moiety. The two mechanisms inherent to the imidazole moiety that we have presented in this subsection should exist in all *E* and *Z* isomers.

3. DISCUSSION AND CONCLUSIONS

We have computed at two levels of theory the singlet vertical excitation energies of the four *E* isomers of urocanic acid that have been shown by Barbatti to contribute most significantly to the UV absorption spectrum in the gas phase[32] as well as of the

dx.doi.org/10.1021/jp411818j | J. Phys. Chem. B 2014, 118, 976−985

four *Z* isomers that are formed via photoisomerization of these four *E* isomers. We have explored the relevant singlet excited-state potential-energy functions for the *E*/*Z* photoisomerization of the four *E* isomers. We have optimized the relevant conical intersections between the $\pi\pi^*$ state and the ground state for the photoisomerization process and have analyzed the branching-space vectors of the conical intersections of these four isomers. The potential-energy surfaces in close proximity of the $\pi\pi^*/S_0$ conical intersection for the photoisomerization process have been analyzed for one isomer. We have shown that $\pi\pi^*/n\pi^*$ conical intersections with twisted geometries exist along the reaction path for the photoisomerization process. We have also shown that additional conical intersections of planar structure between the $\pi\pi^*$ and $n\pi^*$ states exist that are structurally very similar to the $\pi\pi^*$ minima. We have identified three further mechanisms for radiationless excited-state deactivation, some of which are available to all *E* and *Z* isomers (the N−H stretching and the ring-puckering mechanisms inherent to the imidazole moiety), while others are available only in specific isomers (i.e., the electron-driven proton-transfer mechanism in the intramolecularly hydrogen-bonded N3H-*tZtc* isomer). These findings suggest that urocanic acid possesses the intrinsic ability to act as a natural sunscreen, that is, a UV filter. The relative quantum yields of these competing deactivation processes need to be determined via nonadiabatic-dynamics simulations[40,44−51] or via spectroscopic techniques.[41,42,52] The fluorescence excitation and emission spectra of urocanic acid in a supersonic jet reported by Ryan and Levy are, unfortunately, not tautomer-/conformer-resolved.[18] Because of this shortcoming, it is not possible to make specific assignments of these spectra.

The potential-energy function of the bright $\pi\pi^*$ state along the photoisomerization reaction path may be compared with the potential-energy functions of the relevant singlet excited states in ethylene. The $\pi\pi^*$ state in urocanic acid, which intersects with the ground state in the torsion-angle region about −90°, shows similarity to the *V* state in ethylene. The energetic location of the $\pi\pi^*$ state in the Franck−Condon region of the *E* and *Z* isomers is significantly lower than the energetic location of the *V* state in ethylene: the bright $\pi\pi^*$ state is located at ∼5 eV in urocanic acid compared with ∼8 eV for the *V* state. The torsional energy profile of the lowest $\pi\pi^*$ state in urocanic exhibits a gentle slope similar to the *V* state in ethylene. The lowest $\pi\pi^*$ state in urocanic acid is also primarily a HOMO→LUMO transition as is the *V* state in ethylene.[53]

One feature of the excited-state dynamics of urocanic acid has been extensively discussed in the literature. This feature is the unusual wavelength-dependent quantum yield for *E*→*Z* photoisomerization. When urocanic acid absorbs UV light at the red tail of its absorption profile, at ∼310 nm, the photoisomerization quantum yield peaks at ∼50%. When it absorbs at the peak of its absorption spectrum, at ∼266 nm, the quantum yield for *E*→*Z* photoisomerization drops to a mere 5%.[1−3,5] Two explanations have been proposed for this behavior.[1−3,5] The first is the existence of several rotamers that are in equilibrium in the ground state and absorb at different wavelengths.[19,32] The second is the involvement of more than one electronically excited singlet state in the photoreactivity.[2,7−9,11]

Figure 11 shows a compilation of the vertical excitation energies of the lowest $n\pi^*$ state and the lowest $\pi\pi^*$ state at both the CASPT2 (cf. Figure 11 a) and the CC2 (cf. Figure 11 b) level of theory for the eight isomers considered in this work.

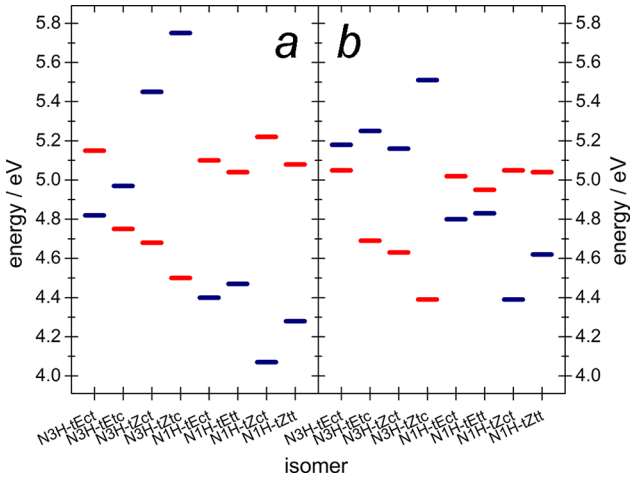

Figure 11. Compilation of the vertical excitation energies of the lowest $n\pi^*$ and $\pi\pi^*$ states of all eight isomers at the CASPT2 level (a) and at the CC2 level (b). Red bars indicate the vertical excitation energy of the $n\pi^*$ state, and blue bars indicate the energy of the $\pi\pi^*$ state of each isomer.

While there are a few differences between the two levels of theory, a clear trend can be recognized. For the following discussion, we consider the CC2 results (cf. Figure 11 b). While the N1H tautomers can be excited to the $\pi\pi^*$ state with photons of energies below 5.1 eV, the N3H tautomers exhibit excitation energies above 5.1 eV. With photons below 5.1 eV, only the N1H tautomers can be excited to the $\pi\pi^*$ state, and all photochemical reaction processes outlined in this work are energetically accessible in these tautomers. Because the $\pi\pi^*$ state is the S_1 state for the N1H tautomers, radiationless deactivation processes compete with the *E*/*Z* photoisomerization process. For the N3H tautomers, the picture is fundamentally different because the $\pi\pi^*$ state is the S_2 state for these tautomers. For photon energies below 5.1 eV, the N3H tautomers can be excited to the $n\pi^*$ state by intensity-borrowing from the higher $\pi\pi^*$ state. From the potential-energy surface of the $n\pi^*$ state, however, only the photoisomerization process is energetically accessible, while the other radiationless deactivation processes are not accessible. Only for excitation energies above 5.1 eV do these processes become accessible in the N3H tautomers and compete with the photoisomerization process. This suggests that the unusual wavelength-dependent quantum yield for *E*/*Z* photoisomerization originates in the ordering of the $n\pi^*$ and the $\pi\pi^*$ states in the N3H tautomers. This also suggests that the N1H tautomers are not responsible for the wavelength-dependent quantum yield. It should be noted, though, that this picture explains the wavelength-dependent quantum yield for *E*/*Z* photoisomerization in the gas phase, which has not been experimentally determined.

In solution, $n\pi^*$ states are known to undergo a blue shift.[33] It is therefore likely that in solvated urocanic acid the lowest $n\pi^*$ state will be higher in energy than the bright $\pi\pi^*$ state in the Franck−Condon region for all tautomers, isomers, and rotamers. Thus, the reversed ordering of these states that is found for N3H tautomers in the gas phase may not be the origin of the unusual wavelength-dependent quantum yield for *E*/*Z* photoisomerization in solution. Instead, it may result from the tautomeric equilibrium and the different UV-absorption profiles of the N3H and N1H tautomers.

dx.doi.org/10.1021/jp411818j | *J. Phys. Chem. B* 2014, 118, 976−985

The next step to advance the understanding of the complex photochemistry of urocanic acid is to perform nonadiabatic trajectory-surface-hopping dynamics simulations of the isolated molecule. With the present work we have paved the way for such dynamics studies because insight into the relevant reaction mechanisms and the topography of the potential-energy surfaces of the relevant excited electronic states is a crucial prerequisite. Furthermore, the above-mentioned difficulties in relating the computational results on the isolated molecule with the experimental findings obtained in solution call for future computational studies that include solvation effects.

We hope that the present study may terminate the recent calm in the research on urocanic acid and will revive the interest that this fascinating biomolecule deserves in view of its physiological significance and its unusual photochemical properties.

4. COMPUTATIONAL METHODS

The ground-state equilibrium geometries were optimized without imposing any symmetry restrictions with the second-order Møller−Plesset (MP2) method and the cc-pVDZ basis set (MP2/cc-pVDZ) using the Turbomole 6.3.1 program package.[54]

Vertical excitation energies were obtained without imposing any symmetry restrictions by single-point calculations using multistate second-order perturbation theory on top of a state-averaged complete-active-space self-consistent-field reference wave function (MS-CASPT2//SA-CASSCF). The cc-pVDZ basis set and a level shift of 0.2 were used. These calculations were performed with the Molcas 7.6 program package.[55] Details of the state-averaging and the composition of the active space are given in the Supporting Information. The vertical excitation energies were also calculated at the approximate second-order coupled-cluster (CC2) level. Here, the cc-pVDZ basis was used as well. These calculations were performed with the Turbomole 6.3.1 program package.[54]

Minimum-energy conical intersections were optimized with the state-averaged complete-active-space self-consistent-field method and the cc-pVDZ basis set (SA-CASSCF/cc-pVDZ) using the Columbus 7.0 program package.[56] Details of the CASSCF parameters used for the optimization of the various conical intersections presented throughout the article are given in the Supporting Information. The data for the nuclear-displacement vectors of the orthogonalized branching-space vectors (the gradient-difference vector **g** and the nonadiabatic-coupling vector **h**) of the optimized conical intersections as well as on the linear approximation of the potential-energy surfaces in close proximity of the conical intersection for the photoisomerization process of the N3H-*tEtc* isomer shown in Figure 4 were also obtained from the Columbus package.

The reaction paths from the Franck−Condon regions to the relevant S_1/S_0 conical intersections were constructed by linear interpolations in internal coordinates without imposing any symmetry constraints. The energy profiles were obtained by MS-CASPT2//SA-CASSCF/cc-pVDZ single-point energy calculations along the interpolated paths. Only for the construction of the reaction path for the N−H hydrogen-detachment process was a rigid scan under C_s symmetry constraint for the wave functions and geometries and the aug-cc-pVDZ basis set used. Details of the CASSCF parameters (number of averaged states as well as size and composition of the active space) of the reference wave functions used for the MS-CASPT2 calculations can be found in the Supporting Information.

■ ASSOCIATED CONTENT

Supporting Information

Energy profiles for the photoisomerization process of the N3H-*tEct*/*tZct* and the N1H-*tEtt*/*tZtt* isomers. Nuclear-displacement vectors of the branching-space vectors of the remaining $\pi\pi^*/S_0$ conical intersections for the photoisomerization processes, of the planar $\pi\pi^*/n\pi^*$ conical intersections, of the $n\pi^*/S_0$ conical intersection for the electron-driven proton-transfer process, of the $\pi\sigma^*_{NH}/S_0$ conical intersection for the N−H stretching process, and of the $\pi\pi^*/S_0$ conical intersection for the ring-puckering process of the imidazole moiety. Description of technical details of the employed computational methods. Cartesian coordinates of all optimized ground-state equilibrium geometries and all conical intersections. This material is available free of charge via the Internet at http://pubs.acs.org.

■ AUTHOR INFORMATION

Corresponding Author

*E-mail: deniz.tuna@ch.tum.de. Tel: +49 89 289 13610.

Notes

The authors declare no competing financial interest.

■ ACKNOWLEDGMENTS

D.T. is grateful for a Ph.D. fellowship granted by the International Max Planck Research School of Advanced Photon Science (IMPRS-APS) and for support by the TUM Graduate School. A.L.S. acknowledges a grant by the National Science Center of Poland (grant no. N N202 126337). This work was partially supported by the Cluster of Excellence "Munich-Centre for Advanced Photonics" (MAP) of the Deutsche Forschungsgemeinschaft (DFG).

■ REFERENCES

(1) Mohammad, T.; Morrison, H.; HogenEsch, H. Urocanic Acid Photochemistry and Photobiology. *Photochem. Photobiol.* **1999**, *69*, 115−135.

(2) Simon, J. D. Spectroscopic and Dynamic Studies of the Epidermal Chromophores *trans*-Urocanic Acid and Eumelanin. *Acc. Chem. Res.* **2000**, *33*, 307−313.

(3) Gibbs, N. K.; Tye, J.; Norval, M. Recent Advances in Urocanic Acid Photochemistry, Photobiology and Photoimmunology. *Photochem. Photobiol. Sci.* **2008**, *7*, 655−667.

(4) Gibbs, N. K.; Norval, M. Urocanic Acid in the Skin: A Mixed Blessing? *J. Invest. Dermatol.* **2011**, *131*, 14−17.

(5) Morrison, H.; Bernasconi, C.; Pandey, G. A Wavelength Effect on Urocanic Acid *E*/*Z* Photoisomerization. *Photochem. Photobiol.* **1984**, *40*, 549−550.

(6) Laihia, J. K.; Lemmetyinen, H.; Pasanen, P.; Jansén, C. T. Establishment of a Kinetic Model for Urocanic Acid Photoisomerization. *J. Photochem. Photobiol., B* **1996**, *33*, 211−217.

(7) Li, B.; Hanson, K. M.; Simon, J. D. Primary Processes of the Electronic Excited States of *trans*-Urocanic Acid. *J. Phys. Chem. A* **1997**, *101*, 969−972.

(8) Hanson, K. M.; Li, B.; Simon, J. D. A Spectroscopic Study of the Epidermal Ultraviolet Chromophore *trans*-Urocanic Acid. *J. Am. Chem. Soc.* **1997**, *119*, 2715−2721.

(9) Hanson, K. M.; Simon, J. D. The Origin of the Wavelength-Dependent Photoreactivity of *trans*-Urocanic Acid. *Photochem. Photobiol.* **1998**, *67*, 538−540.

(10) Kammeyer, A.; Eggelte, T. A.; Bos, J. D.; Teunissen, M. B. M. Urocanic Acid Isomers are Good Hydroxyl Radical Scavengers: A

Comparative Study with Structural Analogues and with Uric Acid. *Biochim. Biophys. Acta* **1999**, *1428*, 117−120.
(11) Haralampus-Grynaviski, N.; Ransom, C.; Ye, T.; Rôzanowska, M.; Wrona, M.; Sarna, T.; Simon, J. D. Photogeneration and Quenching of Reactive Oxygen Species by Urocanic Acid. *J. Am. Chem. Soc.* **2002**, *124*, 3461−3468.
(12) Brookman, J.; Chaćon, J. N.; Sinclair, R. S. Some Photophysical Studies of *cis*- and *trans*-Urocanic Acid. *Photochem. Photobiol. Sci.* **2002**, *1*, 327−332.
(13) Menon, E. L.; Morrison, H. Formation of Singlet Oxygen by Urocanic Acid by UVA Irradiation and Some Consequences Thereof. *Photochem. Photobiol.* **2002**, *75*, 565−569.
(14) Schwarzinger, B.; Falk, H. Concerning the Photodiastereomerization and Protic Equilibria of Urocanic Acid and its Complex with Human Serum Albumin. *Monatsh. Chem.* **2004**, *135*, 1297−1304.
(15) Wallis, R. A.; Smith, G. J.; Dunford, C. L. The Effect of Molecular Environment on the Photoisomerization of Urocanic Acid. *Photochem. Photobiol.* **2004**, *80*, 257−261.
(16) Baier, J.; Maisch, T.; Engel, E.; Landthaler, M.; Bäumler, W. Singlet Oxygen Generation by UVA Light Exposure of Endogenous Photosensitizers. *Biophys. J.* **2006**, *91*, 1452−1459.
(17) Egawa, M.; Nomura, J.; Iwaki, H. The Evaluation of the Amount of *cis*- and *trans*-Urocanic Acid in the Stratum Corneum by Raman Spectroscopy. *Photochem. Photobiol. Sci.* **2010**, *9*, 730−733.
(18) Ryan, W. L.; Levy, D. H. Electronic Spectroscopy and Photoisomerization of *trans*-Urocanic Acid in a Supersonic Jet. *J. Am. Chem. Soc.* **2001**, *123*, 961−966.
(19) Shukla, M. K.; Mishra, P. C. Electronic Spectra, Structure and Photoisomerization of Urocanic Acid. *Spectrochim. Acta* **1995**, *51A*, 831−838.
(20) Lahti, A.; Hotokka, M.; Neuvonen, K.; Äyräs, P. A Theoretical Study of the Conformers of *trans*- and *cis*-Urocanic Acid. *J. Mol. Struct.: THEOCHEM* **1995**, *331*, 169−179.
(21) Lahti, A.; Hotokka, M.; Neuvonen, K.; Äyräs, P. Quantum-Chemical Gas-Phase Calculations on the Protonation Forms of *trans*- and *cis*-Urocanic Acid. *Struct. Chem.* **1997**, *8*, 331−342.
(22) Lahti, A.; Hotokka, M.; Neuvonen, K.; Karlström, G. Quantum Chemical Calculations on the Intramolecular Hydrogen Bond of *cis*-Urocanic Acid. *J. Mol. Struct.: THEOCHEM* **1998**, *452*, 185−202.
(23) Lahti, A.; Hotokka, M.; Neuvonen, K.; Karlström, G. A CASSCF Study on the Lowest $\pi \rightarrow \pi^*$ Excitation of Urocanic Acid. *Int. J. Quantum Chem.* **1999**, *72*, 25−37.
(24) Page, C. S.; Merchán, M.; Serrano-Andrés, L.; Olivucci, M. A Theoretical Study of the Low-Lying Excited States of *trans*- and *cis*-Urocanic Acid. *J. Phys. Chem. A* **1999**, *103*, 9864−9871.
(25) Page, C. S.; Olivucci, M.; Merchán, M. A Theoretical Study of the Low-Lying States of the Anionic and Protonated Ionic Forms of Urocanic Acid. *J. Phys. Chem. A* **2000**, *104*, 8796−8805.
(26) Danielsson, J.; Uličný, J.; Laaksonen, A. A TD-DFT Study of the Photochemistry of Urocanic Acid in Biologically Relevant Ionic, Rotameric, and Protomeric Forms. *J. Am. Chem. Soc.* **2001**, *123*, 9817−9821.
(27) Danielsson, J.; Söderhall, J. A.; Laaksonen, A. Hydration Structure and Conformational Dynamics of Urocanic Acid: A Computer Simulation Study. *Mol. Phys.* **2002**, *100*, 1873−1886.
(28) Danielsson, J.; Laaksonen, A. Gas Phase Photoisomerization of Urocanic Acid − A Theoretical Study. *Chem. Phys. Lett.* **2003**, *370*, 625−630.
(29) Dmitrenko, O.; Reischl, W.; Bach, R. D.; Spanget-Larsen, J. TD-DFT Computational Insight into the Origin of Wavelength-Dependent *E*/*Z* Photoisomerization of Urocanic Acid. *J. Phys. Chem. A* **2004**, *108*, 5662−5669.
(30) Shen, L.; Ji, H.-F. Theoretical Investigation of the Photosensitization Mechanisms of Urocanic Acid. *J. Photochem. Photobiol., B* **2008**, *91*, 96−98.
(31) Tiwari, S.; Mishra, P. C. Urocanic Acid as an Efficient Hydroxyl Radical Scavenger: A Quantum Theoretical Study. *J. Mol. Model.* **2011**, *17*, 59−72.
(32) Barbatti, M. The Role of Tautomers in the UV Absorption of Urocanic Acid. *Phys. Chem. Chem. Phys.* **2011**, *13*, 4686−4692.
(33) Klessinger, M.; Michl, J. *Excited States and Photochemistry of Organic Molecules*; VCH Publishers: New York, 1995.
(34) *Conical Intersections: Electronic Structure, Dynamics & Spectroscopy*; Domcke, W., Yarkony, D. R., Köppel, H., Eds.; World Scientific Publishing: Singapore, 2004.
(35) *Computational Photochemistry*; Olivucci, M., Ed.; Elsevier: Amsterdam, 2005.
(36) *Conical Intersections: Theory, Computation and Experiment*; Domcke, W., Yarkony, D. R., Köppel, H., Eds.; World Scientific Publishing: Singapore, 2011.
(37) Atchity, G. J.; Xantheas, S. S.; Ruedenberg, K. Potential Energy Surfaces Near Intersections. *J. Chem. Phys.* **1991**, *95*, 1862−1876.
(38) Quenneville, J.; Martínez, T. J. Ab Initio Study of *cis-trans* Photoisomerization in Stilbene and Ethylene. *J. Phys. Chem. A* **2003**, *107*, 829−837.
(39) Barbatti, M.; Lischka, H.; Salzmann, S.; Marian, C. M. UV Excitation and Radiationless Deactivation of Imidazole. *J. Chem. Phys.* **2009**, *130*, 034305.
(40) Crespo-Otero, R.; Barbatti, M.; Yu, H.; Evans, N. L.; Ullrich, S. Ultrafast Dynamics of UV-Excited Imidazole. *ChemPhysChem* **2011**, *12*, 3365−3375.
(41) Hadden, D. J.; Wells, K. L.; Roberts, G. M.; Bergendahl, L. T.; Paterson, M. J.; Stavros, V. G. Time Resolved Velocity Map Imaging of H-Atom Elimination from Photoexcited Imidazole and its Methyl Substituted Derivatives. *Phys. Chem. Chem. Phys.* **2011**, *13*, 10342−10349.
(42) Yu, H.; Evans, N. L.; Stavros, V. G.; Ullrich, S. Investigation of Multiple Electronic Excited State Relaxation Pathways Following 200 nm Photolysis of Gas-Phase Imidazole. *Phys. Chem. Chem. Phys.* **2012**, *14*, 6266−6272.
(43) Serrano-Andrés, L.; Merchán, M. Quantum Chemistry of the Excited State: 2005 Overview. *J. Mol. Struct.: THEOCHEM* **2005**, *729*, 99−108.
(44) Martínez, T. J. Insights for Light-Driven Molecular Devices from Ab Initio Multiple Spawning Excited-State Dynamics of Organic and Biological Chromophores. *Acc. Chem. Res.* **2006**, *39*, 119−126.
(45) Barbatti, M.; Aquino, A. J. A.; Szymczak, J. J.; Nachtigallová, D.; Hobza, P.; Lischka, H. Relaxation Mechanisms of UV-Photoexcited DNA and RNA Nucleobases. *Proc. Natl. Acad. Sci. U.S.A.* **2010**, *107*, 21453−21458.
(46) Schapiro, I.; Ryazantsev, M. N.; Frutos, L. M.; Ferré, N.; Lindh, R.; Olivucci, M. The Ultrafast Photoisomerizations of Rhodopsin and Bathorhodopsin Are Modulated by Bond Length Alternation and HOOP Driven Electronic Effects. *J. Am. Chem. Soc.* **2011**, *133*, 3354−3364.
(47) Lasorne, B.; Worth, G. A.; Robb, M. A. Excited-State Dynamics. *WIREs Comput. Mol. Sci.* **2011**, *1*, 460−475.
(48) Lan, Z.; Lou, Y.; Fabiano, E.; Thiel, W. QM/MM Nonadiabatic Decay Dynamics of 9H-Adenine in Aqueous Solution. *ChemPhysChem* **2011**, *12*, 1989−1998.
(49) Mališ, M.; Loquais, Y.; Gloaguen, E.; Biswal, H. S.; Piuzzi, F.; Tardivel, B.; Brenner, V.; Broquier, M.; Jouvet, C.; Mons, M.; et al. Unraveling the Mechanisms of Nonradiative Deactivation in Model Peptides Following Photoexcitation of a Phenylalanine Residue. *J. Am. Chem. Soc.* **2012**, *134*, 20340−20351.
(50) Kuhlman, T. S.; Glover, W. J.; Mori, T.; Møller, K. B.; Martínez, T. J. Between Ethylene and Polyenes - The Nonadiabatic Dynamics of *cis*-Dienes. *Faraday Discuss.* **2012**, *157*, 193−212.
(51) Plasser, F.; Barbatti, M.; Aquino, A. J. A.; Lischka, H. Electronically Excited States and Photodynamics: A Continuing Challenge. *Theor. Chem. Acc.* **2012**, *131*, 1073−1087.
(52) Ashfold, M. N. R.; King, G. A.; Murdock, D.; Nix, M. G. D.; Oliver, T. A. A.; Sage, A. G. $\pi\sigma^*$ Excited States in Molecular Photochemistry. *Phys. Chem. Chem. Phys.* **2010**, *12*, 1218−1238.
(53) Sellner, B.; Barbatti, M.; Müller, T.; Domcke, W.; Lischka, H. Ultrafast Non-Adiabatic Dynamics of Ethylene Including Rydberg States. *Mol. Phys.* **2013**, *111*, 2439−2450.

(54) TURBOMOLE V6.3.1 2011, a development of University of Karlsruhe and Forschungszentrum Karlsruhe GmbH, 1989−2007, TURBOMOLE GmbH, since 2007, available from http://www.turbomole.com.
(55) Aquilante, F.; Vico, L. D.; Ferré, N.; Ghigo, G.; Malmqvist, P.-Å.; Neogrády, P.; Pedersen, T. B.; Pitonak, M.; Reiher, M.; Roos, B. O.; et al. MOLCAS 7: The Next Generation. *J. Comput. Chem.* **2010**, *31*, 224−247.
(56) Lischka, H.; Shepard, R.; Shavitt, I.; Pitzer, R. M.; Dallos, M.; Müller, T.; Szalay, P. G.; Brown, F. B.; Ahlrichs, R.; Böhm, H. J.; et al. *COLUMBUS, an ab initio electronic structure program*, release 7.0., 2012.